

Anisotropic Constitutive Model for Nickel Base Single Crystal Alloys: Development and Finite Element Implementation

(NASA-CR-175015) ANISOTROPIC CONSTITUTIVE
MODEL FOR NICKEL BASE SINGLE CRYSTAL ALLOYS:
DEVELOPMENT AND FINITE ELEMENT
IMPLEMENTATION Final Report (Cincinnati
Univ.) 130 p HC A07/ME A01

N86-21952

Unclas

CSCL 20K G3/39 05770

L.T. Dame and D.C. Stouffer
University of Cincinnati
Cincinnati, Ohio

March 1986



Prepared for
Lewis Research Center
Under Grant NAG 3-511

NASA
National Aeronautics and
Space Administration



TABLE OF CONTENTS

	PAGE
CHAPTER I INTRODUCTION	1
1.1 Alloy Chemistry and Structure	2
1.2 Mechanical Response of the Alloy	5
1.3 Constitutive Modeling History	10
1.3.1 Continuum Mechanics Approach	10
1.3.2 Crystallographic Approach	15
1.4 Scope of the Present Study	16
CHAPTER II DEVELOPMENT OF AN ANISOTROPIC INELASTIC CONSTITUTIVE EQUATION	18
2.1 Observed Deformation Characteristics	18
2.1.1 Tensile Response	18
2.1.2 Creep Response	19
2.2 Metallurgical Models	22
2.3 Kinematics	24
2.4 Inelastic Constitutive Equations	26
2.4.1 Octahedral Flow Equation	27
2.4.2 Cube Flow Equation	33

	PAGE
CHAPTER III EXPERIMENTAL DATA AND MATERIAL CONSTANTS	35
3.1 Rene N4 Composition A Response	36
3.2 Rene N4 VF317 Response	41
3.3 Derivation of the Material Constants	44
3.3.1 Flow Equation Constants	46
3.3.2 Evaluation of Orientation Factors	49
3.3.3 Evaluation of the Hardening Parameters	52
3.3.4 Tensile/Creep Coupling Terms	55
CHAPTER IV FINITE ELEMENT IMPLEMENTATION	58
4.1 Initial Strain Method	58
4.2 Linear Load History	60
4.3 Integration of the Constitutive Equations	62
4.4 Iteration Procedure	63
4.5 Dynamic Time Incrementing	64
4.5.1 Stress Increment Criterion	66
4.5.2 Inelastic Strain Increment Criterion	66
4.5.3 Rate of Change of the Inelastic Strain Rate	67
4.6 Convergence Criteria	67
CHAPTER V COMPARISON OF THE CALCULATED AND EXPERIMENTAL RESULTS	69
5.1 Comparison of Experimental and Calculated Response for Rene N4, Composition A	69
5.1.1 Orientation Dependence and Tension/Compression Asymmetry	70
5.1.2 Cyclic Response	70
5.1.3 Strain Rate Sensitivity	74

5.2	Comparison of Experimental and Calculated Response for Rene N4 VF317, Composition B.....	75
5.2.1	Orientation Dependent Stress Strain Curves	75
5.2.2	Creep Response	78
5.2.3	Stress Relaxation	78
CHAPTER VI	DISCUSSION AND SUMMARY	84
6.1	Constitutive Model Development	84
6.1.1	Coupling of Creep and High Strain Rate Response	84
6.1.2	Nonisothermal Response	85
6.1.3	Thermal Recovery	86
6.1.4	Latent Hardening	86
6.1.5	Cyclic Hardening	88
6.1.6	Other Response Characteristics	88
6.2	Summary of Data Base Requirements	89
6.3	Conclusion	92
APPENDIX A	EIGENSPACE APPROACH	93
A.1	Cubic Materials	98
A.2	Transverse Isotropic Materials	99
A.3	Incompressible Orthotropic Materials	101
A.4	Conditions Necessary for Stationary Eigenvectors	103
A.4.1	Transverse Isotropic Materials	103
A.4.2	Orthotropic Materials	104
APPENDIX B	DEVELOPMENT OF THE KINEMATIC EQUATIONS	108
REFERENCES	119

CHAPTER I

INTRODUCTION

Nickel base single crystal superalloys, because of their superior high temperature properties, have attracted considerable interest for use in gas turbine engines. The initial development of these alloys as turbine blade and vane materials began in the 1960's at Pratt and Whitney Aircraft with the alloy PWA 1409 which is the single crystal version of Mar-M200, [1]-[5]. Since that time a variety of similar alloys have been developed, both by Pratt and Whitney and by other aircraft engine companies. These include the Pratt and Whitney alloy PWA 1480, the AiResearch alloy Mar-M247 and the General Electric alloy Rene-N4, which is the alloy of interest in this research.

During the manufacture of single crystal turbine blades the [001] crystal orientation is the natural growth direction. The [001] axis is parallel to the span of the blade which is also in the direction of the centrifugal loading. At this orientation considerable improvement in creep and fatigue resistance is obtained over conventionally cast turbine blades. There is some variation in the [001] orientation from one blade to another due to the manufacturing process. The transverse orientation of the crystal is generally not controlled, but it can be controlled by using a seed crystal. At the present time it is not possible to adequately evaluate the benefits of controlling the transverse orientation.

One of the basic needs is the development of better mechanical analysis methods for use in the design of single crystal engine

components. Specifically, it is necessary to develop a model to predict the inelastic constitutive behavior of the material and to incorporate the model into a general purpose finite element code. The purpose of this research is to satisfy this need. Presented in this study is a constitutive model for Rene N4 at 760°C and the implementation of this model in a nonlinear three dimensional finite element code.

1.1 Alloy Chemistry and Structure

Rene N4 was developed by General Electric specifically for use as a turbine blade and vane alloy. The nominal chemical compositions of Rene N4 and PWA 1480 are presented in Table I, along with the two specific compositions examined in this study, References [6] and [68]. The elements C, B, and Zr which are typically included in polycrystalline high temperature, nickel base superalloys for the purpose of strengthening the grain boundaries are omitted.

All of the modern single crystal materials are two phase alloys with a large volume fraction of γ' phase. The γ' precipitates have $L1_2$ type crystal structure and are interspersed in a coherent face centered cubic γ solid solution, Figure 1. The strength of the alloy is a function of the γ' size and the percentage of γ' , [7], [15]. Experimentally it has been determined that the peak creep strength is achieved with a volume fraction of γ' of about 60%. In high volume fraction γ' alloys deformation must occur by shearing of the precipitates. Much of the behavior of the alloy can be explained on

this basis. As a result, considerable research has been devoted to crystals with $L1_2$ structure, [8] - [14].

TABLE 1.
Composition and Heat Treatment of Rene N4 and PWA 1480

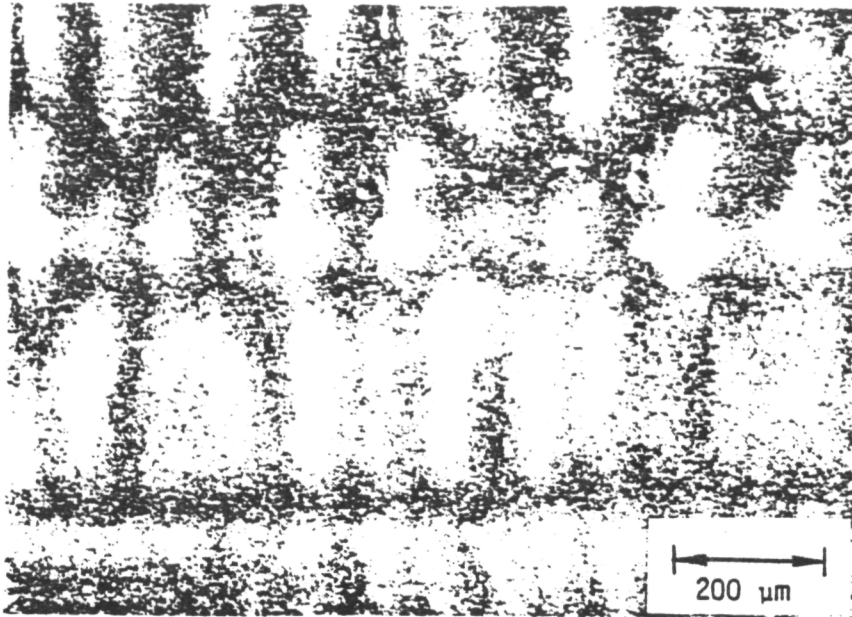
	Element, WT. %										
	Al	Ti	Ta	Nb	Cr	Mo	W	Co	C	B	Zr
^a RENE N4 NOMINAL	3.7	4.2	4.0	0.5	9.25	1.5	6.0	7.5	-	-	-
^c RENE N4 COMPOSITION A	3.77	4.24	3.96	0.5	9.26	1.60	5.88	7.53	-	-	-
^d RENE N4 COMPOSITION B	3.6	4.6	4.1	0.6	8.7	1.6	6.0	7.4	-	-	-
^b PWA-1480	5.0	1.5	12	-	10	-	4.0	5.0	-	-	-

^aHeat Treatment: 1260°C/2h/gas quench + 1080°C/4h/air cool + 900°C/16h/air cool.

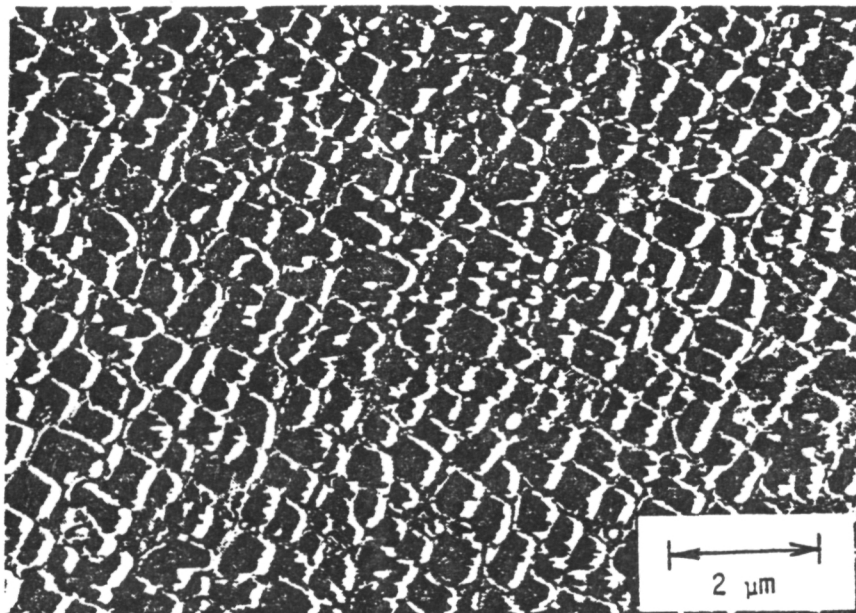
^bHeat Treatment: 1288°C/4h/air cool + 1079°C/4h + 871°C/32h.

^cActual composition for specimens reported in References [6], [37].

^dActual composition for specimens reported in Reference [68] and designated in VF 317.



a) Dendritic Structure at Low Magnification (100X)



b) Gamma Prim Morphology at High Magnification (10,000X)

FIGURE 1. MICROSTRUCTURE OF FULLY HEAT-TREATED RENE' N4

1.2 Mechanical Response of the Alloy

Elastic strains are associated with crystal lattice distortions and are fully recoverable whereas inelastic strains result from the movement of atoms within the lattice and are not recoverable. The effects of inelastic strains on the elastic properties are assumed to be negligible.

Rene N4, as well as other single crystal alloys, exhibits cubic symmetry in the elastic range, Reference [78]. There are three independent elastic constants and in the principal material directions the elastic constitutive equation is written as

$$\begin{Bmatrix} \epsilon_{11} \\ \epsilon_{22} \\ \epsilon_{33} \\ \epsilon_{23} \\ \epsilon_{31} \\ \epsilon_{12} \end{Bmatrix} = \begin{bmatrix} \frac{1}{E} & -\frac{\nu}{E} & -\frac{\nu}{E} & 0 & 0 & 0 \\ -\frac{\nu}{E} & \frac{1}{E} & -\frac{\nu}{E} & 0 & 0 & 0 \\ -\frac{\nu}{E} & -\frac{\nu}{E} & \frac{1}{E} & 0 & 0 & 0 \\ 0 & 0 & 0 & \frac{1}{2G} & 0 & 0 \\ 0 & 0 & 0 & 0 & \frac{1}{2G} & 0 \\ 0 & 0 & 0 & 0 & 0 & \frac{1}{2G} \end{bmatrix} \begin{Bmatrix} \sigma_{11} \\ \sigma_{22} \\ \sigma_{33} \\ \sigma_{23} \\ \sigma_{31} \\ \sigma_{12} \end{Bmatrix} \quad (1.1)$$

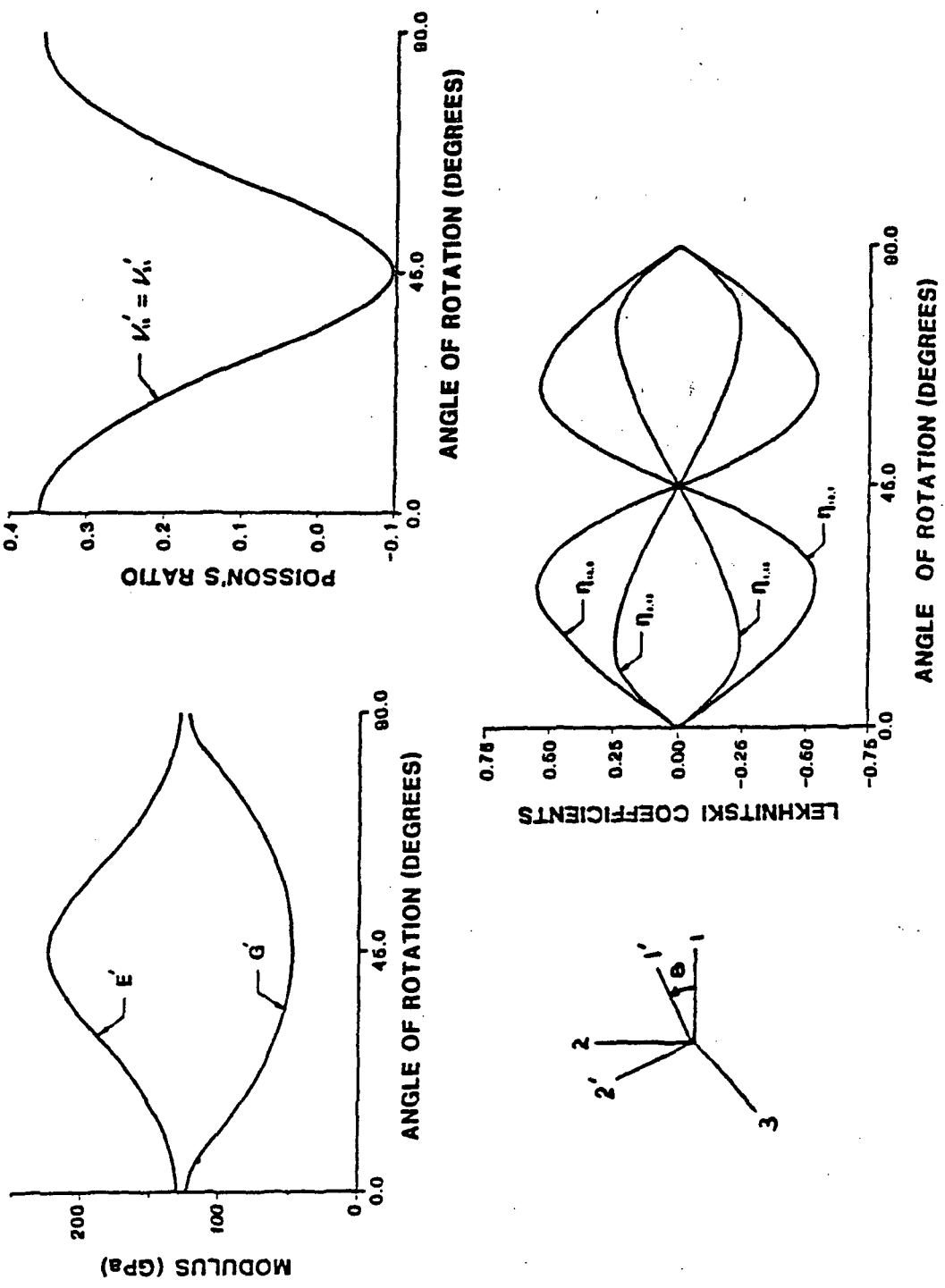
The components of the stress and elastic strain tensors are denoted by σ_{ij} and ϵ_{ij} . Since the elastic modulus, E , shear modulus, G , and Poisson's ratio, ν , are independent elastic constants the terms of the compliance matrix depend on orientation. Rotation of the elastic compliance to another orientation can fully populate the matrix. For example, rotation about the 3 axis gives shear/normal coupling,

Lekhnitski coefficients and variations in the rotated moduli E' , G' and ν' as shown in Figure 2.

The inelastic response of single crystal materials is quite different from the behavior of polycrystalline nickel base superalloys. The yield stress of single crystal alloys is a function of the material orientation relative to the direction of the applied stress. They also exhibit a significant tension/compression asymmetry in yielding. Figure 3, [15] shows the yield stress of PWA 1480 at 593°C as a function of orientation along the $[001]$ - $[011]$ boundary of the standard stereographic triangle for tension and compression. The tension/compression asymmetry is negligible near the $[111]$ orientation. Further, the orientation dependence and tension/compression asymmetry decrease as a function of increasing temperature above a critical temperature. As an example, the variation of yield stress for PWA 1480 at three orientations in tension and compression for a range of temperatures is shown in Figure 4, [15]. In creep, at lower strain rates, single crystal alloys also exhibit orientation dependence even though the deformation mechanisms are expected to be different.

Other observed behavior is similar to that seen in isotropic nickel base superalloys. These materials exhibit both strain rate sensitivity and cyclic hardening. Shown in Figure 5, [17] is the cyclic stress strain response for PWA 1480, 871°C , at different strain rates in the $[111]$ orientation. An initial stress strain hysteresis loop as

FIGURE 2 - VARIATION OF ELASTIC MODULI WITH ORIENTATION FOR A CUBIC SYMMETRIC MATERIAL.



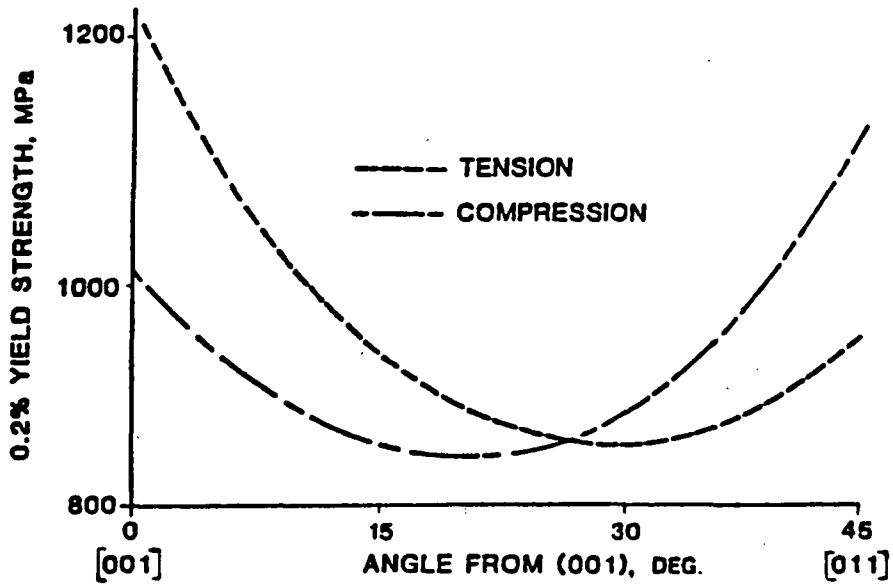


FIGURE 3. YIELD STRENGTH OF PWA 1480 at 593°C (1100°F) WITH ORIENTATION ALONG THE [001] - [011] BOUNDARY OF THE STANDARD STEREOGRAPHIC TRIANGLE. (REFERENCE [15])

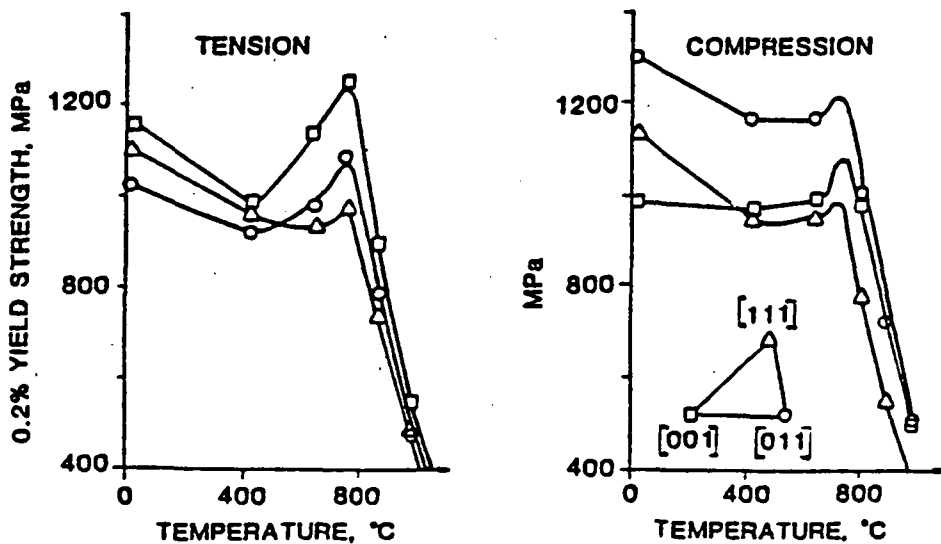


FIGURE 4. YIELD STRENGTH OF PWA 1480 AS A FUNCTION OF TEMPERATURE FOR THE [001], [011] and [111] ORIENTATIONS IN TENSION AND COMPRESSION. (REFERENCE [15])

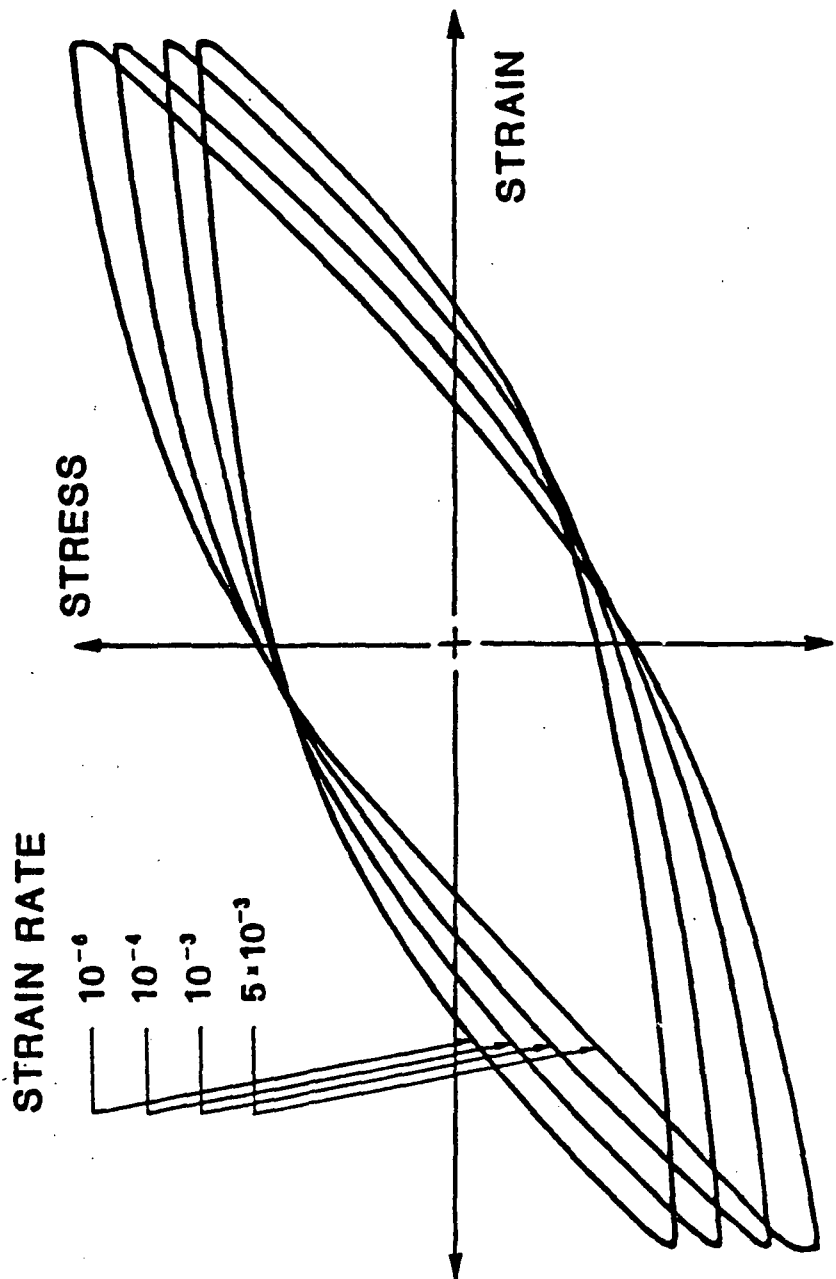


FIGURE 5. STRAIN RATE SENSITIVITY TEST OF PWA 1480 at 871°C FOR THE [111] ORIENTATION. (REFERENCE [17])

compared to a loop after cyclic hardening is shown in Figure 6, [18], for PWA 1480 at 760°C in the [123] orientation.

1.3 Constitutive Modeling History

1.3.1 Continuum Mechanics Approach

A number of investigators have proposed anisotropic plasticity and creep theories. The majority of these are based on a mathematical form similar to yield surface plasticity theory for isotropic materials, [19] - [29]. Material anisotropy is introduced by including an anisotropy matrix in the yield function and kinematic hardening is modeled by utilizing a back stress tensor or a displacement of the yield surface. Isotropic hardening is accounted for with a change in yield surface size. A recent modification of this approach involves using a unified constitutive equation while retaining the basic mathematical structure for the flow law but without an explicit yield surface [38], [49]. In order to demonstrate the general features of the approach it is useful to summarize one of these theories as an example.

Lee, Zaverl, and Shih have developed an anisotropic plasticity and creep theory that successfully predicts many of the features of the inelastic response of Zircaloy, [23], [24], [26], and [30]. The yield function is an extension of Hill's work [28], and is given by

$$M_{ij}(\sigma_i - \alpha_i)(\sigma_j - \alpha_j) - k^2 = 0 \quad (1.2)$$

in a six dimensional stress space, σ_i . The anisotropy matrix M_{ij} describes the variation of yield stress with orientation. The parameter k defines an effective yield surface size and the back stress α_i

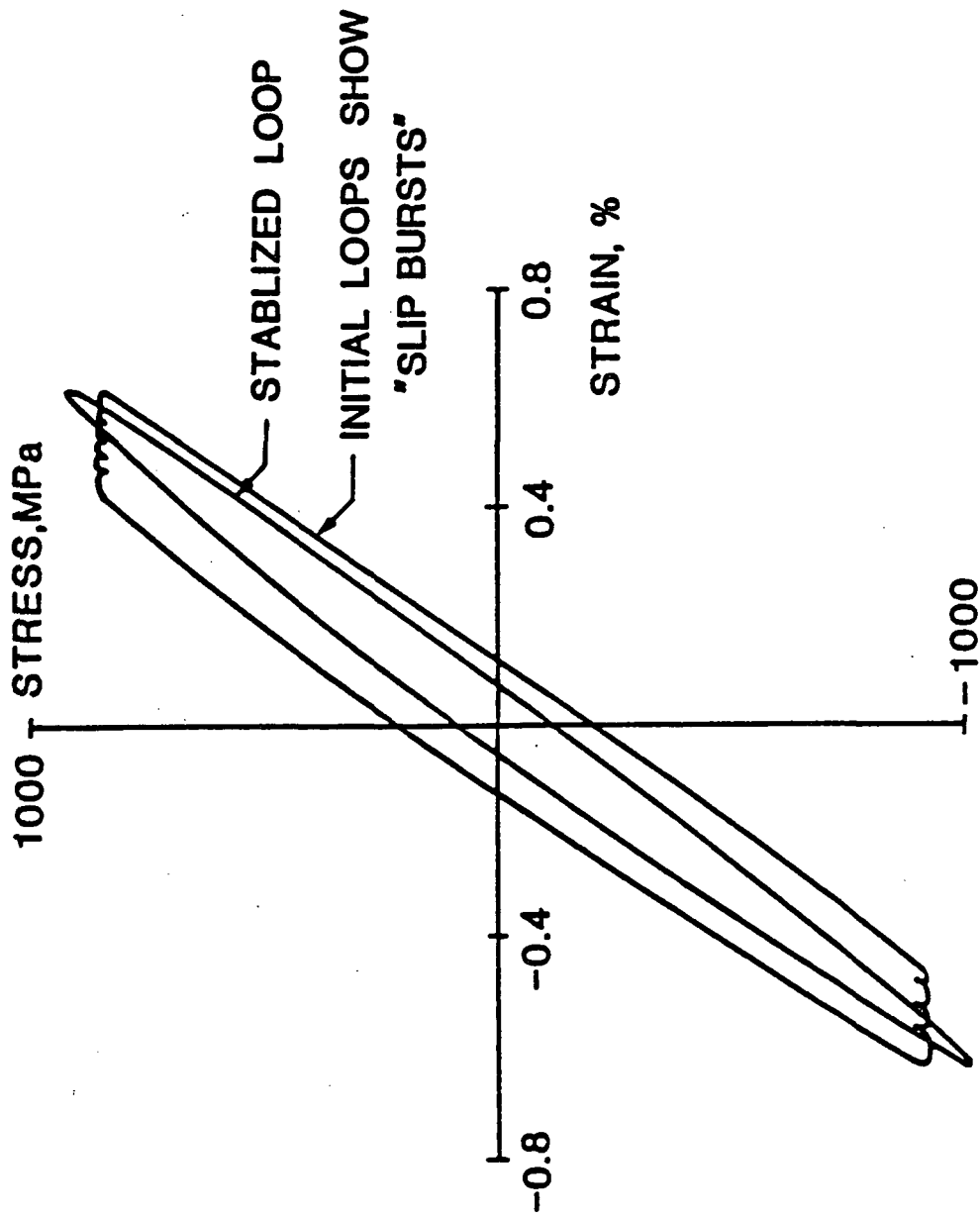


FIGURE 6. CYCLIC HARDENING RESPONSE OF PWA 1480 IN THE [123] ORIENTATION AT 760°C. (REFERENCE 18)

describes the initial tension/compression strength differential and subsequent kinematic hardening. All of the parameters, k , α_i , and M_{ij} are functions of the plastic strain increments. The flow rule,

$$d\epsilon_i^P = \frac{3}{2} \frac{d\bar{\epsilon}^P}{d\bar{\sigma}} S_i \quad (1.3)$$

is a generalization of the Prandtl-Reuss equations for isotropic materials. The effective stress $\bar{\sigma}$ is defined by

$$\bar{\sigma}^2 = M_{ij}(\sigma_i - \alpha_i)(\sigma_j - \alpha_j) \quad (1.4)$$

and the effective plastic strain increment is defined by

$$(d\bar{\epsilon}^P)^2 = M_{ij}^* d\epsilon_i^P d\epsilon_j^P \quad (1.5)$$

where M_{ij}^* is the generalized inverse of M_{ij} and the generalized deviatoric stress is given by

$$S_i = \frac{2}{3} M_{ij} (\sigma_j - \alpha_j) \quad (1.6)$$

To extend the theory into the creep regime an effective creep strain rate $\dot{\epsilon}^C$ is assumed to be a function of the effective stress $\bar{\sigma}$, defined by Equation (1.4), as well as the temperature and shear resistance τ . The shear resistance is assumed to be proportional to k . The flow Equation (1.3) is modified slightly to become

$$\dot{\epsilon}_i^C = \frac{3}{2} \frac{\dot{\bar{\epsilon}}^C}{\bar{\sigma}} S_i \quad (1.7)$$

where $\dot{\epsilon}_i^c$ are the creep strain rate components and the total inelastic strain is then the sum of the creep and plastic strain components. A method for the evaluation of material parameters has been established and the calculated and experimental response of Zircaloy 2 has been presented in References [23] and [26]. The determination of the yield function behavior requires load reversal tests and monotonic tension and compression tests in the three principal directions of anisotropy. The rate dependent material parameters are evaluated from load relaxation tests.

A unified model that falls within the continuum mechanics approach was proposed by Stouffer and Bodner [38], for initial or deformation induced anisotropy. The approach, as summarized in Appendix A, was investigated as part of the study for application to Rene N4. The model is based on transforming the anisotropic flow equation, when written in a six dimensional space, into the eigenspace of the compliance (or stiffness) matrix. This results in a system of six uncoupled scalar flow equations in the compliance eigenvalues which has some advantage for computation. The major disadvantage is that the transformation between the eigenspace and physical space depends upon the evolution of material properties arising from the deformation and is generally unknown. However, as presented in Appendix A, it is possible to determine this transformation exactly for various symmetry classes including cubic symmetry. The results in Appendix A show that once a specific transformation is established; for example, for cubic symmetry,

the response will be forced to follow this symmetry class exactly for all future deformations. Unfortunately, this condition appears to be too restrictive. Relaxation of the symmetry restriction leads to parameters in the eigenspace that are not physically motivated and difficult to determine experimentally. Thus, it was decided to abandon this eigenspace approach in favor of an approach with material parameters that are motivated by the physics of the deformation and directly related to experiments.

The most significant shortcoming of the continuum mechanics approach as described in both of the above examples is that the actual deformation mechanisms are included in the theory only very crudely if at all. This limits the predictive capability of the model outside the range for which it has been calibrated. Another serious problem is modeling the plasticity, creep and fatigue interactions. Lee, Zaverl, and Shih have made an attempt to correct this deficiency by assuming a relationship between the shear resistance in the creep equation and the yield surface size in the yield function. Finally, although not discussed above, the current theories do not contain methods of including temperature history effects. Current technology is based on evaluating model parameters from isothermal data at different temperatures and then interpolating between temperatures to determine the response. This does not account for a change in deformation mechanism due to a temperature excursion.

The principal argument in favor of a continuum mechanics approach is the relative numerical simplicity. For the purpose of implementation

in a finite element code it is somewhat less complicated and generally requires less calculation than a crystallographic approach.

1.3.2 Crystallographic Approach

Early developments in this approach are attributed to Taylor [31], Bishop and Hill [32], [33] and Bishop [34]. The application of the crystallographic approach to single crystal nickel base superalloys began with the work of Paslay, Wells, Leverant and Burck [35], [36], and more recently by Shah [8] to the γ' phase of these alloys.

The crystallographic approach is based on identifying the active slip planes and slip directions. The shear stresses are computed on each of the slip planes from the applied stress. The slip deformation is computed on each slip system and the macroscopic inelastic strain rates or strain increments are then the sum of the contributions of the individual slip systems. This approach is computationally intensive since there are a number of slip systems to be considered at each point in the body. Furthermore the response at the crystallographic level is not necessarily easy to determine.

The classical constitutive assumption is Schmid's law in which it is assumed that the slip on a particular system is a function of the resolved shear stress on the slip plane in the direction of slip. This assumption, however, does not apply for $L1_2$ crystals in general or for single crystal nickel base superalloys. More recently, Pope and others [7]-[12], [14]-[16], have proposed an extension to Schmid's law that includes three components of stress. This approach, which is discussed

in Chapter 2, appears to be successful in correlating the deformation mechanism with several of the macroscopic anisotropic effects.

The principal advantage of this method is that a significant portion of the model is based on the physics of the deformation mechanisms. Presumably, this will enhance the predictive capability of the model. Furthermore, as additional information is obtained about deformation mechanisms at different temperatures and strain rates the local constitutive models can be modified to accommodate the new knowledge. The major disadvantage of this approach is that knowledge of the metallurgy and the interface with mechanics must be understood. A less important objection is the additional difficulty in numerically implementing crystallographic models in finite element codes and the increased computational requirements.

1.4 Scope of the Present Study

The purpose of this research is to provide a tool for the mechanical design and analysis of single crystal turbine blades and vanes. This objective is achieved through the development of an appropriate constitutive model and its implementation in a general purpose three dimensional nonlinear finite element code.

The important features of the nonlinear constitutive response are to be modeled. These include the orientation dependent stress/strain behavior and tension/compression asymmetry. The constitutive model must also predict cyclic and creep response. Because of the extremely limited data base, some important aspects of the material response have not been modeled in this study. The most important aspects of the

response that need further investigation are the nonisothermal behavior and the response of the material in a multiaxial stress state. Also of concern and not currently included in the constitutive model is the cyclic softening/hardening behavior and latent hardening due to intersecting slip systems.

The constitutive model has been developed using the crystallographic approach. The orientation and tension/compression yield asymmetry can be accounted for using the metallurgical models developed in References [7]-[12], [14]-[16]. The development of a constitutive model from metallurgical concepts should provide a basis for further development of both the mechanics and metallurgy associated with single crystal technology.

The intent in developing a finite element program is to produce a code that is general enough to model a wide range of geometries and load histories, flexible enough to easily modify the local constitutive equations and at the same time efficient. The need to model general three dimensional geometries lead to the choice of the twenty noded isoparametric solid element. The code efficiently and accurately integrates the constitutive equations over piecewise linear load histories using an initial strain method with a dynamic time incrementing procedure. Because of the intended application, small displacement and small strain measures are utilized.

CHAPTER II

DEVELOPMENT OF AN ANISOTROPIC INELASTIC CONSTITUTIVE EQUATION

The philosophy in developing the constitutive model is to produce a system of equations that is as simple as possible while still describing the important aspects of the observed material response. As a result of an extremely limited data base, certain effects that could have been included are omitted rather than engaging in speculation. The effort in this report is primarily directed toward modeling isothermal tensile and creep response with some hypothetical extensions to strain rate effects, stress relaxation and initial cyclic response.

2.1 Observed Deformation Characteristics

Slip trace studies of single crystal alloys indicate that one or more types of slip may occur under different temperature, orientation and strain rate conditions. These include: A. (Octahedral Slip) slip on the four octahedral planes in the three directions similar to the $[\bar{1} 0 1]$ direction (see Figure B2, Appendix B); B. (Octahedral Slip) slip on the octahedral planes in the three directions similar to the $[\bar{1} 2 \bar{1}]$ direction; and C. (Cube Slip) slip on the three cube planes in the two directions similar to the $[\bar{1} 0 1]$ direction. The slip conditions occurring during creep and tensile tests are examined for use in development of the model.

2.1.1 Tensile Response

Recent metallurgical research in the behavior of nickel base single crystal superalloys indicates that the tensile response of these

alloys is controlled to a large extent by the behavior of the γ' phase alone, [7], [15] and [16]. Thus, the response of L_{12} ordered alloys and γ/γ' single crystals are discussed together.

In uniaxial tests the critical resolved shear stress (CRSS), or component of stress on the slip plane in the direction of slip required for yielding, is approximately constant or increases slightly up to a critical temperature and is a function of orientation. Below this critical temperature slip occurs primarily on the octahedral $(111)[\bar{1} 0 1]$ slip systems and significant orientation dependence and tension/compression asymmetry is observed. Above the critical temperature there is a sharp drop in the CRSS similar to the yield stress in Figure 4, cube slip, $(010)[\bar{1} 0 1]$ becomes more prominent, and the tension/compression asymmetry is reduced, [16]. There are two exceptions to this behavior. First, test specimens near the $[111]$ orientation exhibit cube slip at all temperatures. Second, loading near the $[0 0 1]$ orientation is thought to produce only octahedral slip at all temperatures since the resolved shear stress on the cube planes is zero.

2.1.2 Creep Response

The understanding of the creep properties and the active slip systems during creep in γ/γ' alloys is much less complete than the tensile response. Only a limited number of studies have been reported in the literature; however, a few important observations can be included in this review.

Unlike the tensile yield response, the creep properties of ordered L_{12} crystals are much different than the creep response of the γ/γ' alloys [69]. The creep rate of γ' is significantly higher than that of γ/γ' alloys under identical conditions.

Some nickel base superalloy single crystals exhibit an incubation period in addition to the usual primary, secondary and tertiary creep, see Figure 7b [7]. The incubation period and primary creep are attributed to $(111) [\bar{1} 2 \bar{1}]$ slip. In single crystal Rene N4 at temperatures from 760°F to 1150°C the response did not include an incubation period similar to that in Mar-M200, see Figure 7 and 11.

In secondary creep at temperatures above the critical temperature slip is inferred to occur by $(111) [\bar{1} 0 1]$ slip [8]. However, cube slip is considered to be present near the $[111]$ orientation and absent near the $[0 0 1]$ orientation similar to the tensile response. These deformation modes have been verified by transmission electron microscopy (TEM) studies for PWA 1444, [63] and in addition dodecahedral slip, (011) planes, was observed for loading in the (001) and (011) directions. In this study a tension/compression asymmetry was observed and typical response showed a creep rate that is higher in tension than compression for a creep in the $[1 1 0]$ direction. This response is similar to the tension/compression asymmetry observed in the yield stress.

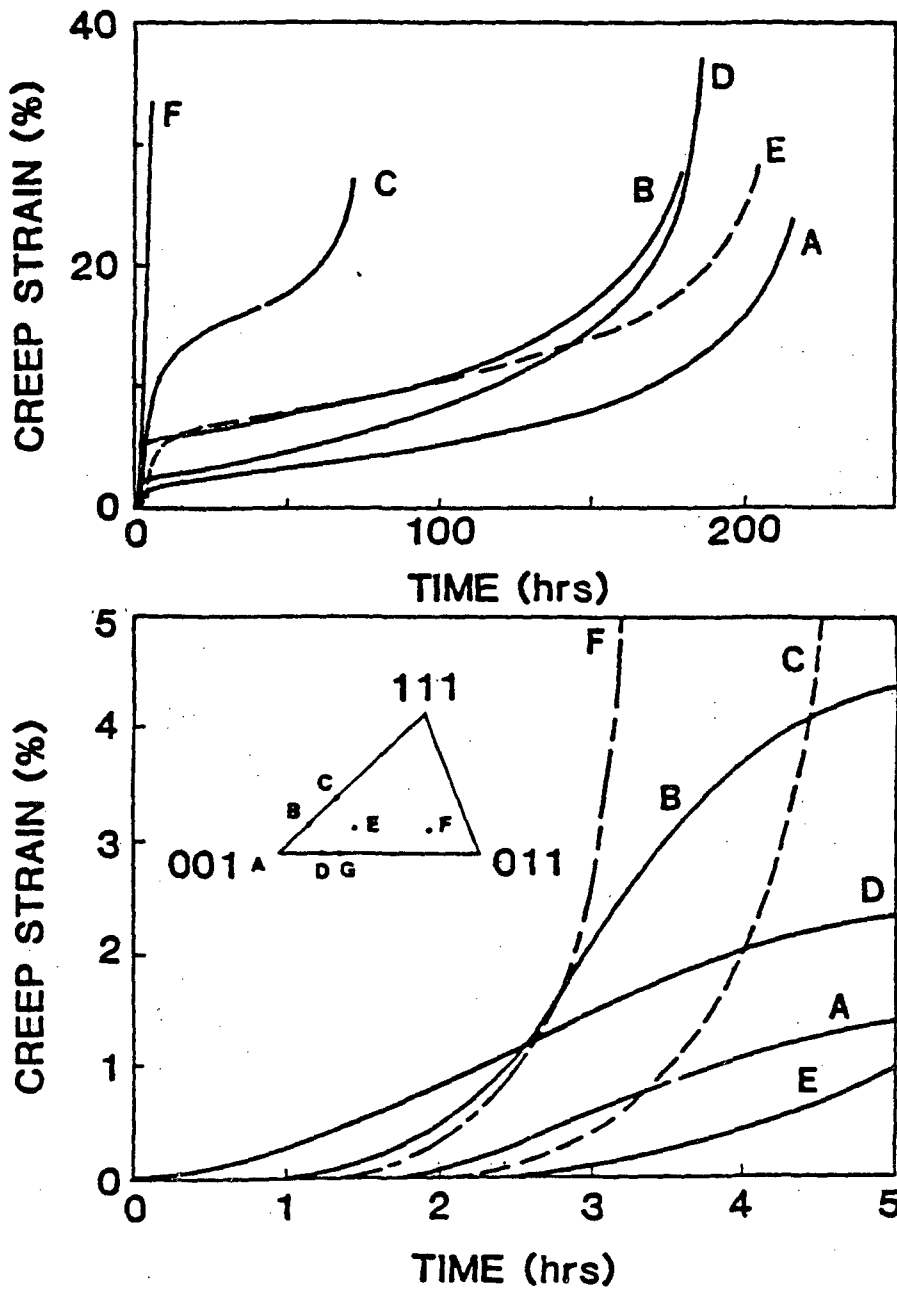


FIGURE 7. CREEP CURVES OF MAR-M200 CRYSTALS AT 760°C AND 690 MPa.
(REFERENCE 7)

2.2 Metallurgical Models

A major step in understanding this behavior was made by Takeuchi and Kuramoto [10] in their study of Ni_3Ga single crystals. They proposed that the increase in CRSS up to the critical temperature and non Schmid's law behavior is a result of cross slip of screw dislocation segments from the octahedral to cube planes. The cross slipped segments pin the dislocations and therefore increase the flow stress. They further proposed that the cross slip mechanism is thermally activated and is driven by the resolved shear stress in the $(010)[\bar{1} 0 1]$ system. However, their model did not fully explain the tension/compression asymmetry or the orientation dependence observed in other Li_2 alloys.

An improvement in the Takeuchi-Kuramoto model was proposed by Lall, Chin and Pope in [11]. In their theory the octahedral $\frac{a}{2} [\bar{1} 0 1]$ dislocation is an extended dislocation consisting of two Shockley partial dislocation pairs, $\frac{a}{6} [\bar{2} 1 1] + \frac{a}{6} [\bar{1} \bar{1} 2]$. In order to cross slip the pair must constrict into a single $\frac{a}{2} [\bar{1} 0 1]$ dislocation. The constriction is aided by a shear stress on the (111) plane in the $[1 \bar{2} 1]$ direction. It is important to note that a shear stress in the opposite direction extends the dislocation pair and thus inhibits cross slip. This effect is generally referred to as the "core width effect" and gives rise to the tension/compression asymmetry observed in these alloys. Lall, Chin and Pope also proposed that the change in flow

stress $\Delta\tau_{(111)}$ on the octahedral plane in the $[\bar{1} 0 1]$ direction, for example, from a reference state at 0°K is given by

$$\Delta\tau_{(111)} = A \exp -\frac{H}{kT}, \quad (2.1)$$

where A is a constant, T is temperature, and k is Boltzmann's constant. The parameter H is a function of the resolved shear stress on the (111) plane in the $[\bar{1} 2 \bar{1}]$ direction, τ_1 , and the resolved shear stress on the (010) plane in the $[\bar{1} 0 1]$ direction, τ_2 . The stress components τ_1 and τ_2 are shown in Figures B1 and B2. By expanding H in a Taylor series about the reference condition H_0 , Equation (2.1) becomes

$$\Delta\tau_{(111)} = A \exp \frac{-H_0 + V_1\tau_1 + V_2\tau_2 + \dots}{kT}, \quad (2.2)$$

where V_1 and V_2 are constants.

In the orientations and at temperatures where cube slip is dominant the orientation dependence and tension/compression asymmetry is reduced considerably. Therefore, it is believed that Schmid's law can be used to relate the slip rate to the resolved shear stress on the cube planes.

A major effort in this work is to recast the above results, both experimental and theoretical, into the form of a constitutive equation involving state variables that characterize the change in material properties due to the deformation history. These results are valuable

for determining the appropriate independent variables and functional forms.

2.3 Kinematics

It is necessary to develop the kinematic equations that relate the shear stresses on the crystallographic planes and in the directions of interest to the stress tensor relative to the principal material axes. The constitutive equations are applied at the crystallographic level and it is therefore necessary to also develop the relationship between the crystallographic shear strain rates and the macroscopic inelastic strain rate tensor. The required stress and infinitesimal strain relations were derived by Bishop in [34] and are summarized below. The sign convention used in this research and the details of the calculations are presented in Appendix B.

The relative rate of displacement of a point located at x_i due to a uniform shear strain rate $\dot{\gamma}^{\alpha\beta}$ parallel to the α plane in the β direction is given by

$$\dot{u}_i = \sum_j \dot{\gamma}^{\alpha\beta} n_j^\alpha x_j l_i^{\alpha\beta} \quad (2.3)$$

where n_j^α is the unit normal to the α plane and $l_i^{\alpha\beta}$ is the unit vector in the β direction on the α plane (no summation of repeated indices). Summing for all planes and slip directions gives

$$\dot{u}_i = \sum_{\alpha\beta j} \dot{\gamma}^{\alpha\beta} n_j^\alpha x_j l_i^{\alpha\beta} \quad (2.4)$$

Applying the linear strain displacement relation

$$\dot{\epsilon}_{ij} = \frac{1}{2} \left[\frac{\partial \dot{u}_i}{\partial x_j} + \frac{\partial \dot{u}_j}{\partial x_i} \right] \quad (2.5)$$

gives the desired relationship between the crystallographic shear strain rates $\dot{\gamma}^{\alpha\beta}$, and global strain rates $\dot{\epsilon}_j$,

$$\dot{\epsilon}_{ij} = \sum_{\alpha\beta} \frac{1}{2} \dot{\gamma}^{\alpha\beta} (\ell_i^{\alpha\beta} n_j^\alpha + \ell_j^{\alpha\beta} n_i^\alpha) \quad (2.6)$$

The stress vector σ_j on a plane α is given by

$$\sigma_j = \sum_i \sigma_{ij} n_i^\alpha \quad (2.7)$$

where σ_{ij} is the applied stress tensor in the principal material axes.

The local shear stress component in the β direction on the α plane is given by

$$\tau^{\alpha\beta} = \sum_j \sigma_j \ell_j^{\alpha\beta} \quad (2.8)$$

Combining the above two equations gives

$$\tau^{\alpha\beta} = \sum_{ij} \sigma_{ij} n_i^\alpha \ell_j^{\alpha\beta} \quad (2.9)$$

the transformation between the global applied and local stress components.

In summary, the constitutive model is based on separating the total global strain at a point in a body into elastic and inelastic components. The elastic strains are computed using Equation (1.1) and the applied stress tensor. Inelastic strains are obtained by integrating the inelastic strain rate with time. The inelastic strain

rate is calculated by summing the contributions from each of the crystallographic slip systems using Equation (2.6). The inelastic shear strain rate on each of the slip systems is computed from the inelastic constitutive equations which are developed in the remainder of this chapter. In addition, the inelastic shear strain rates on the active slip systems are a function of the local shear stresses which are computed from Equation (2.9).

2.4 Inelastic Constitutive Equations

There are at least two separate flow equations required to describe the tensile response of single crystals, i.e., cube slip and octahedral slip in the $[\bar{1} 0 1]$ direction. In addition dodecahedral slip and octahedral slip in the $[\bar{1} \bar{1} 2]$ direction have been reported in creep for some single crystal superalloys. Since no incubation period has been observed for Rene N4 in creep at any temperature, it appears that octahedral slip in the $[\bar{1} \bar{1} 2]$ directions may not be present. Creep deformation is attributed to the immediate operation of (111) $[\bar{1} 0 \bar{1}]$ or (001) $[\bar{1} 0 1]$ slip depending on orientation. Further, dodecahedral slip has not been observed for Rene N4 in a recent study of tensile and fatigue response, [6], [37]. Thus in this work it is assumed that only cube slip and octahedral slip in the $[\bar{1} 0 1]$ directions are active, and the model will be developed on this basis.

In addition, there appear to be at least two deformation mechanisms present. At the higher strain rates, such as in tensile tests, deformation occurs by dislocations cutting the γ' precipitate.

The deformation rate depends on the size and volume fraction of γ' . The orientation dependence of the CRSS at temperatures below the critical temperature depends on the core width effect and the cross slip mechanism. The creep strength of γ/γ' alloys appears to be controlled by the γ/γ' interfaces in the material. This explains the difference in creep behavior of γ' and γ/γ' alloys. The activation energy during creep is much higher than expected from a vacancy diffusion process. Tien, et al [70], proposed that during steady state creep the presence of γ' particles leads to a dislocation network that exhausts the vacancy concentration. Deformation occurs by the less favorable process of emitting and diffusing interstitials, which is consistent with the higher activation energies. This model has been supported by many observations as summarized in [7].

The modeling effort should include both the tensile and creep mechanisms. In addition, it appears there should be a strong interaction effect since the dislocation network and γ' particles are important in both cases. Unfortunately, there is very little or no evidence available for the development of a model to characterize these interaction effects. In the next two subsections a constitutive equation for cube and octahedral slip is proposed.

2.4.1 Octahedral Flow Equation

The octahedral slip system is active for both tensile and creep deformation, but the deformation mechanisms are different as discussed above. The model for octahedral slip is proposed as the sum of two components i.e.,

$$\dot{\gamma}_{\text{OCT}}^{\alpha\beta} = \left(\dot{\gamma}_{\text{OCT}}^{\alpha\beta} \right)_1 + \left(\dot{\gamma}_{\text{OCT}}^{\alpha\beta} \right)_2 \quad (2.10)$$

The first component is used to characterize dislocation cutting of the γ' particles and the second is motivated by the interstitial emission and diffusion mechanism. The two terms must be coupled to characterize the effect of the dislocation network on both mechanisms. Equation (2.10) is typical of classical models involving the use of both plastic and creep strain components. The origin of this approach is clearly based on the physical motivation of two or more deformation mechanisms. The thrust of the unified strain measure is to eliminate the need to identify the coupling between the two mechanisms. Unfortunately, many of the unified models are reasonable for modeling plasticity or creep but are not completely adequate for both. In the present study a coupling parameter is proposed in combination with the flow laws for $\dot{\gamma}_1^{\alpha\beta}$ and $\dot{\gamma}_2^{\alpha\beta}$ that appears to be an improvement.

The functional form of the octahedral flow equations for $\dot{\gamma}_{\text{OCT}}^{\alpha\beta}$ is similar to the exponential form developed by Bodner et. al. for isotropic materials. This form has been used with success for a number of materials including isotropic nickel base superalloys at high temperatures, [39], [40], [50]-[60]. The Bodner flow equation was taken from an expression for mobile dislocation velocity proposed by Gilman, [61], [62] and is expected to capture the essential features of the

response for Rene N4 at the higher strain rates below the critical temperature. The form of the equation used in this study is

$$\dot{\gamma}_{\text{OCT}_1}^{\alpha\beta} = D_1 \exp \left[- \left(\frac{Z_1^{\alpha\beta}}{|\tau^{\alpha\beta}|} \right)^{n_1} \right] \frac{\tau^{\alpha\beta}}{|\tau^{\alpha\beta}|} \quad (2.11)$$

where $Z_1^{\alpha\beta}$ is a state variable introduced to characterize the resistance to inelastic flow. The parameters D_1 and n_1 are used to characterize the limiting strain rate and the strain rate sensitivity. The octahedral flow equation and state variable $Z_1^{\alpha\beta}$ must also characterize the orientation and tension/compression asymmetry properties. Since the form of the flow equation is similar to the Lall, Chin and Pope model their results can easily be incorporated into Equation (2.11).

The functional form of the octahedral flow equation for $\dot{\gamma}_{\text{OCT}_2}^{\alpha\beta}$ is taken in a form similar to Equation (2.11), i.e.

$$\dot{\gamma}_{\text{OCT}_2}^{\alpha\beta} = D_2 \exp \left[- \left(\frac{Z_2^{\alpha\beta}}{|\tau^{\alpha\beta}|} \right)^{n_2} \right] \frac{\tau^{\alpha\beta}}{|\tau^{\alpha\beta}|} \quad (2.12)$$

This form is selected because it is consistent with representations used to characterize thermally driven diffusion processes as well as mobile dislocation velocities. Further, maintaining a similar structure allows for the same interpretation of the state variables $Z_1^{\alpha\beta}$ and $Z_2^{\alpha\beta}$, which should aid in establishing coupling between the two terms.

Combining Equations (2.10), (2.11) and (2.12) gives

$$\dot{\gamma}_{\text{OCT}}^{\alpha\beta} = \left\{ D_1 \exp \left[- \left(\frac{Z_1^{\alpha\beta}}{|\tau^{\alpha\beta}|} \right)^{n_1} \right] + D_2 \exp \left[- \left(\frac{Z_2^{\alpha\beta}}{|\tau^{\alpha\beta}|} \right)^{n_2} \right] \right\} \frac{\tau^{\alpha\beta}}{|\tau^{\alpha\beta}|} \quad (2.13)$$

The constants D_1 and D_2 are chosen to be 10^4 sec^{-1} and 1 sec^{-1} to allow uncoupling at high and low strain rates. The first term is negligible during creep and the second term is negligible during high rate tensile tests. Both terms are active at intermediate values of stress or strain rate. The constants n_1 and n_2 characterize the strain rate sensitivity and are determined independently. This is consistent with the observed response of single crystal alloys [7]. The state variables $Z_1^{\alpha\beta}$ and $Z_2^{\alpha\beta}$ include work hardening arising from the development of a dislocation microstructure and include core width and cross slip effects.

The flow resistance at high strain rates, $Z_1^{\alpha\beta}$, is assumed to be similar to the Lall, Chin and Pope result, Equation (2.2), and is given by

$$Z_1^{\alpha\beta} = Z^{\alpha\beta} + \phi_1 - V_{11} \tau_1^{\alpha\beta} + V_{12} \tau_2^{\alpha\beta} \quad (2.14)$$

where ϕ_1 is the initial value of $Z_1^{\alpha\beta}$, $Z^{\alpha\beta}(0) = 0$ and V_{11} and V_{12} are constants. The parameter $Z^{\alpha\beta}$ is a measure of work hardening and $\tau_1^{\alpha\beta}$ and $\tau_2^{\alpha\beta}$ are the shear stress components associated with the core width effect and the cross slip mechanism previously discussed. The shear stress $\tau_1^{\alpha\beta}$ is on the same octahedral plane and is perpendicular to $\tau^{\alpha\beta}$.

The sign convention used for $\tau^{\alpha\beta}$ and $\tau_1^{\alpha\beta}$ is given in Appendix B. The shear stress $\tau_2^{\alpha\beta}$ is the magnitude of the resolved shear stress on the cube plane in the same direction as $\tau^{\alpha\beta}$. The increase in flow resistance due to work hardening $Z^{\alpha\beta}$, is given by the evolution equation

$$\dot{Z}^{\alpha\beta} = M_1 (W_1 - Z^{\alpha\beta}) \tau^{\alpha\beta} \dot{\gamma}^{\alpha\beta} \quad (2.15)$$

where M_1 and W_1 are material constants. The functional form of the evolution equation involving inelastic work rate $\tau^{\alpha\beta} \dot{\gamma}^{\alpha\beta}$ rather than $\dot{\gamma}^{\alpha\beta}$ alone is very similar to the form used in the Bodner model for isotropic materials. A major difference is that there is no recovery term included in Equation (2.15). Also absent is an explicit function to model the effect of hardening due to intersecting slip systems. Even though some theoretical work has been done on latent hardening due to intersecting slip systems, [64]-[67], data to support the inclusion in the constitutive model currently do not exist for Rene N4.

The expression for the state variable $Z_2^{\alpha\beta}$ at low strain rates is similar in form to Equation (2.14) and is given by

$$Z_2^{\alpha\beta} = aZ^{\alpha\beta} + \phi_2 - \frac{v_{21} \tau_1^{\alpha\beta}}{\sqrt{3J_2}} + \frac{v_{22} \tau_2^{\alpha\beta}}{\sqrt{3J_2}} \quad (2.16)$$

where V_{21} and V_{22} are material parameters associated with the shear stress components, $\tau_1^{\alpha\beta}$ and $\tau_2^{\alpha\beta}$, and J_2 is the second invariant of the deviatoric stress tensor. Equations (2.14) and (2.16) are coupled since the same work hardening term $Z^{\alpha\beta}$ appears in both equations. The parameters a and ϕ_2 define the development of the dislocation structure (hardening) at the stress-strain rate levels associated with creep. Equation (2.16) is valid for primary and secondary creep only. A thermal recovery term may also be necessary at high temperature. Tertiary creep is neglected because it occurs at strain levels beyond the range of interest for this study.

It is possible to include a component of kinematic hardening into the model. Two values are assigned to each state variable, $Z_+^{\alpha\beta}$ and $Z_-^{\alpha\beta}$, corresponding to the direction of slip. Equation (2.15) is used to calculate $\dot{Z}_{SD}^{\alpha\beta}$ in the direction of slip. In the opposite direction the hardening rate, $\dot{Z}_{OD}^{\alpha\beta}$, is given by

$$\dot{Z}_{OD}^{\alpha\beta} = q \dot{Z}_{SD}^{\alpha\beta} \quad (2.17)$$

where q is a material parameter. Isotropic hardening occurs when $q = 1$ and kinematic hardening occurs when $q = -1$. This form is similar to the system used by Bodner et al [38] for tension/compression response of isotropic materials.

2.4.2 Cube Flow Equation

Cube slip occurs in specimens where the loading is near the [1 1 1] material direction and becomes increasingly important at high temperature. Furthermore, Schmid's law is a good approximation for cube slip.

The inelastic shear strain rate, $\dot{\gamma}_{\text{CUBE}}^{\alpha\beta}$, on an α cube plane in the β direction is formulated with two terms similar to Equation (2.10) for octahedral slip and is given by

$$\dot{\gamma}^{\alpha\beta} = \left\{ D_3 \exp \left[- \left(\frac{Z_3^{\alpha\beta}}{|\tau^{\alpha\beta}|} \right)^{n_3} \right] + D_4 \exp \left[- \left(\frac{Z_4^{\alpha\beta}}{|\tau^{\alpha\beta}|} \right)^{n_4} \right] \right\} \frac{\tau^{\alpha\beta}}{|\tau^{\alpha\beta}|}. \quad (2.18)$$

Once again the constants D_3 and D_4 are the limiting strain rates and are chosen to be 10^4 sec^{-1} and 1 sec^{-1} to allow separation of the two terms. The constants n_3 and n_4 reflect the strain rate sensitivity of the material in cube slip, and $Z_3^{\alpha\beta}$ and $Z_4^{\alpha\beta}$ are the state variables that include work hardening.

The evolution equations that account for the work hardening are similar to that for octahedral slip except that the orientation factors are excluded. These can be summarized as

$$Z_3^{\alpha\beta} = \phi_3 + Z^{\alpha\beta} \quad (2.19)$$

and

$$Z_4^{\alpha\beta} = \phi_4 + bZ^{\alpha\beta} \quad (2.20)$$

where the evolution of $Z^{\alpha\beta}$ is given by

$$\dot{z}^{\alpha\beta} = M_3 (W_3 - z^{\alpha\beta}) \tau^{\alpha\beta} \dot{\gamma}^{\alpha\beta} , \quad (2.21)$$

where $z^{\alpha\beta}(0) = 0$ and W_3 and M_3 are determined from the high rate data.

The parameters ϕ_4 and b relate the hardening in the high rate and low rate response for cube slip.

CHAPTER III

EXPERIMENTAL DATA AND MATERIAL CONSTANTS

Most of the experimental data available for Rene N4 are from tensile and creep tests with the specimens oriented in the [0 0 1] material direction. Unfortunately, this is not particularly useful when developing a constitutive model for a material that exhibits orientation dependence and tension/compression asymmetry. The two temperatures at which the best data base for Rene N4 is currently available are 760°C and 980°C. In this study the temperature is limited to 760°C because the orientation dependence and tension/compression asymmetry are more predominant and the repeatability of the data is better.

At 760°C the stress-strain response for several orientations in both tension and compression, and fatigue response was determined by Gabb, Gayda, Miner, and Voigt [6], [37]. Also available at 760°C are tensile stress-strain and creep data at three orientations for an earlier version of Rene N4, designated as VF317, Reference [68]. The slightly different chemistry for VF317 may be the source of differences in the observed response. The tensile response reported by Gabb, Gayda, Miner and Voigt for specimens oriented in the [0 0 1] was about 30 percent weaker than VF317 in tension. Since the response characteristics are significantly different for the two data sets it was not possible to develop a single set of material constants for the constitutive model.

The Gabb, Gayda, Miner and Voigt data were used to develop the constants and test the model for octahedral and cube slip at high strain.

rates in tension, compression and fatigue. The VF317 data were used to develop the constants for octahedral slip at high strain rates in tension and low stress levels in creep.

3.1 Rene N4 Composition A Response

The tensile data reported by Gabb, Gayda, Miner and Voigt, Reference [6], consist of seven tests at three orientations. The specimens had a cylindrical gage section 19 mm long by 4.7 mm in diameter. The tests were run at a constant crosshead rate with an initial strain rate of about $2 \times 10^{-4} \text{ sec}^{-1}$. Data recorded were load and crosshead displacement. Plastic strain was estimated using the offset from the elastic loading line and the specimen gage length. The resulting stress strain curves are shown in Figure 8.

It was confirmed by TEM analysis that slip in the $[0\ 0\ 1]$ and $[0\ 1\ 1]$ specimens was in the octahedral system while cube slip was observed with orientations near the $[\bar{1}\ 1\ 1]$ orientation. Tensile axis rotation was observed in the specimens tested to failure. The variability of the yield stress within a crystal was small; however, the variability between crystals was as large as 23%. This difference which is attributed to the orientation and tension/compression asymmetry is typical of other single crystals near this temperature. However, at 980°C the orientation and asymmetry properties are much less important and Schmid's law appears to be applicable, Reference [6]. Stresses beyond yield increased initially and flattened out for the $[0\ 0\ 1]$ and $[\bar{1}\ 1\ 2]$ specimens. The $[0\ 1\ 1]$ specimen exhibited decreasing loads

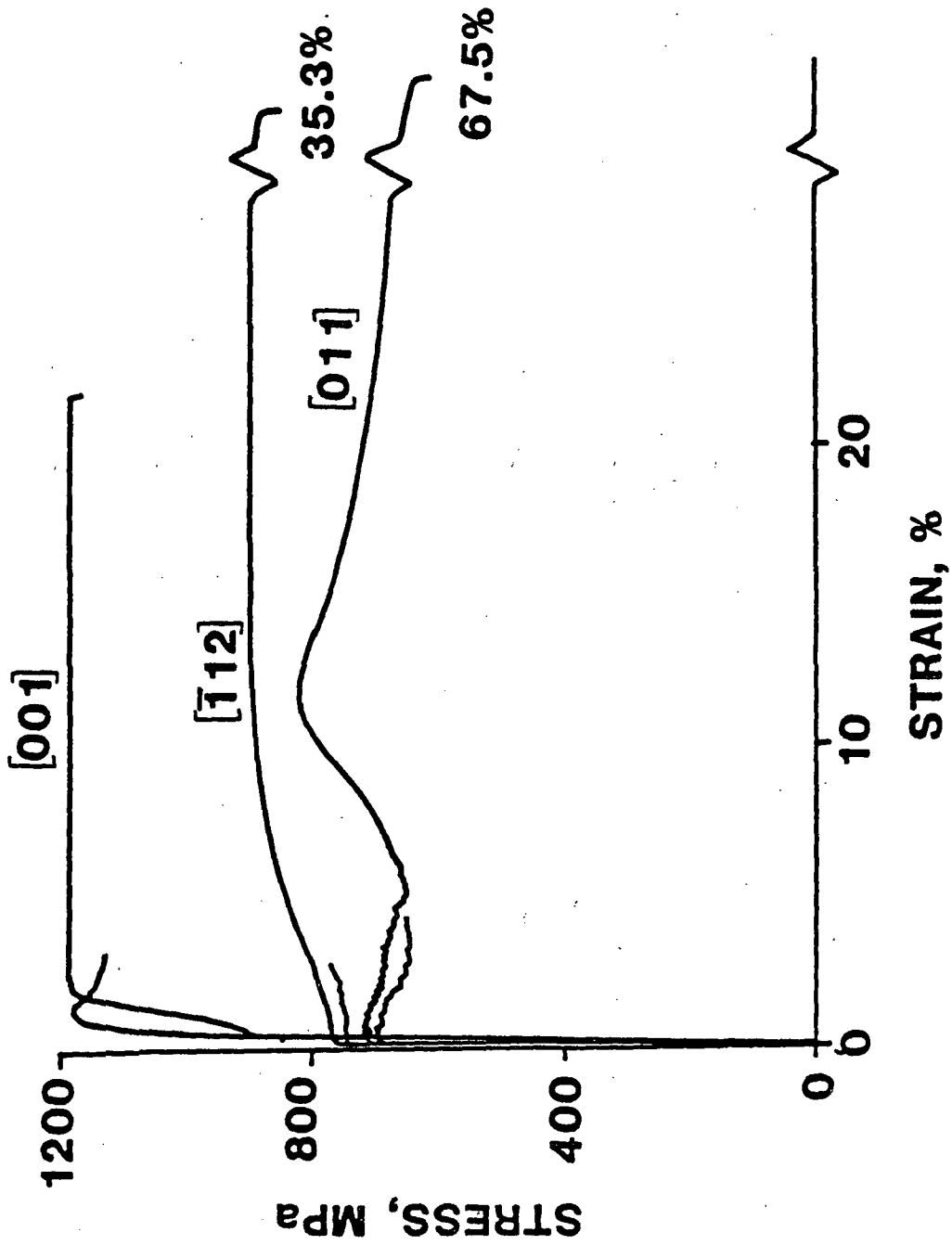


FIGURE 8. TENSILE RESPONSE OF RENE N4 AT 760°C. (REFERENCE 6)

sharp serrations to about 5% strain. The serrated yielding, which is observed in PWA 1480 and Mar M200, is attributed to the operation of a small number of slip planes, typically one, two or four.

The fatigue response at 760°C reported in Part II of Reference [37], consisted of the monotonic yield points for specimens at six orientations in tension and compression and first cycle hysteresis loops for three orientations. The specimens had a cylindrical gage section 15mm long by 5mm in diameter. The control waveform was sinusoidal with a frequency of .1 Hz.

The tensile and compressive yield stresses at several orientations are shown in Table 2. The [0 0 1] specimen had the greatest initial yield in tension and the [0 1 1] specimen was strongest in compression. Both specimens displayed significant tension/compression asymmetry while the $[\bar{1} 1 1]$, [0 2 3] and $[\bar{2} 3 6]$ specimens displayed very little or none.

The initial hysteresis loops for [0 0 1], [0 1 1] and $[\bar{1} 1 1]$ orientations are shown in Figure 9. The [0 1 1], $[\bar{1} 4 5]$, $[\bar{2} 3 6]$ and [0 2 3] specimens had serrated flow characteristics. All specimens displayed slight hardening with continued cycling which increased with increasing strain range but was generally less than 10%. For all tests the response stabilized well before half life.

TABLE 2.* Monotonic Yield Strength (0.02% offset) of Rene N4 at 760°C

Orientation	Elastic Modulus GPa	Tensile Y. S. MPa	Comp. Y. S. MPa
[001]	104	956	818
[011]	185	748	905
[$\bar{1}11$]	253	817	842
[023]	170	695	747
[$\bar{2}36$]	166	716	714
[$\bar{1}45$]	181	656	792

*Reference [37]

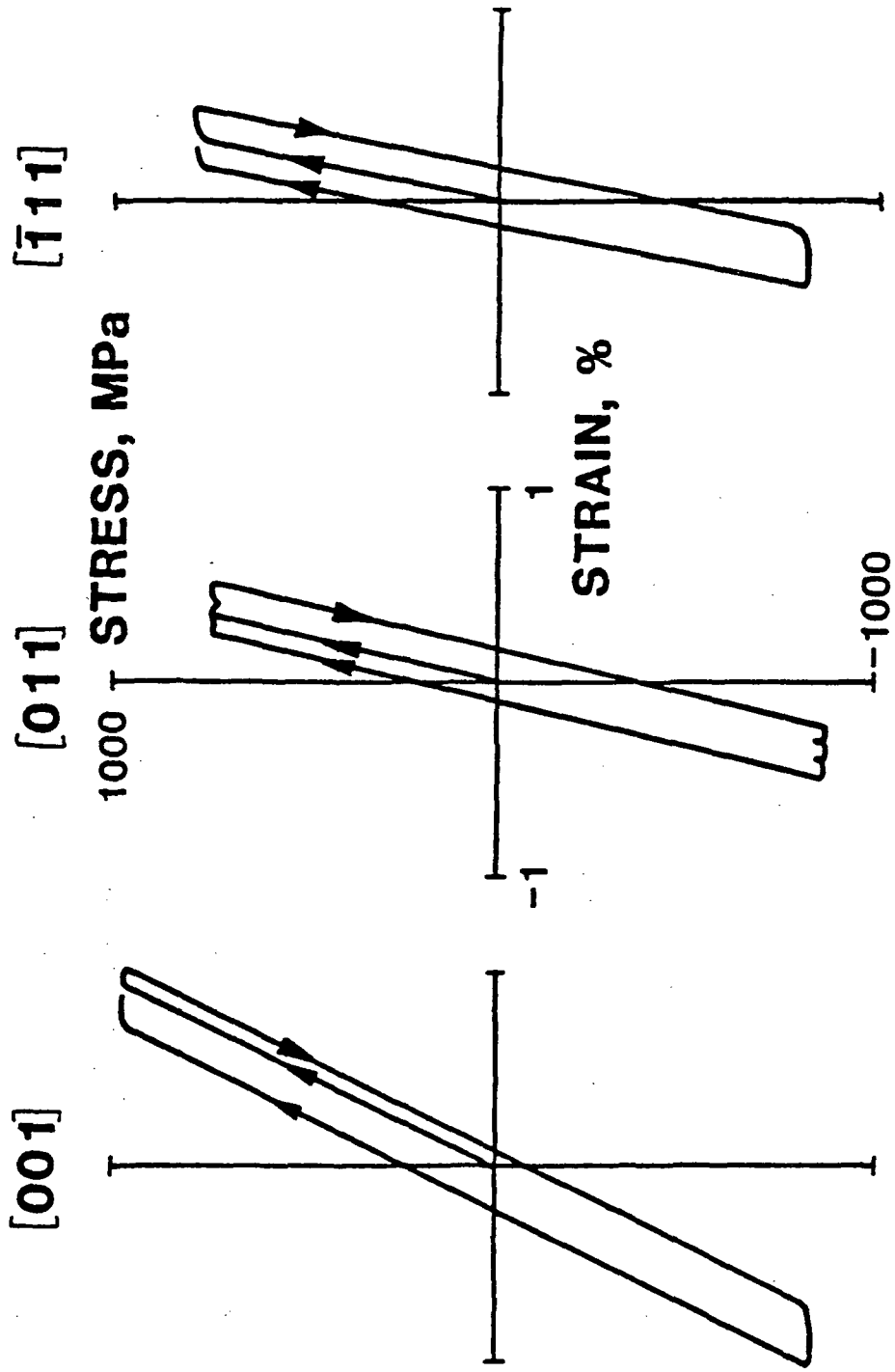


FIGURE 9. TYPICAL FIRST CYCLE HYSTERESIS LOOPS FOR RENE N4 AT 760°C.
(REFERENCE 37)

3.2 Rene N4 VF317 Response

The tensile data for Rene N4 VF317 at 760°C consist of three specimens at three orientations. The specimens had a Codep coated cylindrical gage section 18mm long by 3.3mm in diameter. The tensile tests were run at a constant strain rate of $8.333 \times 10^{-5} \text{ sec}^{-1}$ to inelastic strains of .2%. At .2% yield the extensometers were removed and the specimens were pulled to failure at a constant head rate of .02117 mm/sec.

The response to approximately 1% strain, as shown in Figure 10, displays considerable orientation dependence. The stress increased about 30% between the .02% yield stress and ultimate stress for all specimens. Although no TEM work was done to determine active slip systems it is reasonable to assume that cube slip is not active for these orientations.

Tensile creep rupture tests were performed on Rene N4 VF317 at 760° for the same three orientations. The 3.175 mm diameter specimens were Codep coated. A total of seven creep tests at three orientations were conducted and the results are shown in Figure 11. Two of the test at 620 MPa were terminated prior to failure. The reduction in area ranged from 17% to 48%.

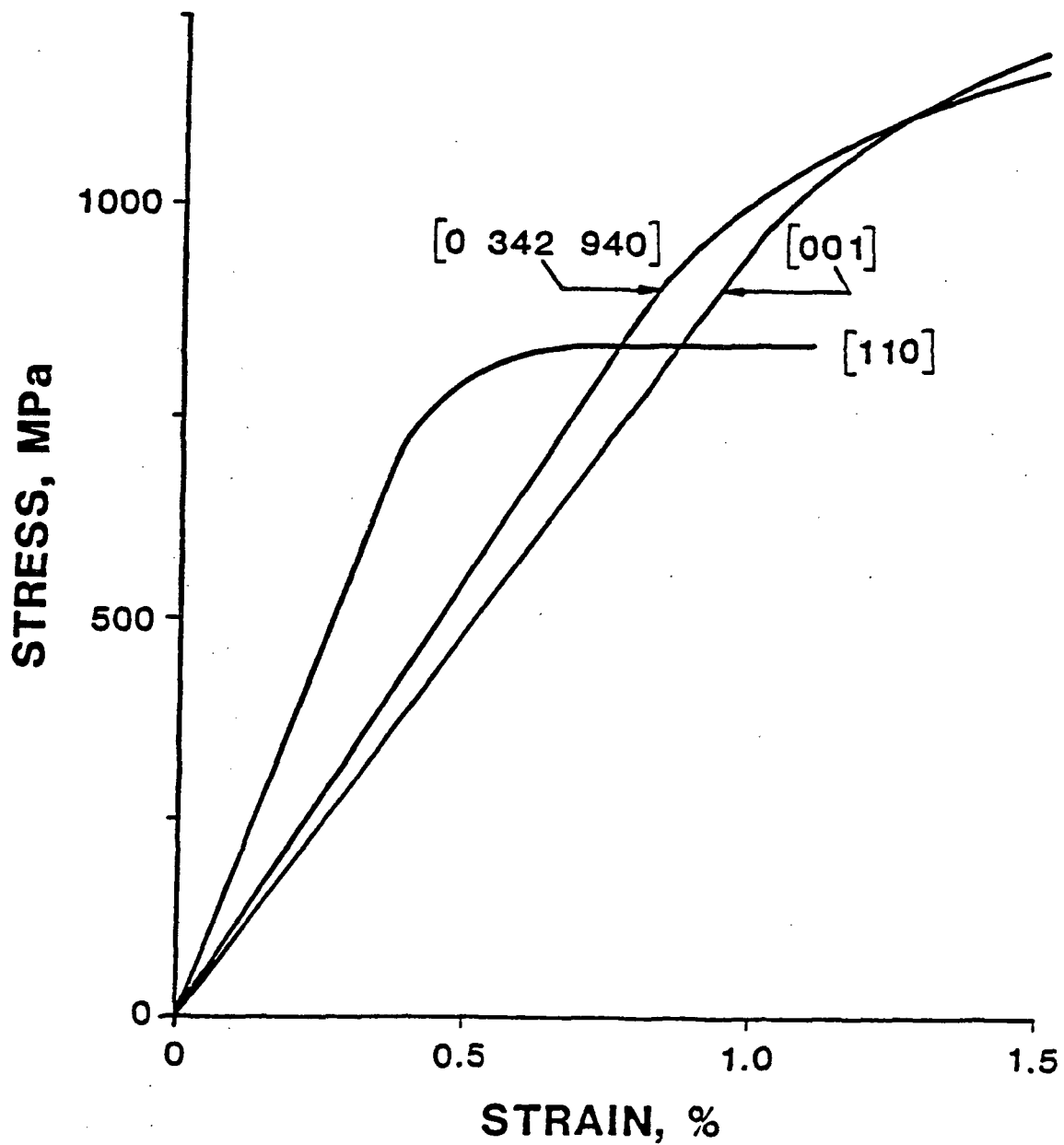


FIGURE 10. TENSILE RESPONSE OF RENE N4 VF 317 AT 760°C.

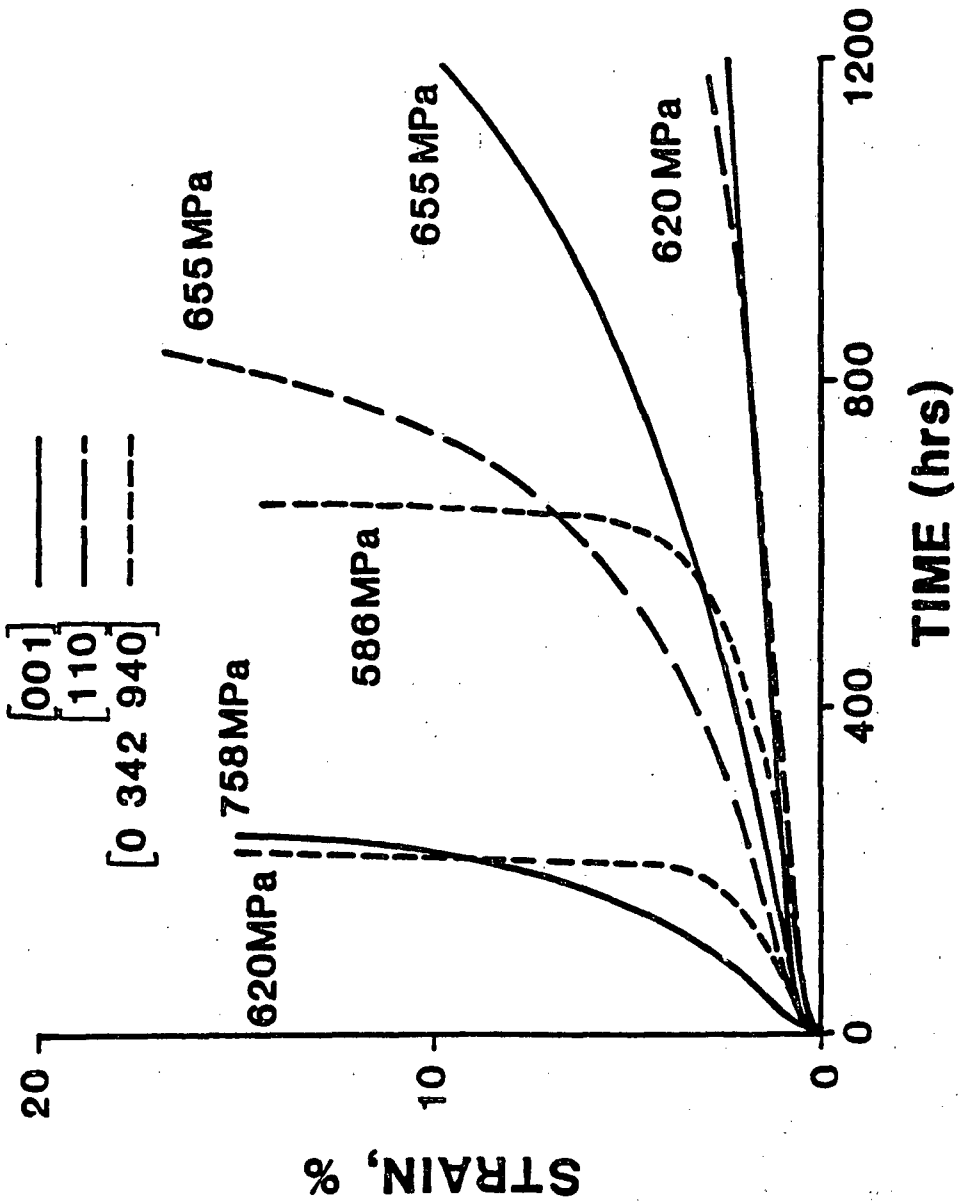


FIGURE 11. CREEP RESPONSE OF RENE N4 VF 317 AT 760°C.

Note that the specimens in the $[0\ 342\ 940]$ orientation were stronger in the tensile tests and in creep than expected when compared to the other data set or to PWA 1480 (Figure 3). The specimens at this orientation were nearly as strong as the specimens in the $[0\ 0\ 1]$ orientation. The reason for this anomaly is not known.

3.3 Derivation of the Material Constants

The octahedral slip constants are derived from tests where cube slip is not present, for example, the $[0\ 0\ 1]$ and $[0\ 1\ 1]$ orientations. Conversely, the cube slip constants are derived from tests where octahedral slip is not present i.e., $[1\ 1\ 1]$ orientation. In addition, the first term in the octahedral or cube flow equation is negligible in creep and the second term is negligible at high strain rates. When a choice of orientations is available for developing constants the data from the $[0\ 0\ 1]$ orientation is used since it is the primary loading direction in turbine blade applications.

Since the constitutive model is developed on the individual slip systems it is essential to know the relationship between the applied stress tensor and local shear stresses and the relationship between local slip rates and the global strain rate tensor. To simplify this task the kinematic equations in Appendix B were implemented in a computer code. For example, the shear stress components from an applied stress of 100 MPa in each of four directions is shown in Table 3. The local stress in every slip direction on each of the octahedral and cube planes is shown. The notation is described in Appendix B. The stresses in the (111) $[\bar{1}\ 2\ \bar{1}]$ system are used only for determining τ_1 in the

TABLE 3. LOCAL STRESS FOR AN APPLIED STRESS OF 100 MPa IN THE
[001], [011], [111] AND [0 342 940] DIRECTIONS

SLIP SYSTEM	PLANE	DIRECTION	[001] SHEAR STRESS	[011] SHEAR STRESS	[111] SHEAR STRESS	[0 342 940] SHEAR STRESS
(111) $\bar{1}01$	1	1	-40.825	-40.825	0.	-49.169
	1	2	40.825	0.	0.	31.280
	1	3	0.	-40.825	0.	-17.889
	2	1	40.825	0.	0.	22.936
	2	2	0.	0.	-27.217	-8.345
	2	3	-40.825	0.	-27.217	-31.280
	3	1	0.	-40.825	-27.217	-17.889
	3	2	-40.825	0.	0.	-31.280
	3	3	-40.825	-40.825	-27.217	-49.169
	4	1	40.825	0.	-27.217	31.280
	4	2	40.825	0.	-27.217	22.936
	4	3	0.	0.	0.	-8.345
(111) 112	1	1	-23.570	23.570	0.	-7.731
	1	2	-23.570	-47.140	0.	-38.716
	1	3	47.140	23.570	0.	46.448
	2	1	-23.570	0.	-31.427	-22.877
	2	2	47.140	0.	15.713	31.301
	2	3	-23.570	0.	15.713	-8.424
	3	1	47.140	23.570	15.713	46.448
	3	2	-23.570	-47.140	-31.427	-38.716
	3	3	-23.570	23.570	15.713	-7.731
	4	1	-23.570	0.	15.713	-8.424
	4	2	-23.570	0.	15.713	-22.877
	4	3	47.140	0.	-31.427	31.301
(100) 101	1	1	0.	0.	47.140	0.
	1	2	0.	0.	0.	0.
	2	1	0.	35.355	47.140	22.719
	2	2	0.	-35.355	0.	-22.719
	3	1	0.	35.355	47.140	22.719
	3	2	0.	35.355	0.	22.719

model, τ_2 is determined from the $(001)[\bar{1} 0 1]$ slip system and τ is determined for either the $(111)[1 \bar{0} 1]$ or $(001)[\bar{1} 0 1]$ slip system depending on the active system.

For the purpose of developing material constants it is also important to choose test orientations where the local stress and strain rate on each of the slip planes can be determined. For example, a load in the $[0 0 1]$ direction will produce equal stresses on eight of the $(111)[\bar{1} 0 1]$ slip systems and no stress on the other $(111)[\bar{1} 0 1]$ systems or the cube systems. It is expected that slip on all eight systems will be the same. By comparison, a load on a $[0 342 940]$ specimen will have shear stresses in all of the $(111)[\bar{1} 0 1]$ slip directions. Further, it is expected that these shear stress will produce slip on more than one system and the slip rates are not expected to be equal. Thus, the tests in the $[0 0 1]$, $[0 1 1]$ and $[1 1 1]$ are preferred to evaluating constants due to the uniformity of stress and strain rate in the octahedral and cube systems. Table 3 also shows why only octahedral slip is found near the $[0 0 1]$ orientation (no stress on the cube planes) and only cube slip is found near the $[1 1 1]$ direction (dominant stress on the cube planes).

3.3.1 Flow Equation Constants

The octahedral and cube slip systems are assumed to have limiting strain rates, D_1 and D_3 , of 10^4 sec^{-1} in high strain rate tests and the limiting strain rate in creep, D_2 , is chosen to be 1 sec^{-1} . Neither

data set contains creep tests near the [111] orientation that would activate cube slip. As a result, it is not possible to evaluate any of the constants associated with cube slip in creep and D_4 is set to zero for all of the numerical exercises. The value 10^4 sec^{-1} has been accepted as a constant for many materials except under extreme loading rates. The value $D_2 = 1 \text{ sec}^{-1}$ was chosen since creep rates are about 10^{-4} less than tensile rates.

The constants n_1 , n_2 , and n_3 are all evaluated using essentially the same method. To compute n_1 two or more tensile tests at different strain rates with the specimens in the [001] orientation are necessary. Two or more creep tests with specimens in the [001] orientation and at different stress levels are required to determine n_2 . The evaluation of n_3 can be accomplished with two or more tensile tests at different strain rates with specimens oriented in the [111] direction. The tensile tests are loaded under constant strain rate conditions to failure and the saturated values of stress are determined. The secondary creep rates are used from the creep tests.

At high strain rates where the contribution of the creep rate term is negligible, Equation (2.11) may be rewritten as

$$\ln \left[\ln \left(\frac{\dot{\gamma}_{\text{OCT}}^{\alpha\beta}}{D_1} \right) \right] = n_1 \ln Z_1^{\alpha\beta} - n_1 \ln \tau^{\alpha\beta} \quad (3.1)$$

where $Z_1^{\alpha\beta}$ is the fully saturated value at that strain rate. The [001] orientation has eight equally active octahedral systems and $\dot{\gamma}_{OCT}^{\alpha\beta}$ and $\tau^{\alpha\beta}$ are easily calculated from the applied stress and the measured inelastic strain rate. When $\ln \left[\ln \left(\frac{\dot{\gamma}_{OCT}^{\alpha\beta}}{D_1} \right) \right]$ is plotted against $\ln \tau^{\alpha\beta}$ the slope of the line will be $-n_1$. Once n_1 is known the saturated value of $Z_1^{\alpha\beta}$ can be calculated from Equation (3.1) or the ordinate of the line.

The constants n_2 and $Z_2^{\alpha\beta}$ are calculated in a similar manner from the secondary creep rates while neglecting the contribution from the high strain rate term. The values for n_3 and n_4 and the saturated values $Z_3^{\alpha\beta}$ and $Z_4^{\alpha\beta}$ are obtained from tensile and creep tests using [111] oriented specimens. The parameters n_1 , n_2 , n_3 and n_4 are independent of orientation and are also assumed constant for constant temperature. The values $Z_1^{\alpha\beta}$, and $Z_2^{\alpha\beta}$ depend on orientation.

Since the required tensile tests were not available for either of the current data sets, the value for n_1 was estimated from an analysis of PWA-1480 data at 1600°F and 1800°F. The value for n_3 was assumed to be the same. Data were available for the calculation of n_2 for the Rene N4 VF317 chemistry. Obviously the strain rate sensitivity

predicted by the current set of material constants is at best an estimate.

3.3.2 Evaluation of Orientation Factors

The orientation dependence and tension/compression asymmetry of the material in octahedral slip is characterized by the constants V_{11} and V_{12} at tensile strain rates and V_{21} and V_{22} in creep. The constants can be evaluated from any three tensile tests at constant strain rate (or any three creep tests) as long as the orientations and/or tension/compression sense is different and cube slip is not involved. Best results, however, are obtained if the orientations are not close together and both tensile and compressive data are used. Tests close together tend to magnify the experimental variability. In addition, it is very helpful if the active slip systems are equally stressed as explained earlier. An optimum set of tests is probably [001] in tension and compression and [011] in either tension or compression. This choice of orientation is well away from the cube slip regime, there is a large variation in τ_1 and τ_2 , and the model is calibrated for the orientation of greatest interest.

For the high strain rate tests where the contribution of the creep rate term is negligible the saturated value for $Z_1^{\alpha\beta}$ for the three tests can be calculated. Rearranging Equation (2.11) gives

$$Z_1^{\alpha\beta} = \left[-\ln \left(\frac{\dot{\gamma}_{OCT}^{\alpha\beta}}{D_1} \right) \right]^{\frac{1}{n_1}} |\tau^{\alpha\beta}| \quad , \quad (3.2)$$

where $\dot{\gamma}_{\text{OCT}}^{\alpha\beta}$ and $\tau^{\alpha\beta}$ are the values when the inelastic strain rate and stress become constant. Letting

$$S_1 = Z^{\alpha\beta} + \phi_1 = \text{constant} \quad , \quad (3.3)$$

Equation (2.14) can be written for each of the three tests, i.e.

$$\begin{aligned} \left(Z_1^{\alpha\beta} \right)_1 &= S_1 - V_{11} \left(\tau_1^{\alpha\beta} \right)_1 + V_{12} \left(\tau_2^{\alpha\beta} \right)_1 \quad , \\ \left(Z_1^{\alpha\beta} \right)_2 &= S_1 - V_{11} \left(\tau_1^{\alpha\beta} \right)_2 + V_{12} \left(\tau_2^{\alpha\beta} \right)_2 \quad , \\ \left(Z_1^{\alpha\beta} \right)_3 &= S_1 - V_{11} \left(\tau_1^{\alpha\beta} \right)_3 + V_{12} \left(\tau_2^{\alpha\beta} \right)_3 \quad . \end{aligned} \quad (3.4)$$

Since $\tau_1^{\alpha\beta}$ and $\tau_2^{\alpha\beta}$ are known from Table 3 or equivalent and $Z_1^{\alpha\beta}$ can be computed from Equation (3.2) for each test, the constants S_1 , V_{11} , and V_{12} can be determined.

The calculation of the orientation factors V_{21} and V_{22} for the creep regime is similar. Neglecting the contribution of the high strain rate term, Equation (2.12) can be rearranged to give

$$Z_2^{\alpha\beta} = \left[- \ln \left(\frac{\dot{\gamma}_{\text{OCT}}^{\alpha\beta}}{D_2} \right)^{\frac{1}{n_2}} \right]_{\tau^{\alpha\beta}} \quad , \quad (3.5)$$

where $\dot{\gamma}_{\text{OCT}}$ is the value during secondary creep. Once again letting

$$S_2 = aZ^{\alpha\beta} + \phi_2 \quad . \quad (3.6)$$

Equation (2.16) can be written for each of the three tests, i.e.

$$\begin{aligned} (z_2^{\alpha\beta})_1 &= S_2 - v_{21} \left(\frac{\tau_1^{\alpha\beta}}{\sqrt{3J_2}} \right)_1 + v_{22} \left(\frac{\tau_2^{\alpha\beta}}{\sqrt{3J_2}} \right)_1, \\ (z_2^{\alpha\beta})_2 &= S_2 - v_{21} \left(\frac{\tau_1^{\alpha\beta}}{\sqrt{3J_2}} \right)_2 + v_{22} \left(\frac{\tau_2^{\alpha\beta}}{\sqrt{3J_2}} \right)_2 \quad \text{and} \quad (3.7) \\ (z_2^{\alpha\beta})_3 &= S_2 - v_{21} \left(\frac{\tau_1^{\alpha\beta}}{\sqrt{3J_2}} \right)_3 + v_{22} \left(\frac{\tau_2^{\alpha\beta}}{\sqrt{3J_2}} \right)_3. \end{aligned}$$

Since $\tau_1^{\alpha\beta}$, $\tau_2^{\alpha\beta}$ and J_2 are known and $z_2^{\alpha\beta}$ can be computed from Equation (3.5) for each test, the constants S_2 , v_{21} , and v_{22} can be calculated.

For the Rene N4 VF317 data set, the tensile stress strain curves for the three orientations were used to obtain the constants S_1 , v_{11} , and v_{12} . These tests were not optimal for this calculation since the strain rate was changed before the stress level was saturated and none of the tests were in compression. The constants S_2 , v_{21} , and v_{22} were calculated for the secondary creep rates for three specimens in different orientations. These tests also were not optimal since none were in compression.

The Rene N4 data of Gabb, Gayda, Miner and Voigt contains only two stress-strain curves at a constant rate that activated octahedral slip. Recall that the test in the $[\bar{1}12]$ orientation activated cube slip. This is not sufficient to establish the orientation factors. Alternatively, the data set contains yield stresses for the initial quarter cycle of the fatigue loops for specimens in several orientations. Since the

control wave form is sinusoidal, the total strain range varies from test to test and the strain rate varies during the loading quarter cycle, it is not possible to determine the orientation factors as described above.

Thus, to test the orientation and tension/compression aspects of the constitutive model, some assumptions were made. It was assumed that the yield stress variation in the sinusoidal first quarter cycle is representative of the saturated stress in constant strain rate tensile tests. Furthermore, a strain rate of 2×10^{-4} was assumed. The constants were calculated from [011] tension and [001] tension and compression yield stresses from the first cycle. It is obvious that this procedure will not generate the actual constants, but it does provide a means for exercising the constitutive model with the data that are available.

3.3.3 Evaluation of the Hardening Parameters

The evaluation of the constants in the state variable evolution Equations, (2.15) and (2.21), for both the octahedral and cube slip systems proceeds in a similar way. The evaluation of M_1 , W_1 and ϕ_1 for octahedral slip and M_3 , W_3 and ϕ_3 for cube slip is based using the high strain rate tensile data.

For the octahedral system, Equation (2.15) can be integrated to give

$$Z^{\alpha\beta} = W_1 [1 - \exp(-M_1 \tau^{\alpha\beta} \dot{\gamma}^{\alpha\beta})] \quad (3.8)$$

Combining Equations (2.14), (3.3) and (3.8) yields

$$\ln(W_1) - M_1 \tau^{\alpha\beta} \dot{\gamma}^{\alpha\beta} = \ln [S_1 - V_{11} \tau_1^{\alpha\beta} + V_{12} \tau_2^{\alpha\beta} - Z_1^{\alpha\beta}] \quad (3.9)$$

The quantity $\ln [S_1 - V_{11} \tau_1^{\alpha\beta} + V_{12} \tau_2^{\alpha\beta} - Z_1^{\alpha\beta}]$ is log linear in the local rate of inelastic working, $\tau^{\alpha\beta} \dot{\gamma}^{\alpha\beta}$. The parameter $Z_1^{\alpha\beta}$ can be evaluated using Equation (3.2) and stress-strain test data since $\tau^{\alpha\beta}$, $\dot{\gamma}^{\alpha\beta}$, D_1 and n_1 are all known. By plotting Equation (3.9) for the [001] tensile data, Figure 12, the constants W_1 and M_1 are obtained. Notice that at $\tau^{\alpha\beta} \dot{\gamma}^{\alpha\beta} = 0$, $\ln(W_1) = \ln[S_1 - V_{11} \tau_1^{\alpha\beta} + V_{12} \tau_2^{\alpha\beta} - Z_1^{\alpha\beta}]$. Once W_1 is obtained, ϕ_1 can be calculated from Equation (3.3).

In cube slip the calculation of M_3 , W_3 and ϕ_3 is identical to the procedure for octahedral slip. Since the creep strain rate is negligible at high strain rates the cube flow Equation (2.18), becomes

$$\dot{\gamma}^{\alpha\beta} = D_3 \exp \left[- \left(\frac{Z_3^{\alpha\beta}}{|\tau^{\alpha\beta}|} \right)^{n_3} \right] \quad (3.10)$$

for a high strain rate test with the specimen loaded in the [111] orientation. Rearranging Equation (3.10) gives

$$Z_3^{\alpha\beta} = \left[- \ln \left(\frac{\dot{\gamma}^{\alpha\beta}}{D_3} \right) \right]^{\frac{1}{n_3}} |\tau^{\alpha\beta}| \quad (3.11)$$

and at saturation

$$Z_3^{\alpha\beta} = \phi_3 + W_3 = \text{constant} \quad (3.12)$$

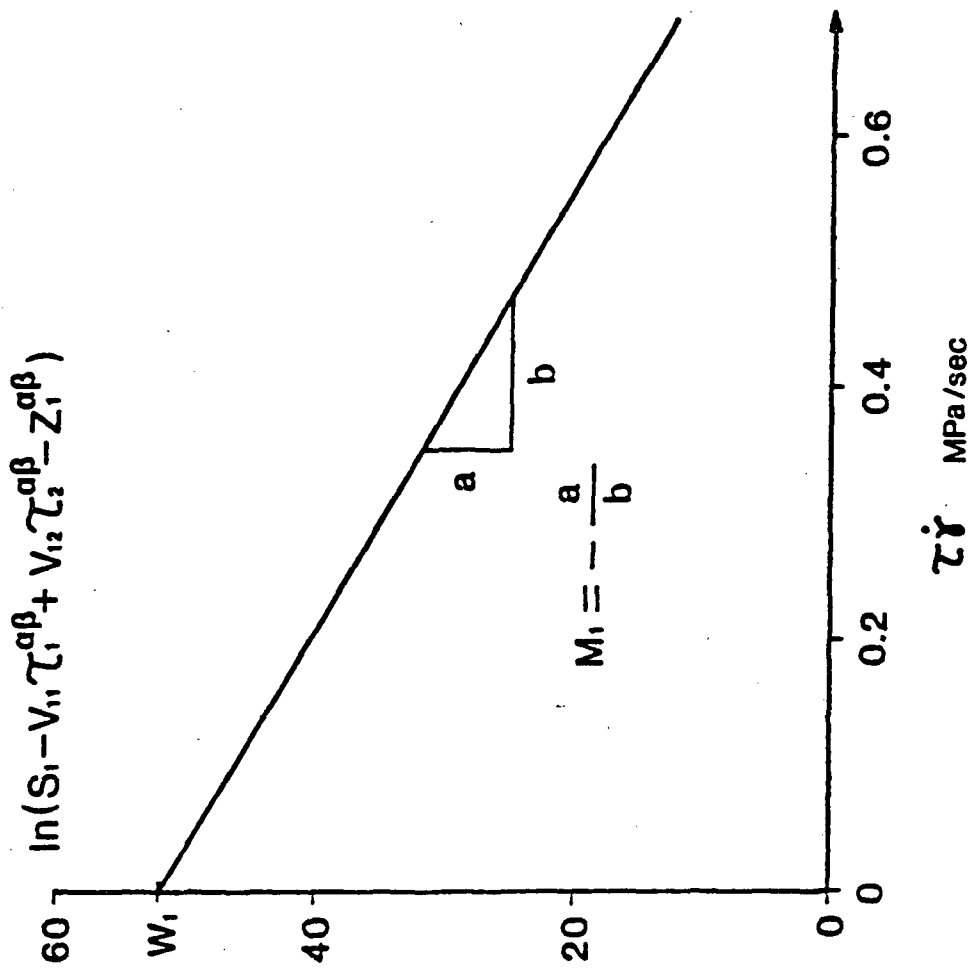


FIGURE 12. EVALUATION OF HARDENING PARAMETERS M_1 AND W_1 FOR RENE N4 VF 317 AT 760°C

Integrating the evolution Equation (2.21) results in

$$Z^{\alpha\beta} = W_3 [1 - \exp(-M_3 \tau^{\alpha\beta} \dot{\gamma}^{\alpha\beta})] \quad (3.13)$$

Using Equations (2.19) and (3.13) gives

$$\ln(W_3) - M_3 \tau^{\alpha\beta} \dot{\gamma}^{\alpha\beta} = \ln[Z_3^{\alpha\beta} - \phi_3] \quad (3.14)$$

The parameter $Z_3^{\alpha\beta}$ can be evaluated using Equation (3.11) and the stress strain test data since $\tau^{\alpha\beta}$, $\dot{\gamma}^{\alpha\beta}$, D_3 and n_3 are all known. A plot similar to Figure 12 is used to find W_3 and M_3 . Using the saturated value of $Z_3^{\alpha\beta}$, Equation (3.12) is used to find ϕ_3 .

Unfortunately, a constant strain rate tensile test with loading in the [111] direction was not available and M_3 and W_3 were assumed to be the same as for octahedral slip for the numerical exercises.

3.3.4 Tensile/Creep Coupling Terms

The tensile/creep coupling constants, a and ϕ_2 for octahedral slip and b and ϕ_4 for cube slip can be calculated from the tensile constants and creep response. The constants a and ϕ_2 are calculated for an orientation where octahedral slip is dominant, such as [001]. The calculation of b and ϕ_4 requires data for an orientation where cube slip is dominant, such as [111].

The value of $Z_2^{\alpha\beta}$ can be obtained from Equation (3.5) for the primary and secondary creep rates. At the beginning of the creep test

prior to any hardening, the hardening parameter $Z^{\alpha\beta}$ will be zero and Equation (2.16) reduces to

$$Z_2^{\alpha\beta} = \phi_2 - \frac{V_{21}\tau_1^{\alpha\beta}}{\sqrt{3J_2}} + \frac{V_{22}\tau_2^{\alpha\beta}}{\sqrt{3J_2}}, \quad (3.15)$$

so ϕ_2 can be calculated. During secondary creep $Z^{\alpha\beta}$ is saturated and equal to W_1 , Equation (2.16) becomes

$$Z_2^{\alpha\beta} = aW_1 + \phi_2 - \frac{V_{21}\tau_1^{\alpha\beta}}{\sqrt{3J_2}} + \frac{V_{22}\tau_2^{\alpha\beta}}{\sqrt{3J_2}}, \quad (3.16)$$

and a may be calculated.

The constants for cube slip in creep may be similarly calculated using the initial creep strain rate and the secondary creep strain rate. The data were not available in the current data base for the calculation of b and ϕ_4 .

A summary of all the constants for both data sets is presented in Table 4. There are a total of 22 constants in addition to the 3 elastic constants. However, D_1 , D_2 , D_3 and D_4 are assumed known, thus there are effectively 18 constants required to model the inelastic response.

TABLE 4 - MATERIAL CONSTANTS

CONSTANT	VF317	GABB, GAYDA, MINER VOIGT DATA
D_1	10000 SEC ⁻¹	10000 SEC ⁻¹
n_1	2.02	2.02
D_2	1 SEC ⁻¹	----
n_2	.708	----
ϕ_1	959.1 MPa	1109 MPa
V_{11}	3.7454	.5752
V_{12}	3.5799	-.5799
M_1	5.656 MPa ⁻¹	8.194 MPa ⁻¹
W_1	177.9 Mpa	437.5 MPa
a	52.52	----
ϕ_2	5626 MPa	----
V_2	20070 MPa	----
V_{22}	18690 MPa	----
D_3	----	10000 sec ⁻¹
n_3	----	2.02
D_4	----	----
n_4	----	----
ϕ_3	----	1198 MPa
M_3	----	8.194 MPa ⁻¹
W_3	----	437.5 MPa
b	----	----
ϕ_4	----	----

The elastic constants at 760°C are $E = 100.0$ GPa, $G = 96.5$ GPa and $\nu = .38$.

CHAPTER IV

FINITE ELEMENT IMPLEMENTATION

The finite element implementation of the constitutive model was done using a twenty noded isoparametric solid element. This element was chosen because it is possible to model almost any three dimensional geometry and also allows for any orientation of the material principal axes. Order two Gaussian integration was used both for stiffness generation and the calculation of body forces.

The ability to model piecewise linear load histories was also included in the finite element code. This capability is particularly useful when modeling stress strain tests or fatigue loops and also for certain analysis applications. Since the inelastic strain rate could be expected to change dramatically during a linear load history it is important to include a dynamic time incrementing procedure. The current study is restricted to isothermal conditions, consequently the finite element code is limited to steady state thermal conditions during a load case. The term "load case" is used to denote a time period for which the initial and final loads and boundary conditions are defined and vary linearly between the end points.

4.1 Initial Strain Method

The initial strain method is an efficient technique for incorporating time dependent constitutive models in nonlinear finite element codes [71], [72]. It is an economical technique because it is necessary to reform the stiffness matrix only for temperature changes.

The derivation of the nodal equilibrium equations follows directly from the principle of virtual work as described below. Element strains $\{\epsilon^T\}$, in terms of nodal displacement $\{x\}$ are given by

$$\{\epsilon^T\} = [B]\{x\} \quad , \quad (4.1)$$

where $[B]$ is the element strain displacement matrix. Since the total strains are the sum of the elastic strains $\{\epsilon^E\}$ and the inelastic strains $\{\epsilon^I\}$ it follows that

$$\{\epsilon^T\} = \{\epsilon^E\} + \{\epsilon^I\} \quad . \quad (4.2)$$

The stresses are related to the elastic strains by

$$\{\sigma\} = [E]\{\epsilon^E\} \quad , \quad (4.3)$$

where $[E]$ is the matrix of elastic constants. Defining $\{f\}$ as the element nodal forces and $\{\hat{x}\}$ as the associated virtual displacements and applying the method of virtual work yields

$$\{\hat{x}\}^T \{f\} = \int_V \{\hat{\epsilon}\}^T \{\sigma\} dV \quad , \quad (4.4)$$

where $\{\hat{\epsilon}\}$ are the strains associated with the displacements $\{\hat{x}\}$. The integration is over the volume of the element. Substituting Equations (4.1), (4.2) and (4.3) into (4.4) gives

$$\{\hat{x}\}^T \{f\} = \int_V ([B]\{\hat{x}\})^T [E] (\{\epsilon\} - \{\epsilon^I\}) dV \quad . \quad (4.5)$$

Since $\{\hat{x}\}$ is arbitrary and independent of the integration (4.5) becomes

$$\{f\} + \{f^I\} = [k]\{x\} \quad , \quad (4.6)$$

where the inelastic pseudo force $\{f^I\}$ is defined as

$$\{f^I\} = \int_V [B]^T [E] \{\epsilon^I\} dV \quad , \quad (4.7)$$

and the elastic stiffness matrix $[k]$ is defined by

$$[k] = \int_V [B]^T [E] [B] dV \quad . \quad (4.8)$$

When the elemental equations are assembled the global equilibrium equation

$$[K]\{d^T\} = \{F\} + \{F^I\} \quad (4.9)$$

is obtained. The matrix $[K]$ is the global stiffness matrix, $\{d^T\}$ is the total displacement vector, $\{F\}$ is the vector of applied thermomechanical forces, and $\{F^I\}$ is the vector of inelastic pseudo forces.

The calculation of the inelastic strain rates and the state variable evolution rate is accomplished in the constitutive subroutines. The integration over the element volume is generally performed numerically and in this study order two Gaussian quadrature was used. The total inelastic force vector is then assembled by summing the contributions from all of the elements.

4.2 Linear Load History

In order to incorporate linear load histories into this scheme the total displacement vector is decomposed into elastic and inelastic components i.e., let

$$\{d^T\} = \{d^E\} + \{d^I\} \quad . \quad (4.10)$$

The vector $\{d^E\}$ is the displacement due to applied thermomechanical forces and $\{d^I\}$ is the displacement due to the inelastic pseudo-forces.

These displacement vectors can be calculated using

$$\{d^E\} = [K]^{-1}\{F\} \quad , \quad (4.11)$$

and

$$\{d^I\} = [K]^{-1}\{F^I\} \quad . \quad (4.12)$$

The elastic displacements are obtained for the initial and final thermomechanical loads in the load case. Assuming a linear variation the elastic displacements at any time in the load case are given by

$$\{d^E\} = \{d^E\}_0 + \left(\frac{t-t_0}{t_f-t_0}\right)(\{d^E\}_f - \{d^E\}_0) \quad . \quad (4.13)$$

The vectors $\{d^E\}_0$ and $\{d^E\}_f$ are the elastic displacements due to the initial and final applied thermomechanical forces. The current time in the load case is t , and t_0 and t_f are the initial and final times in the load case. The displacements due to the inelastic strains at any time during the load case are given by

$$\{d^I\} = \{d^I\}_0 + \sum_{\substack{\text{TIME} \\ \text{INCREMENTS}}} \{\Delta d^I\} \quad . \quad (4.14)$$

The vector $\{d^I\}_0$ is the vector of displacements due to inelastic strains at the beginning of the load case, and $\{\Delta d^I\}$ is a displacement increment due to the inelastic strains during a time step. The increment in displacements $\{\Delta d^I\}$ due to the change in inelastic strains $\{\Delta \epsilon^I\}$ during a time step is computed using

$$\{\Delta d^I\} = [K]^{-1}\{\Delta F^I\} \quad . \quad (4.15)$$

The inelastic pseudo force increment $\{\Delta F^I\}$ is calculated from

$$\{\Delta F^I\} = \sum_{\text{ELEMENTS}} \int_V [B]^T [E] \{\Delta \epsilon^I\} dV \quad , \quad (4.16)$$

where $\{\Delta \epsilon^I\}$ is the change in inelastic strain during the time increment.

4.3 Integration of the Constitutive Equations

Although the integration of the constitutive equations to obtain the inelastic strain increment could be achieved by any number of schemes, [4.3], [4.4], the second order Adams-Moulton predictor-corrector method lends itself readily to the required equilibrium iteration. The global inelastic strain and the state variables (written as Z_i for convenience) are integrated using

$$\{\Delta \epsilon^I\} = \frac{(t_i - t_{i-1})}{2} (\{\dot{\epsilon}^I\}_{i-1} + \{\dot{\epsilon}^I\}_i) \quad , \quad (4.17)$$

and

$$Z_i = \frac{(t_i - t_{i-1})}{2} (\dot{Z}_{i-1} + \dot{Z}_i) + Z_{i-1} \quad . \quad (4.18)$$

The vectors $\{\dot{\epsilon}^I\}_i$ and $\{\dot{\epsilon}^I\}_{i-1}$ are the inelastic strain rates at times t_i and t_{i-1} and Z_i and Z_{i-1} are the state variable at times t_i and t_{i-1} .

Since the inelastic response of the material is computed on the crystallographic planes, there is a state variable for each slip system at every integration point. The inelastic strain rate is computed by summing the contribution from each of the active slip systems. The inelastic strain rate on each of the active slip systems is a function of the stress state and the state variable for each system as described in Chapter II.

4.4 Iteration Procedure

At the beginning of a load case the initial and final elastic displacements are computed using Equation (4.11) and the displacements due to prior inelastic strains are computed using Equation (4.12). The total strains at the beginning of the load case are recovered for each integration point and the elastic strains are computed from

$$\{\epsilon^E\} = \{\epsilon^T\} - \{\epsilon^{\alpha\Delta T}\} - \{\epsilon^I\} \quad , \quad (4.19)$$

where $\{\epsilon^T\}$ are the total strains and $\{\epsilon^{\alpha\Delta T}\}$ are the thermal strains.

The stresses are computed, transformed to the material axis system and Equation (2.9) is used to find the shear stresses on each of the slip systems.

Using the current values of the state variables and the stress state allows the calculation of the initial values of the shear strain rates and state variable evolution rates on each of the slip systems. Equation (2.6) is then used to compute the macroscopic inelastic strain rates. Before entering the time loop an initial time increment is computed and the inelastic strain increments are estimated using a forward Euler integration formula. From the estimated inelastic strain increments an initial estimate is made for the inelastic pseudo force increment using Equation (4.16). The usual technique employed with the initial strain method is to assume that the incremental inelastic force $\{\Delta F^I\}$, the corresponding displacements $\{\Delta d^I\}$, and the inelastic strain increments $\{\Delta \epsilon^I\}$ are all zero on the first iteration of a time step. The stability of the method can be improved considerably when a forward Euler integration of the inelastic strain rates is used to make an

estimate of $\{\Delta\epsilon^I\}$, $\{\Delta F^I\}$, and $\{\Delta d^I\}$ on the first iteration. This method results in an initial estimate which is much closer to the solution. In sample cases the overall number of iterations was reduced by more than one half.

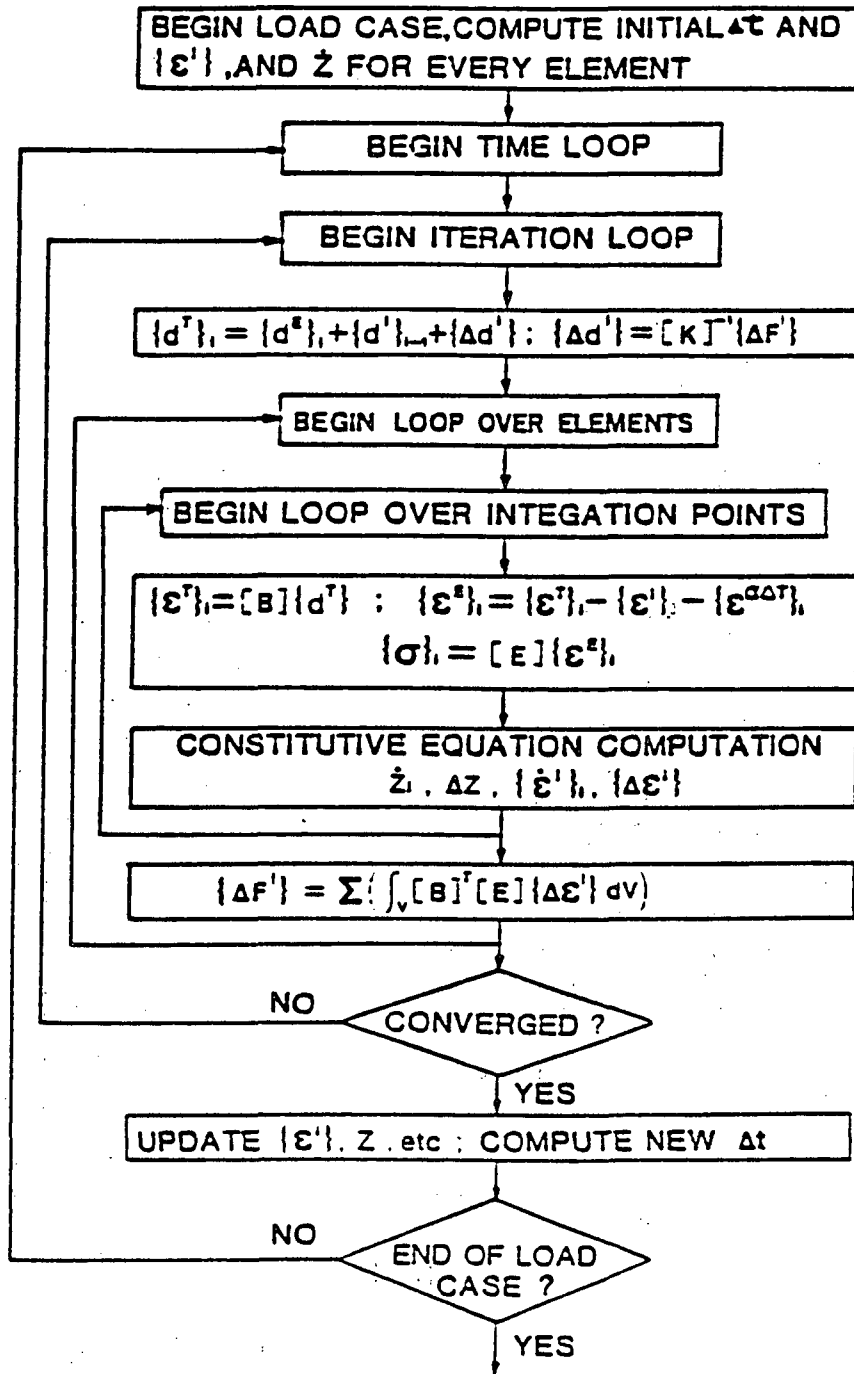
The procedure during a time increment is to estimate the solution on the first iteration using a forward Euler scheme as outlined above. Then displacements, strains, stresses, inelastic strain rates, and state variable evolution rates are computed at the end of the time increment. The inelastic strains and state variables are integrated over the time increment and an improved inelastic force is computed. The procedure is repeated until convergence is achieved at the end of the time increment. Figure 13 summarizes the logic.

4.5 Dynamic Time Incrementing

In a computer code that allows a linear variation of loads with time a dynamic time incrementing scheme is very desirable since large excursions in stress and inelastic strain rate are to be expected. The procedure used to compute the time increments requires a certain amount of initial experimentation to determine appropriate time step control parameters. However, once this has been done the procedure works quite well and is a tremendous improvement in economy over a constant time increment.

The time increment is based on three separate time step control criteria. These are the maximum stress increment, maximum inelastic strain increment, and maximum rate of change of the inelastic strain rate. The minimum time step calculated from the three criteria is the value used. Since the calculations are based on values readily

FIGURE 13. FLOW CHART OF FINITE ELEMENT SOLUTION PROCEDURE



available from the previous time step, little computational effort is required.

4.5.1 Stress Increment Criterion

A maximum stress increment criterion is used to control the time increment during primarily elastic excursions. This criterion is necessary to prevent overshoot of the point where significant inelastic strain rates begin. The calculation for the time increment is given by

$$\Delta t_k = \Delta t_{k-1} \frac{\Delta \sigma_{INC}}{(\Delta \sigma_{k-1})_{MAX}} \quad (4.20)$$

where Δt_{k-1} is the previous time increment, $(\Delta \sigma_{k-1})_{MAX}$ is the maximum change in effective stress for all integration points during the previous time increment, and $\Delta \sigma_{INC}$ is the maximum desired stress increment. The value for $\Delta \sigma_{INC}$ is program input and will vary somewhat, depending on material constants. Typical values are about 15 MPa.

4.5.2 Inelastic Strain Increment Criterion

The inelastic strain increment criterion controls the time step when the stress and inelastic strain rates are not changing significantly. This is given by

$$\Delta t_k = \Delta t_{k-1} \frac{\Delta \epsilon_{INC}^I}{(\Delta \epsilon_{k-1}^I)_{MAX}} \quad (4.21)$$

The maximum change in effective inelastic strain for all integration points during the previous time increment is $(\Delta \epsilon_{k-1}^I)_{MAX}$ and $\Delta \epsilon_{INC}^I$ is the maximum desired inelastic strain increment. The value for $\Delta \epsilon_{INC}^I$ is program input and typical values are about .000100.

4.5.3 Rate of Change of the Inelastic Strain Rate

This criterion controls the time increment when the inelastic strain rate is changing rapidly such as in the "knee" of a stress strain curve. The quantity $\ddot{\epsilon}^I$ is a measure of how close the initial forward Euler estimation is to the final converged solution. The backward difference formula

$$\ddot{\epsilon}_1^I = (\dot{\epsilon}_{1-1}^I - \dot{\epsilon}_{1-2}^I) / \Delta t_{k-1} \quad (4.22)$$

is used to estimate $\ddot{\epsilon}_1^I$. The maximum value of $\ddot{\epsilon}^I$ for all integration points $(\ddot{\epsilon}^I)_{MAX}$ is used to estimate the next time step using

$$\Delta t_k = \sqrt{\frac{2\Delta t_{k-1} \Delta \epsilon_{INC}^I e}{(\ddot{\epsilon}_1^I)_{MAX}}} \quad (4.23)$$

The parameter e is the maximum desired error by which the initial forward Euler estimation is in error. The value for e is program input and typical values are about .01. Equation (4.23) is derived simply from taking the difference between an Euler integration scheme and the more accurate second order Adams-Moulton method.

4.6 Convergence Criteria

Convergence is required at every integration point. Two separate criteria must be satisfied for convergence. First, the difference in the effective inelastic strain increment from subsequent iterations must be less than a prescribed value, i.e.

$$|\Delta \epsilon_k^I - \Delta \epsilon_{k-1}^I| < \delta_\epsilon \quad (4.24)$$

Second the change in effective stress from subsequent iterations must also be less than a prescribed value, i.e.

$$|\sigma_k - \sigma_{k-1}| < \delta_\sigma \quad (4.25)$$

For all of the calculations done in this study the convergence tolerances were set at one percent of the maximum desired effective stress increment and one percent of the maximum desired inelastic strain increment used in computing the time step.

CHAPTER V

COMPARISON OF THE CALCULATED AND EXPERIMENTAL RESULTS

All of the numerical calculations were performed using the finite element code described in the previous chapter. Since all of the calculations were for uniaxial tests it was not necessary to model the actual specimen geometry. However, to test the force and stiffness assembly routines a model with two twenty noded bricks was used to simulate the specimen response. The calculations were performed to compare with test results and also to exercise the constitutive model and computer code under conditions for which no data are available.

5.1 Comparison of Experimental and Calculated Response for Rene N4, Composition A

The calculations were performed using the constants derived from the data presented by Gabb, Gayda, Miner and Voigt in References [6] and [37]. The constants are for octahedral and cube slip at high strain rate (Table 4). The features of the model that are exercised are the orientation dependence, tension/compression asymmetry, strain rate dependence and isotropic vs kinematic hardening for hysteresis loops. Because of the assumptions required in the derivation of the material constants due to the limited data base, most of the exercises for this data set are intended to demonstrate features of the constitutive model rather than correlation with experimental data.

5.1.1 Orientation Dependence and Tension/Compression Asymmetry

Recall that in Chapter III the constants were derived by hypothesizing that the .02% yield stress for the first quarter cycle of sinusoidal loading was representative of the orientation dependence and tension/compression asymmetry for constant strain rate tests. The octahedral constants were derived using the [001] tension and compression tests and the [011] tension data. The cube slip constants were derived using the [$\bar{1}11$] tension data. The stress response was calculated for these tests and for the tests at other orientations. The calculated results are compared to the experimental results in Table 5. All of the predicted results are within 6% of the experimental values and within the confidence level for the experiments. It can be concluded that the constitutive model successfully predicts the orientation dependence and tension/compression asymmetry in octahedral slip. It can also be seen that the octahedral and cube flow equations produce good results when simultaneously activated.

5.1.2 Cyclic Response

The first 1.25 cycles of the fatigue response presented in Reference [37] are compared to the predicted results using both isotropic hardening and kinematic hardening (Figures 14 and 15). The stress ranges for the kinematic hardening assumption are generally better than for the isotropic hardening assumption.

TABLE 5. COMPARISON OF MONTONIC YIELD STRESSES (REFERENCE [37]) AND CALCULATED SATURATION STRESSES WITH OCTAHEDRAL AND CUBE SLIP CONSTITUTIVE MODELS ACTIVE, RENE N4, 760°C

ORIENTATION	TENSION OR COMPRESSION	.02% YIELD STRESS (REF [37]) (MPa)	CALCULATED SATURATION STRESS (MPa)	ERROR (%)
[001]*	T	956	956	0
[001]*	C	-818	-819	.1
[011]*	T	748	752	.5
[011]	C	-905	-865	4.4
[$\bar{1}11$]*	T	817	827	1.3
[$\bar{1}11$]	C	-842	-828	1.7
[023]	T	695	705	1.5
[023]	C	-747	-741	.9
[$\bar{2}36$]	T	716	725	1.2
[$\bar{2}36$]	C	-714	-752	5.3
[$\bar{1}45$]	T	656	692	5.5
[$\bar{1}45$]	C	-792	-763	3.6

* CONSTANTS WERE DERIVED USING THIS DATA

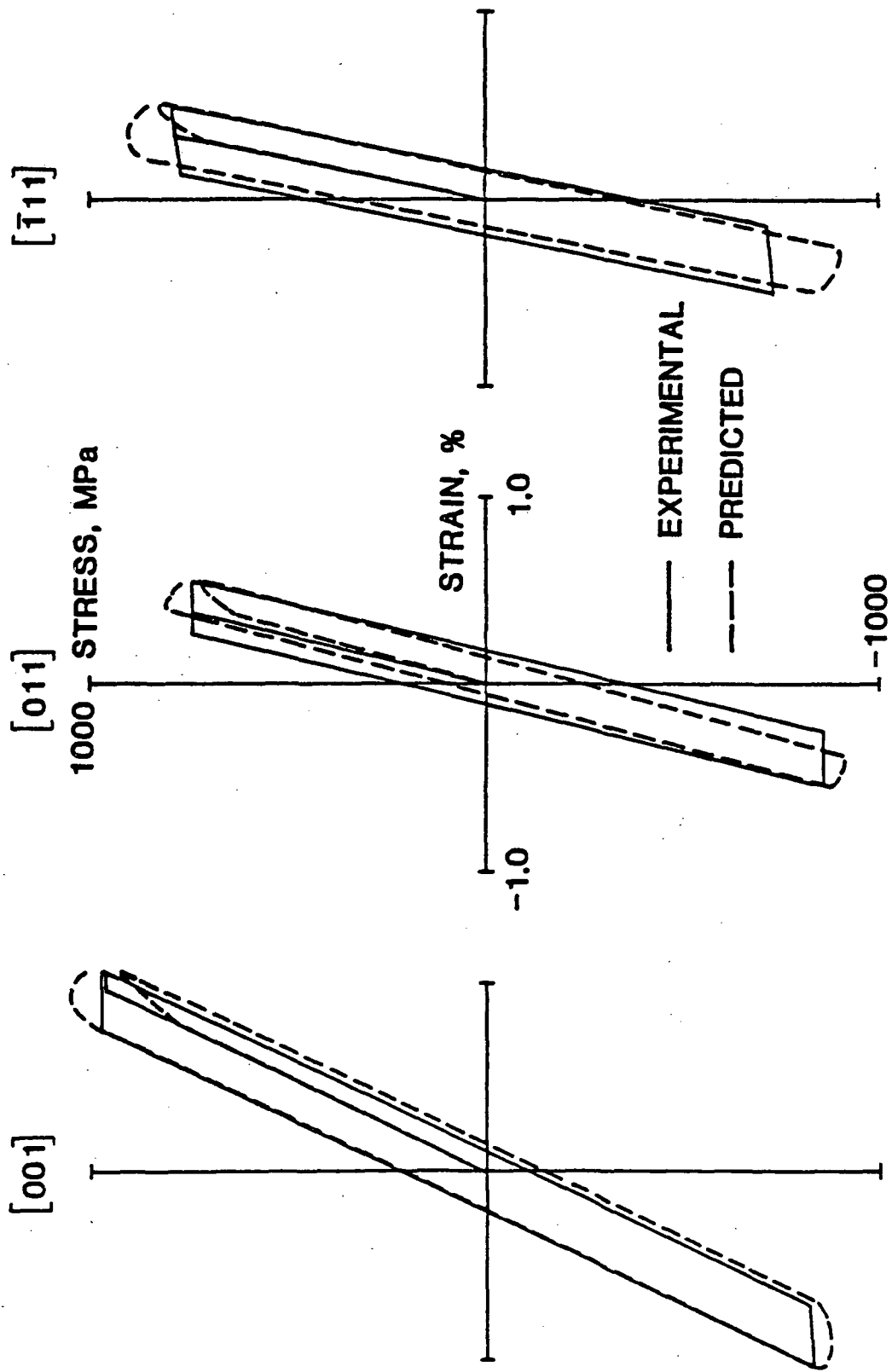


FIGURE 14. PREDICTED AND EXPERIMENTAL RESPONSE OF FIRST CYCLE FATIGUE LOOPS FOR RENE N4 AT 760°C, ISOTROPIC HARDENING

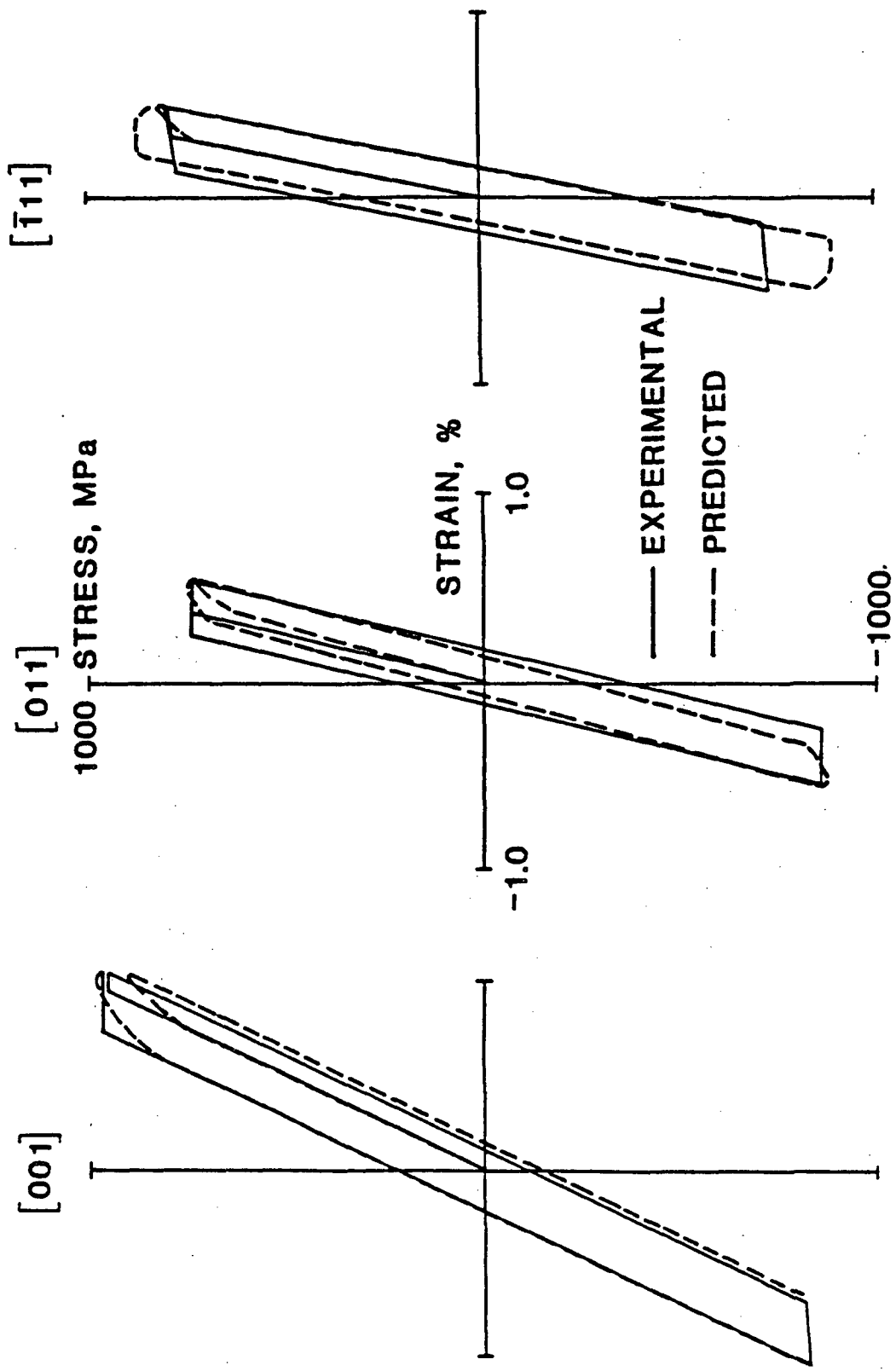


FIGURE 15. PREDICTED AND EXPERIMENTAL RESPONSE OF FIRST CYCLE FATIGUE LOOPS FOR RENE N4 AT 760°C, KINEMATIC HARDENING

There is a significant difference in the shapes of the curves. The use of a sinusoidal wave form has a tendency to produce flat curves but the predicted response even shows a stress drop near the peak strain points. Probably the most significant variation between the predicted and experimental results is seen in the response of the specimen in the $[\bar{1}11]$ orientation after the first 1/4 cycle. These differences can at least partially be attributed to the assumptions that were required to derive the constants. Recall, that the values for n_1 and n_2 were estimated from PWA 1480 data at 871^oc and 982^oc. This may not be representative of Rene N4 at 760^oc. In addition, the hardening constants were estimated from Rene N4 VF317. These extrapolations could cause significant errors in the predicted hardening and strain rate sensitivity.

A slight mismatch in elastic modulus is seen between the predicted and experimental results for the specimen oriented in the [011] direction. The elastic moduli used in the analysis are the nominal values and are entered in the principal material directions. A slight variation in elastic modulus from the nominal value is not surprising.

5.1.3 Strain Rate Sensitivity

In order to demonstrate the strain rate sensitivity of the constitutive model, first cycle fatigue loops were calculated for two different orientations and three different rates using the sinusoidal total strain history. The results of this exercise are shown in Figure 16. Qualitatively, it can be stated that the observed trend is as

expected. Since no data are available, quantitative comparisons are not possible.

5.2 Comparison of Experimental and Calculated Response for Rene N4 VF317, Composition B

The calculations were performed using the constants derived from the Rene N4 VF317 data, Reference [68]. The constants are for octahedral slip at high strain rate and creep (Table 4). The features of the model that are exercised are orientation dependent stress strain curves, orientation dependent creep response and stress relaxation behavior.

5.2.1 Orientation Dependent Stress Strain Curves

The stress strain response was calculated for a constant strain rate of $8.333 \times 10^{-5} \text{ sec}^{-1}$ for three orientations. The calculated response compared to the experimental data is shown in Figure 17. The orientation constants were determined using all three curves so the variation in the yield stress levels is reproduced well. The hardening parameters were calculated from the [001] curve only.

Notice that there is a significant mismatch in the elastic modulus for the predicted and experimental response for the [0 342 940] orientation. Recall the observed VF317 response does not agree with the PWA 1480 response shown in Figure 3 because the yield stress for the [0 342 940] specimen, 20° from [001] in the [011] direction, is far above the expected level. The difference in the experimental and calculated elastic modulus suggests that the specimens in this data set designated as being in the [0 342 940] direction are probably much

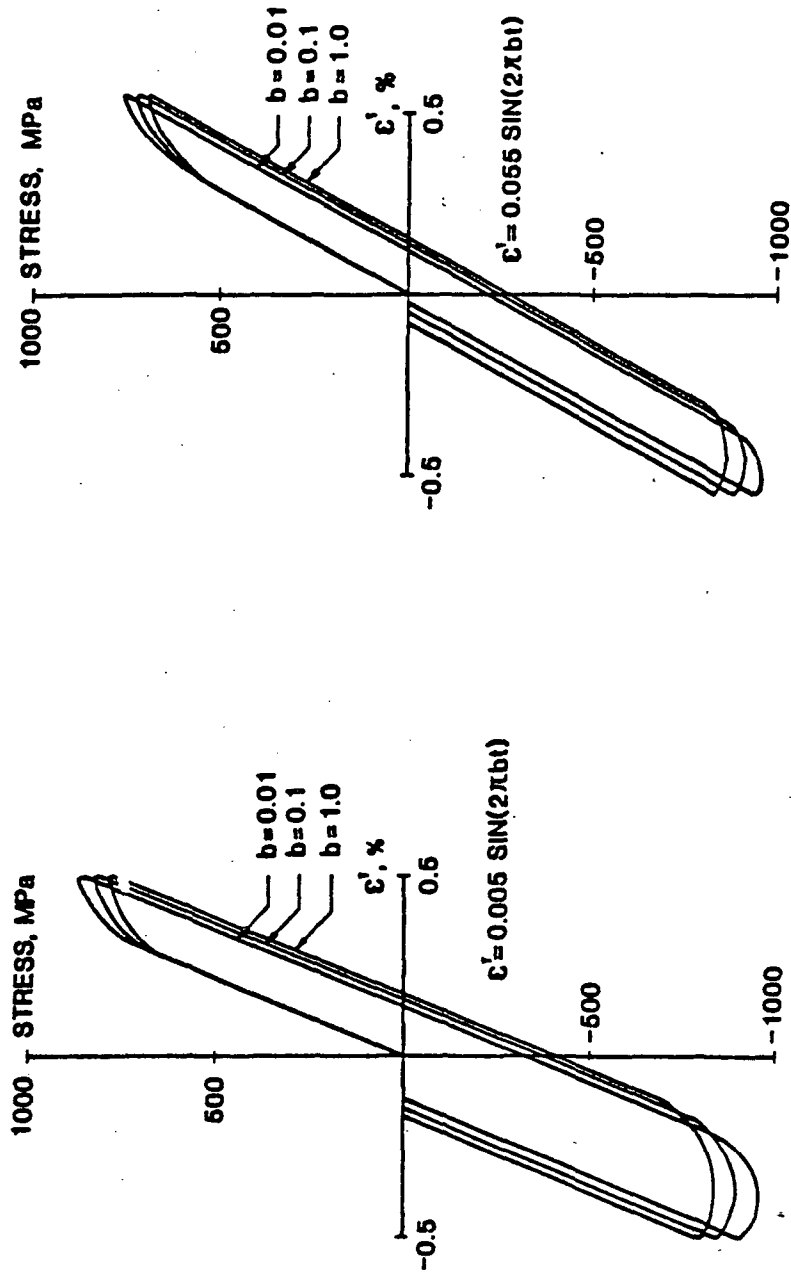
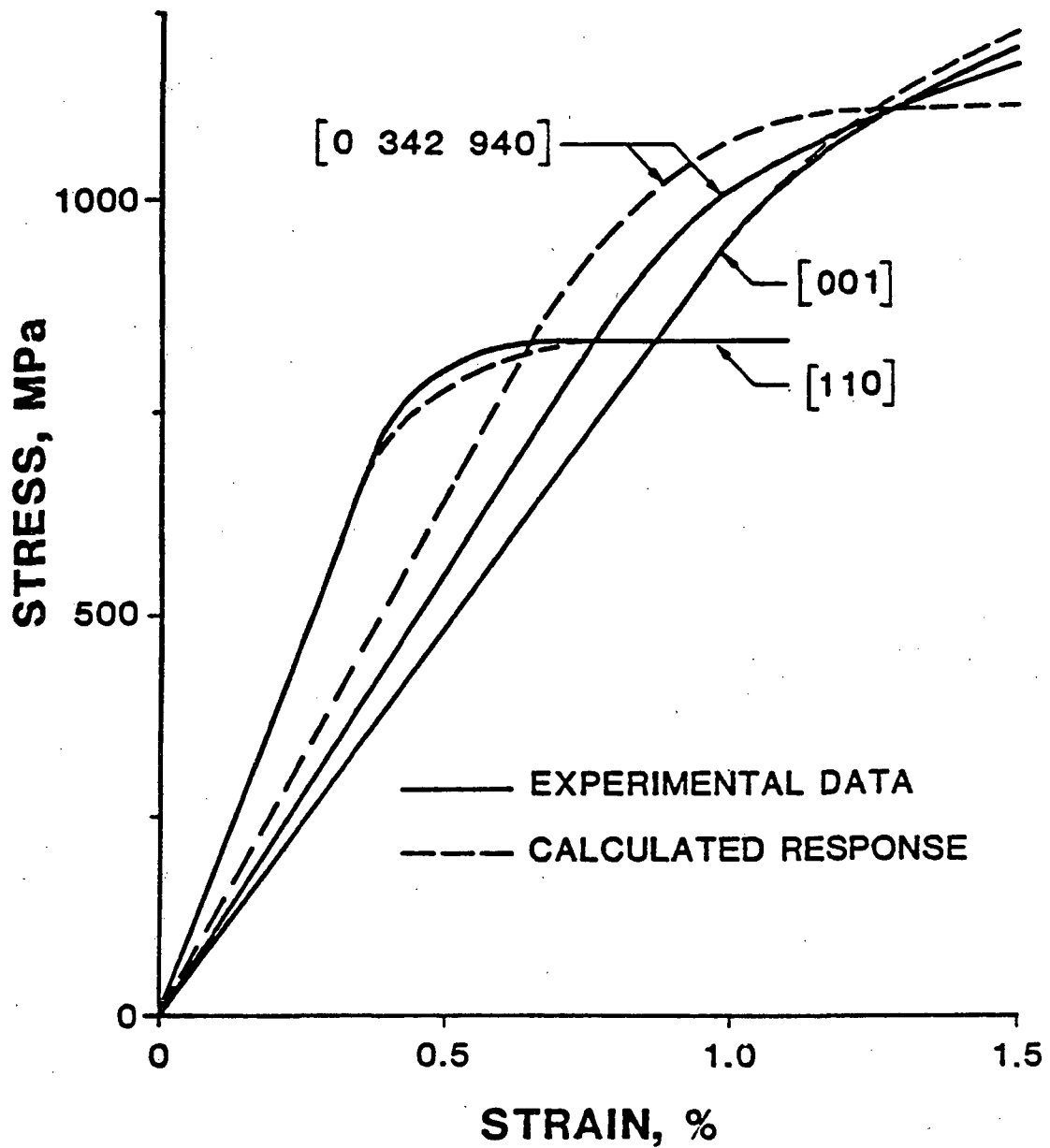


FIGURE 16b. PREDICTED RESPONSE AT THREE STRAIN RATES, [111]

FIGURE 16a. PREDICTED RESPONSE AT THREE RATES, [011]

FIGURE 16. PREDICTED STRAIN RATE SENSITIVITY OF RENE N4 AT 760°C.

FIGURE 17. PREDICTED AND EXPERIMENTAL STRESS STRAIN CURVES FOR RENE N4 VF317 AT 760°C.



closer to the [001] direction. This inconsistency is further verified through an example compression calculation. The predicted saturation stress response for a [001] specimen in compression was less than a third of the corresponding tensile [001] response. This is not realistic, especially since the model worked very well for the previous tension/compression exercises

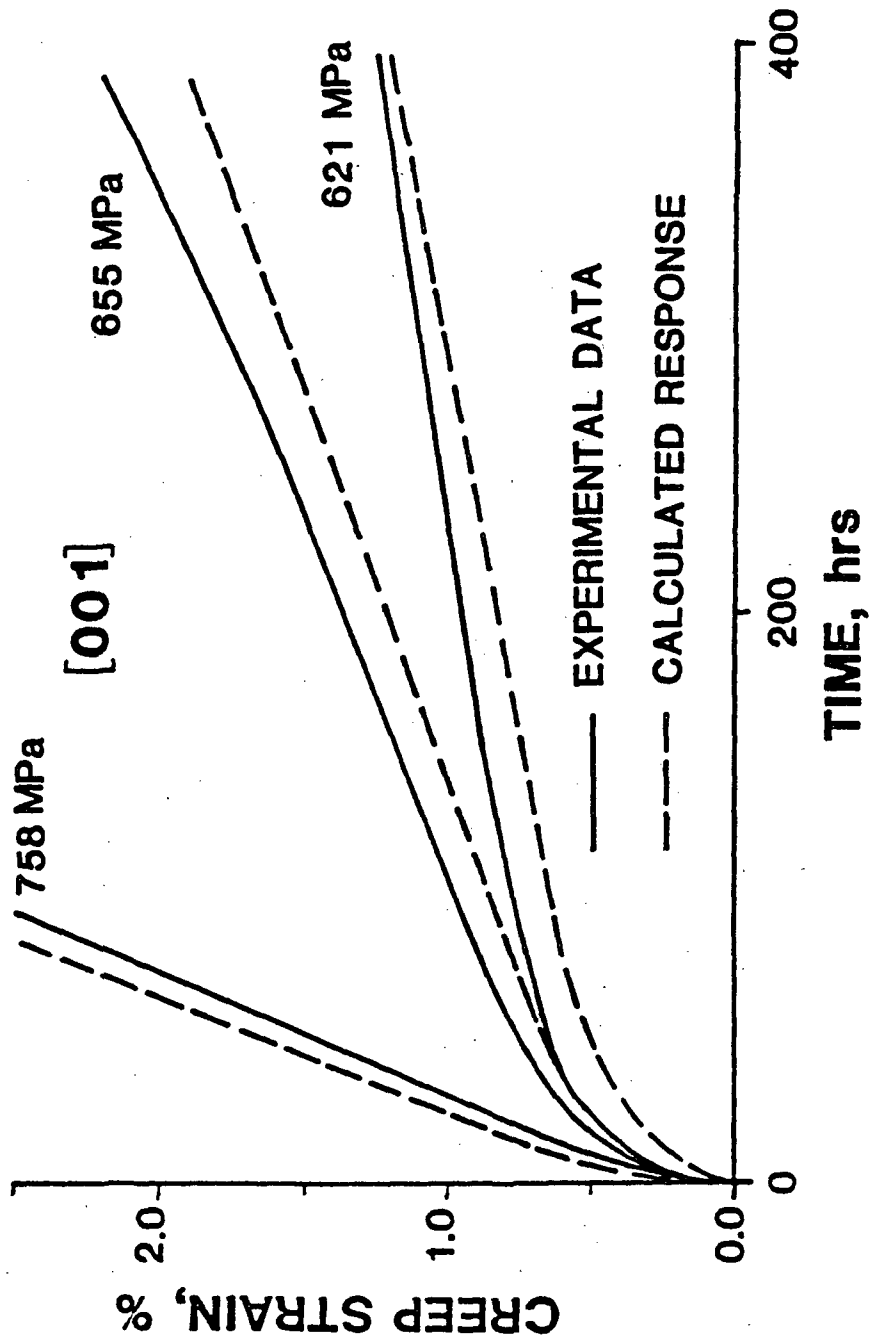
5.2.2 Creep Response

The tensile creep curves for seven specimens at three orientations were calculated and are compared with experimental data in Figures 18-20. The experimental data are from creep rupture tests which usually do not yield reliable data at the beginning of a test. Usually this type of test produces significant variation from test to test due to poor alignment and strain measuring systems as well as inherent differences from specimen to specimen. The correlation between the predicted and actual response for this type of test must be considered to be excellent.

5.2.3 Stress Relaxation

Although no stress relaxation data are available the stress relaxation response for specimens oriented in the [001] and [011] directions was calculated. Both predictions are for a constant displacement boundary condition with an initial stress level of 758 MPa. The qualitative behavior is as expected with the stress in the [011] oriented specimen relaxing faster than in the [001] oriented specimen, Figure 21. The strain rates in the [001] oriented specimen are in the same range as in the creep tests. However, the strain rates in the

FIGURE 18. CREEP RESPONSE OF RENE N4 VF317 LOADED IN THE [001] DIRECTION AT 760°C.



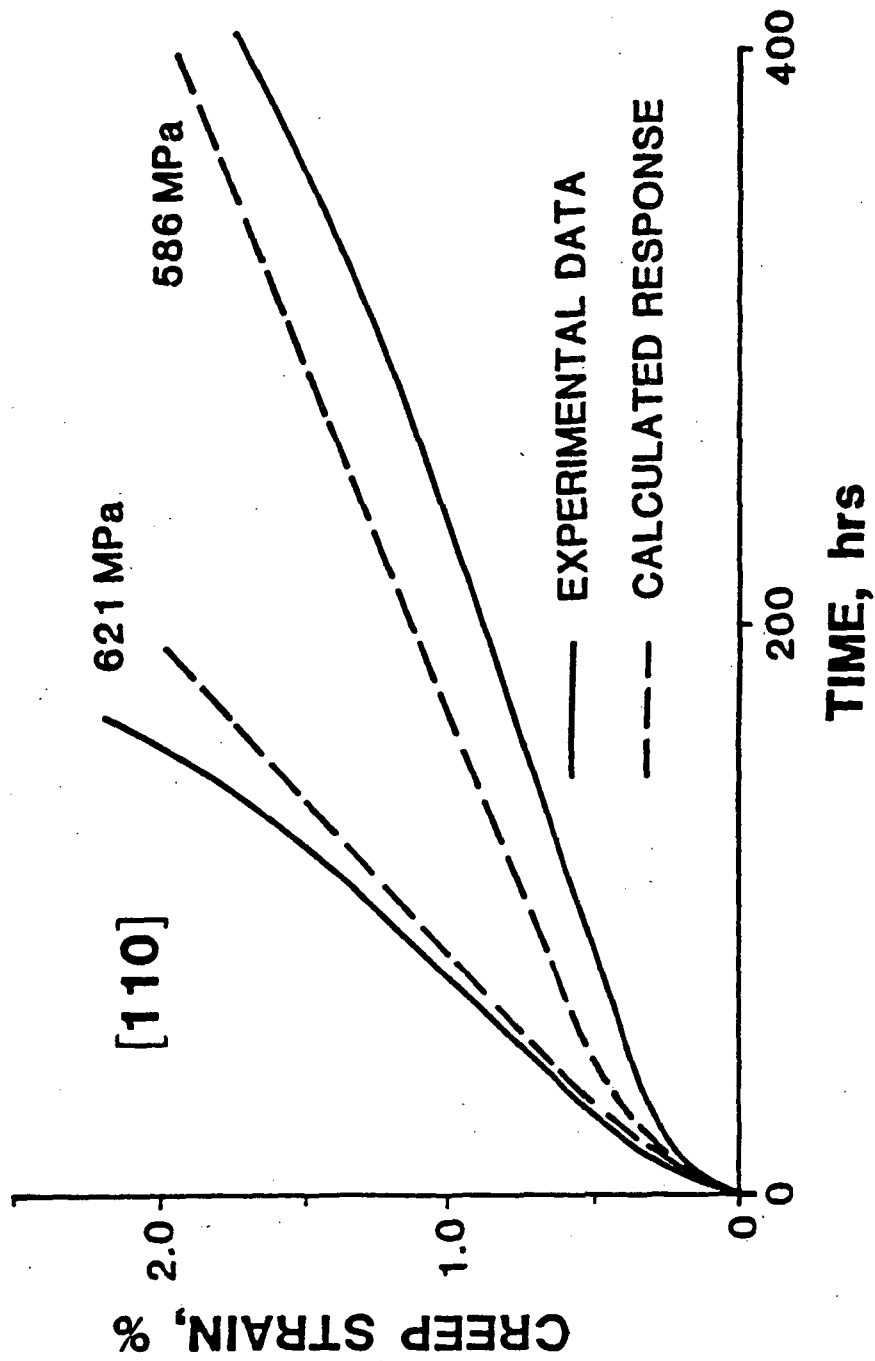


FIGURE 19. CREEP RESPONSE OF RENE N4 VF317 LOADED IN THE [110] DIRECTION AT 760°C.

FIGURE 20. CREEP RESPONSE OF RENE N4 VF317 LOADED IN THE [0 342 940] DIRECTION AT 760°C.

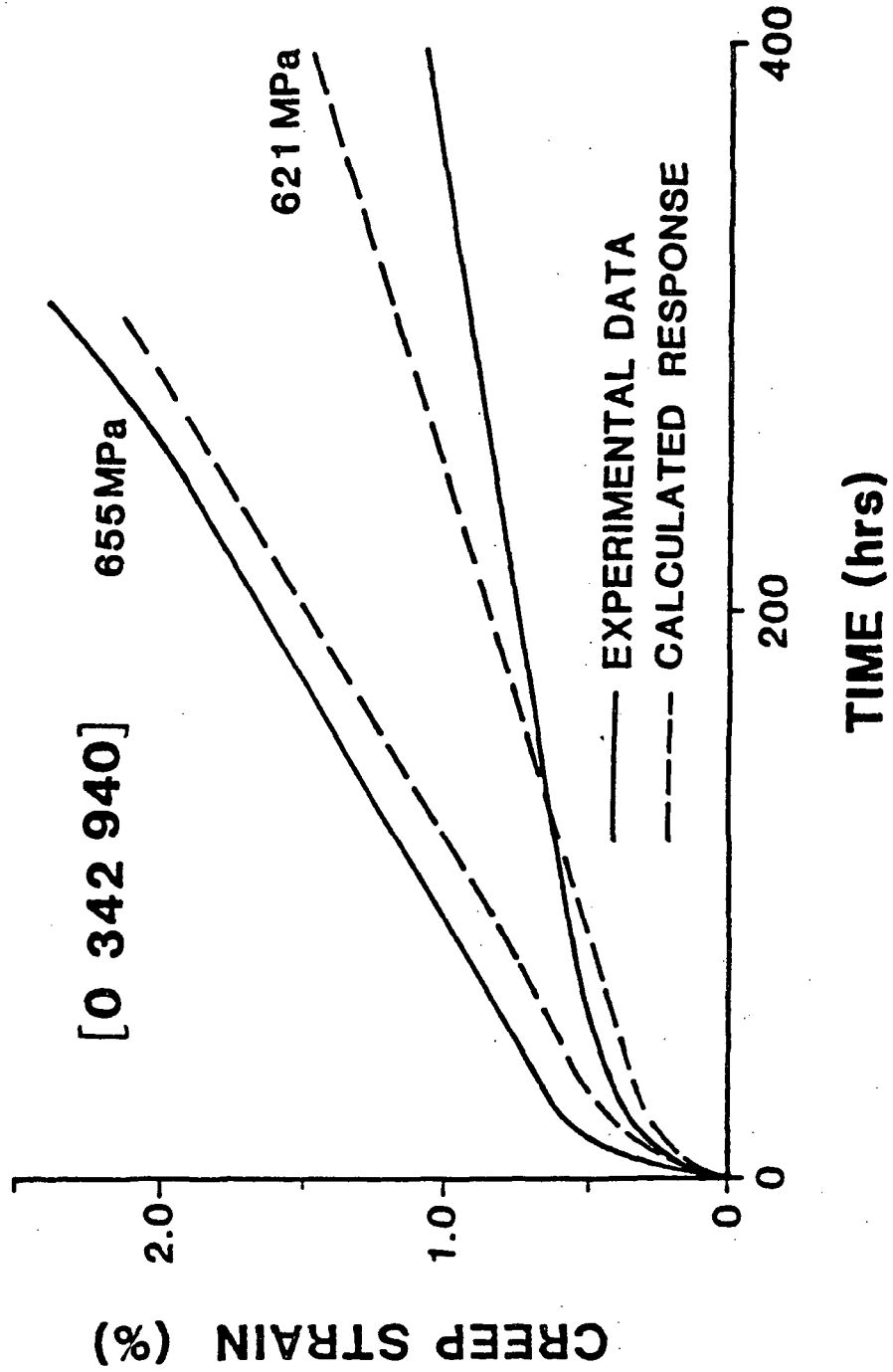
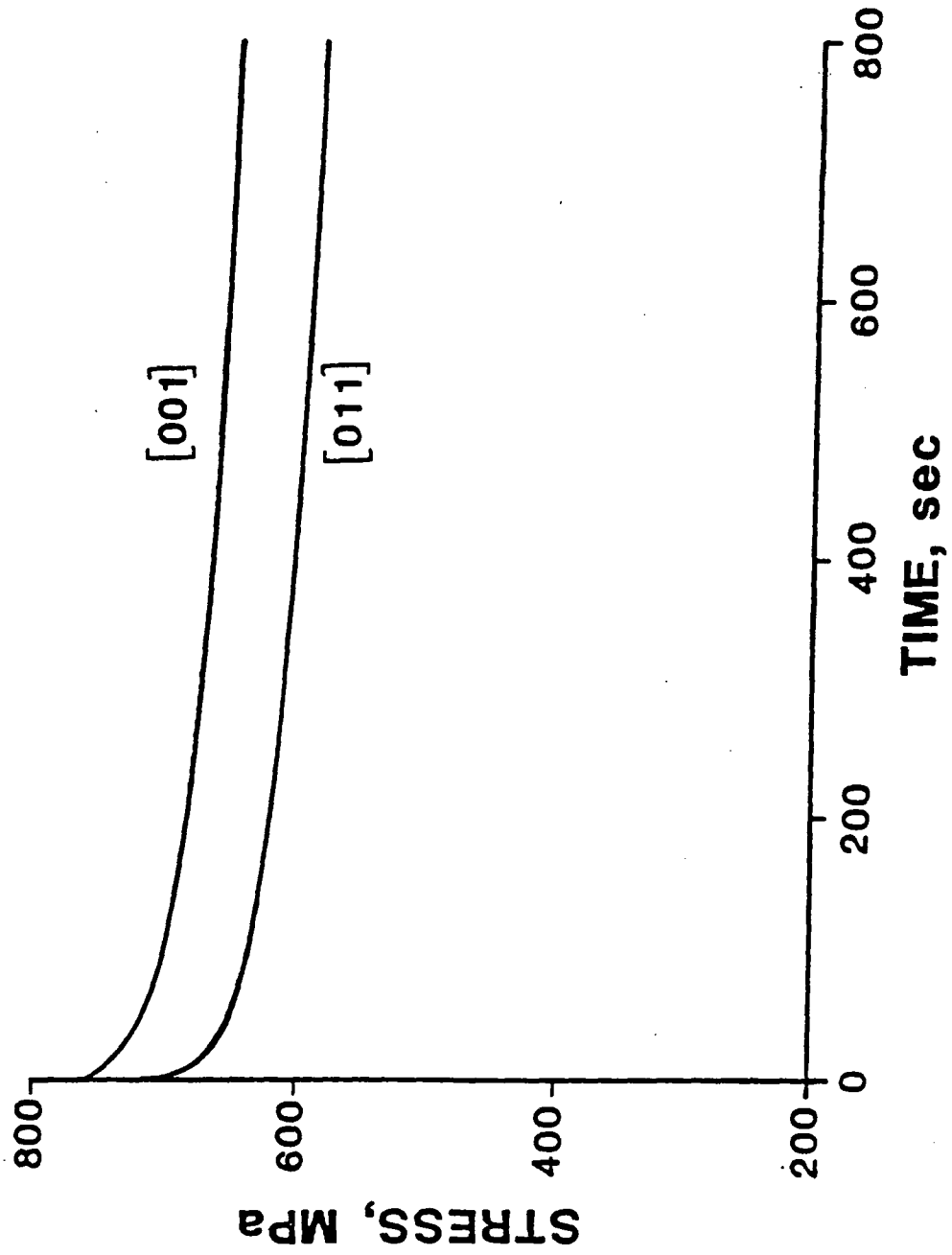


FIGURE 21. PREDICTED STRESS RELAXATION CURVES, RENE N4 VF317, 760°C.



[011] oriented specimen span the range between the tensile and creep data. Although the model behaved as expected it would be interesting to compare it to actual data in this intermediate strain rate range.

CHAPTER VI

DISCUSSION AND SUMMARY

The constitutive model as developed in this report is physically based and is capable of modeling most of the relevant material behavior at constant temperature. However, consideration must be given to future development needs. In addition, it is useful to specify the data base required to fully characterize the material parameters in the constitutive model as it now exists.

6.1 Constitutive Model Development

In the short term it should be possible to utilize the current constitutive model and finite element code as a viable mechanical analysis tool with little further development. For the future a number of potential refinements in the constitutive model are anticipated as outlined below.

6.1.1 Coupling of Creep and High Strain Rate Response

The work hardening in the flow equation for each slip system is characterized by a state variable $Z^{\alpha\beta}$. This state variable is a measure of flow resistance at high strain rates and in creep. In the current data base this approach appeared satisfactory, but questions remain for load histories in which both high strain rates and creep occur. To evaluate the coupling as it is formulated in this study requires a high strain rate loading followed by creep and/or a creep test followed by a tensile test.

Since different deformation mechanisms are postulated for high strain rates and creep it is reasonable to assume that two work

hardening state variables may be necessary. If this is the case, it is logical that coupling would occur in the state variable evolution equations.

6.1.2 Nonisothermal Response

The most obvious problem in modeling the nonisothermal response of Rene N4 is the lack of a data base sufficient to derive the material parameters over a range of temperatures. A simple nonisothermal implementation can be accomplished in the same manner as an isotropic formulation. The material constants are interpolated for temperature, and temperature rate and history effects are neglected.

Although the model has not been calibrated for any other temperatures it is possible to propose a method for interpolating some of the material parameters. In the flow Equations (2.13) and (2.18) the parameters D_1 , D_2 , D_3 and D_4 are interpreted as limiting strain rates and are expected to be constant with temperature. The strain rate sensitivity parameters n_1 , n_2 , n_3 and n_4 can be represented by an equation of the form

$$n = \frac{a}{T} + b \quad (6.1)$$

as proposed by Bodner in Reference [53], where a and b are constants and T is the absolute temperature. The thermal dependence of the orientation parameters ϕ_1 , ϕ_2 , V_{11} , V_{12} , V_{21} and V_{22} should be in the form of an Arrhenius function, (Equation (2.2)). The variation of the material parameters in the state variable evolution Equations (2.15) and

(2.21) with temperature is unknown and would be postulated from the data.

The validity of this approach needs to be investigated. A reasonable approach would be to compare predictions of the current model with nonisothermal experiments. It is anticipated that the state variable evolution Equations (2.15) and (2.21) may require a thermal rate term to include thermal history effects.

6.1.3 Thermal Recovery

The treatment of secondary creep as a balance between strain hardening and recovery was originally proposed by Orowan in 1947, Reference [76]. Nearly all of the recently developed unified constitutive models include a hardening term and a recovery term in the work hardening state variable evolution equations. This form has been successful in modeling the inelastic response of many isotropic metals. In this formulation an adequate data base for evaluating a recovery term did not exist and the term was not included. Also at the temperature studied, recovery is probably not as important as at higher temperatures. Future work should include the investigation of a thermal recovery term in the state variable evolution equations.

6.1.4 Latent Hardening

The work hardening state variable evolution Equations (2.15) and (2.21) include "self hardening" only. That is, the work hardening on a slip system is assumed to be effected only by slip on that system. The hardening of inactive slip systems by intersection with active slip systems or "latent hardening" is generally considered to be an important

part of the theoretical basis for hardening in single crystal plasticity, References [64]-[67]. In a recent review, Reference [77], the ratios of latent hardening to self hardening for single crystal aluminum and copper are reported in the range of 1 to 2.

There are two methods for determining the effects of latent hardening mentioned in the literature. The first is to plastically deform a large crystal oriented for single slip, cut the crystal into specimens oriented to activate previously latent systems and compare the response of the initially latent systems to that in the original test. The second method involves measuring the crystal axis rotations in a tension test. During finite straining the slip direction rotates toward the loading direction and eventually a second slip system, or "conjugate" system, becomes equally stressed. If the latent hardening of the conjugate system is identical to the self hardening of the primary system it will slip equally under the same stress. If the latent hardening on the conjugate system is greater than the self hardening on the primary system equal inelastic straining will not be achieved until the stress on the conjugate system is greater than that on the primary system.

Since Rene N4 is a high temperature alloy and the specimens are coated to prevent environmental degradation, the testing procedures outlined above would be further complicated. It seems that a viable alternative testing procedure for investigating latent hardening would be to run a combination of proportional and nonproportional tension-torsion tests.

For small strains and proportional loading, latent hardening will have little or no effect on the material's response or the predictive capability of the constitutive model. For nonproportional loading or large strains the effect of latent hardening for Rene N4 is probably important but cannot be investigated with the current data base. Extension of the present theory to large strains and/or nonproportional loading will require consideration of latent hardening effects.

6.1.5 Cyclic Hardening

Nickel base single crystal alloys experience cyclic hardening resulting in up to a 10% increase in stress between initial and stabilized loops in a strain range controlled test, see Figure 6. Because of the limited data base this behavior has not been modeled. One way to model this effect is to include an additional term in the state variable hardness equation. A commonly used measure correlated with cyclic hardening is accumulated inelastic work which could be the independent variable in the cyclic hardening term.

6.1.6 Other Response Characteristics

There are a number of other response characteristics not modeled in this study. For example, slip bursts are observed at some orientations but have not been considered analytically. This effect is of little importance and in fact would present serious numerical problems if these effects were included in the constitutive model.

Anelastic recovery, or negative creep strain rates at a positive stress following a stress drop, are commonly observed in nickel base superalloys. For isotropic materials this behavior is usually modeled

by including a back stress tensor. A similar approach could be used for single crystal materials by including a back stress term on each slip system. In addition, the back stress model is important for isotropic modeling because it allows the direction of the deviatoric stress and inelastic strain rate vectors to be different and to vary as a function of the deformation. This effect has been observed and documented in the literature for a variety of multiaxial loading conditions. The current formulation does not force the stress and inelastic strain rate vectors to be parallel; however, there are no multiaxial tests of nickel base single crystal alloys to evaluate this effect.

Tertiary creep is not predicted by the current model. The usual technique for isotropic materials to account for tertiary creep is by including a damage measure in the constitutive model. A similar approach could be used for Rene N4 by including another state variable and evolution equation. However, since tertiary creep occurs at strains above 2% to 3%, there is little need to model tertiary creep for turbine blade and vane applications.

6.2 Summary of Data Base Requirements

For the nonlinear finite element code with the Rene N4 constitutive model to be a useful tool it is necessary to develop the data base to generate the required material parameters. In addition, it is necessary to evaluate the model at other temperatures. The development of the data base can also be used for refining the constitutive model. In fact, part of the value of the constitutive

model is to provide a framework for alloy development and for understanding experimental results.

The temperature environment for turbine blades and vanes varies from ambient up to about 1200°C. Inelastic behavior during operation would occur mostly at temperatures over 550°C. The test data for the inelastic response of the material should therefore span the range from about 550°C to about 1200°C. Considering the variation in response with temperature, it is desirable to obtain data at about 100°C intervals. A hypothetical test matrix at a single temperature is presented in Table 6. The matrix is based on the tests required to determine the material parameters as discussed in Chapter III. The data base must be chosen to activate the octahedral and cube slip systems separately. Further, the tests should fully span the space of the stereographic triangle in both tension and compression. The [001] orientation is favored (half of the tests are in this orientation) since this direction is coincident with the radial direction of the blade or vane. In addition, tests should be run at other orientations to verify the model. The matrix in Table 6 is only for the model as presented in this report. The testing should also include a number of fatigue tests to evaluate cyclic hardening and further verify the model. It is not expected that the full test matrix should be run at all temperatures; however, the full matrix should be run at least one temperature above and below the critical temperature, about 800°C, since the deformation mechanisms appear to be different.

TABLE 6 - CONSTITUTIVE MODEL TEST MATRIX

TYPE OF TEST	SPECIMEN ORIENTATION	TENSION OR COMPRESSION	NUMBER OF DIFFERENT STRAIN RATES	NUMBER OF DIFFERENT STRESS LEVELS
CONSTANT STRAIN RATE	[001]	T	2	-
CONSTANT STRAIN RATE	[001]	C	1	-
CONSTANT STRAIN RATE	[011]	T	1	-
CONSTANT STRAIN RATE	[111]	T	2	-
CONSTANT LOAD	[001]	T	-	3
CONSTANT LOAD	[001]	C	-	2
CONSTANT LOAD	[011]	T	-	2
CONSTANT LOAD	[111]	T	-	3

* TESTS IN THE [111] ORIENTATION ARE FOR EVALUATION OF CUBE SLIP CONSTANTS, TESTS IN THE OTHER ORIENTATIONS ARE FOR EVALUATION ON OCTAHEDRAL SLIP CONSTANTS.

6.3 Conclusion

The constitutive model developed in this study successfully predicts an important part of the observed material behavior. A method has been developed for the derivation of material constants and no special or difficult tests are required.

The implementation of the constitutive model in a nonlinear finite element code has been accomplished. It is computationally more intensive than comparable rate dependent isotropic models or rate independent anisotropic models, but it is not significantly more expensive. Some of the features in the finite element code enhance its usability and decrease its cost.

The goal of developing a practical design tool for Rene N4 gas turbine engine components has substantially been achieved.

APPENDIX A

EIGENSPACE APPROACH

In the early stages of this research a considerable effort was made to further develop and apply the unified constitutive theory proposed by Stouffer and Bodner in 1979 [38]. The theory as proposed included initial or deformation induced anisotropy.

The form of the deformation rate equation is an extension of the Prandtl-Reuss flow law to anisotropic inelasticity. The rate of inelastic deformation tensor is related to the deviatoric stress tensor by a fourth order linear transformation whose components are functions of the stress and state variables. The constitutive equations are an extension of earlier work by Bodner and Partom [39], [40] and do not employ the use of a yield criteria or separate loading and unloading conditions. The state variables are introduced to characterize the work hardening of the material due to inelastic deformation. These variables are shown to transform as a fourth order tensor and are a central part of the anisotropic model.

The tensorial structure of the constitutive theory is typical of most anisotropic constitutive models, namely

$$\dot{\epsilon}_{ij} = \lambda_{ijkl} \sigma_{kl} \quad (\text{A.1})$$

where ϵ_{ij} is the strain or strain rate, σ_{kl} is the Cauchy or deviatoric stress and λ_{ijkl} is a fourth order tensor that characterizes all of the material properties. The components of λ_{ijkl} may be constants as in linear elasticity or may be functions of stress and the previous history

as required by the particular choice of material and deformation mechanisms. Frequently Equation (1.1) is written in a six dimensional vector space as

$$\epsilon_{\alpha} = \lambda_{\alpha\beta} \sigma_{\beta} \quad (\text{A.2})$$

Where $\alpha, \beta = 1, 2, \dots, 6$ and ϵ_{ij} and σ_{ij} are written as vectors. In Reference [38] these vectors were defined as $\sigma_1 = \sigma_{11}$, $\sigma_2 = \sigma_{22}$, $\sigma_3 = \sigma_{33}$, $\sigma_4 = \sqrt{2} \sigma_{23}$, $\sigma_5 = \sqrt{2} \sigma_{31}$, $\sigma_6 = \sqrt{2} \sigma_{12}$ and similarly for the strain tensor ϵ_{ij} .

The coupling between stress and deformation is obvious in Equation (A.2). That is a single stress, σ_1 for example, will produce six components of deformation. One approach to modeling is to transform Equation (A.2) into diagonal matrix; that is

$$\epsilon_{\alpha}^* = \lambda_{\alpha\alpha}^* \sigma_{\alpha}^* \quad , \quad (\text{A.3})$$

with no sum on α , ϵ_{α}^* and σ_{α}^* are the transformed variables and $\lambda_{\alpha\alpha}^*$ are the eigenvalues of $\lambda_{\alpha\beta}$. This approach has the advantage that the stress and deformation are completely uncoupled; that is, one component of stress produces only one component of deformation. This could be particularly convenient in computational and experimental work. However, the major complication is that the eigenvectors are expected to be functions of $\lambda_{\alpha\beta}$ and, in general depend on the deformation history.

C-2

The philosophy behind the proposed approach is to specify the eigenvalues and eigenvectors rather than the components of $\lambda_{\alpha\beta}$ directly. In Ref. [38], it was assumed that there existed a class of materials for which the eigenvectors are invariant.

Let us begin by calculating the eigenvalues and eigenvectors for an inelastic compressible isotropic material with a constitutive equation as described by Equation (A.2). Designate ϵ_{α} as the inelastic strain rate and σ_{α} as the Cauchy stress. The tensor $\lambda_{\alpha\beta}$ is assumed to be symmetric, and since the components are real, then $\lambda_{\alpha\beta}$ will have real eigenvalues. Rice [41], Ponter and Leckie [42], Ponter [43] and Abuelfoutouh [44] have shown that the strain rate can be expressed as the derivative of a potential function with respect to the stress for history dependent polycrystalline materials. This result can be used to establish symmetry in $\lambda_{\alpha\beta}$. The constitutive equation for an isotropic material in a six dimensional vector space can be written as

$$\begin{Bmatrix} \epsilon_1 \\ \epsilon_2 \\ \epsilon_3 \\ \epsilon_4 \\ \epsilon_5 \\ \epsilon_6 \end{Bmatrix} = \begin{bmatrix} \lambda_{11} & \lambda_{12} & \lambda_{12} & 0 & 0 & 0 \\ \lambda_{12} & \lambda_{11} & \lambda_{12} & 0 & 0 & 0 \\ \lambda_{12} & \lambda_{12} & \lambda_{11} & 0 & 0 & 0 \\ 0 & 0 & 0 & \lambda_{11} - \lambda_{12} & 0 & 0 \\ 0 & 0 & 0 & 0 & \lambda_{11} - \lambda_{12} & 0 \\ 0 & 0 & 0 & 0 & 0 & \lambda_{11} - \lambda_{12} \end{bmatrix} \begin{Bmatrix} \sigma_1 \\ \sigma_2 \\ \sigma_3 \\ \sigma_4 \\ \sigma_5 \\ \sigma_6 \end{Bmatrix} \quad (\text{A.4})$$

using two independent material functions λ_{11} and λ_{12} . The eigenvalues are

$$\begin{Bmatrix} \varepsilon_1^* \\ \varepsilon_2^* \\ \varepsilon_3^* \\ \varepsilon_4^* \\ \varepsilon_5^* \\ \varepsilon_6^* \end{Bmatrix} = \begin{bmatrix} \lambda_{11} + 2\lambda_{12} & 0 & 0 & 0 & 0 & 0 \\ 0 & \lambda_{11} - \lambda_{12} & 0 & 0 & 0 & 0 \\ 0 & 0 & \lambda_{11} - \lambda_{12} & 0 & 0 & 0 \\ 0 & 0 & 0 & \lambda_{11} - \lambda_{12} & 0 & 0 \\ 0 & 0 & 0 & 0 & \lambda_{11} - \lambda_{12} & 0 \\ 0 & 0 & 0 & 0 & 0 & \lambda_{11} - \lambda_{12} \end{bmatrix} \begin{Bmatrix} \sigma_1^* \\ \sigma_2^* \\ \sigma_3^* \\ \sigma_4^* \\ \sigma_5^* \\ \sigma_6^* \end{Bmatrix} \quad (\text{A.5})$$

where ε_α^* and σ_α^* are the transformed strain rate and stress vectors in the eigenvector basis. The eigen configuration is defined as $\underline{\lambda}^* = \underline{Q} \underline{\lambda} \underline{Q}^T$ where \underline{Q} is the proper orthogonal transformation that can be written as the matrix of the components of the eigenvectors. For this case the eigenvalues are not all distinct and the six eigenvectors are not unique. The only unique eigenvector is in the one direction. The other five eigenvectors are arbitrary, however, they should form an orthonormal basis. A typical orthogonal transformation, written with eigenvectors arranged as the rows of the matrix, can be defined as

$$Q = \begin{bmatrix} \frac{1}{\sqrt{3}} & \frac{1}{\sqrt{3}} & \frac{1}{\sqrt{3}} & 0 & 0 & 0 \\ \frac{1}{\sqrt{2}} & -\frac{1}{\sqrt{2}} & 0 & 0 & 0 & 0 \\ \frac{1}{\sqrt{6}} & \frac{1}{\sqrt{6}} & -\frac{2}{\sqrt{6}} & 0 & 0 & 0 \\ 0 & 0 & 0 & 1 & 0 & 0 \\ 0 & 0 & 0 & 0 & 1 & 0 \\ 0 & 0 & 0 & 0 & 0 & 1 \end{bmatrix} \quad (A.6)$$

Using Q , the components of the transformed strain rate and stress vectors can be calculated in terms of the untransformed components. The eigenvector $(1/\sqrt{3}, 1/\sqrt{3}, 1/\sqrt{3}, 0, 0, 0)$ is the hydrostatic line in stress space and the other two normal stress eigenvectors are in the deviatoric stress plane. Budiansky and O'Connell [45] recently developed a method to evaluate the properties of isotropic polycrystalline material using this transformation.

A.1 Cubic Materials

Anisotropic materials with cubic symmetry have three independent material parameters λ_{11} , λ_{12} and λ_{44} . The constitutive equation, [8], can be written as

$$\begin{Bmatrix} \epsilon_1 \\ \epsilon_2 \\ \epsilon_3 \\ \epsilon_4 \\ \epsilon_5 \\ \epsilon_6 \end{Bmatrix} = \begin{bmatrix} \lambda_{11} & \lambda_{12} & \lambda_{12} & 0 & 0 & 0 & 0 \\ \lambda_{12} & \lambda_{11} & \lambda_{12} & 0 & 0 & 0 & 0 \\ \lambda_{12} & \lambda_{12} & \lambda_{11} & 0 & 0 & 0 & 0 \\ 0 & 0 & 0 & \lambda_{44} & 0 & 0 & 0 \\ 0 & 0 & 0 & 0 & 0 & \lambda_{44} & 0 \\ 0 & 0 & 0 & 0 & 0 & 0 & \lambda_{44} \end{bmatrix} \begin{Bmatrix} \sigma_1 \\ \sigma_2 \\ \sigma_3 \\ \sigma_4 \\ \sigma_5 \\ \sigma_6 \end{Bmatrix} \quad (\text{A.7})$$

in the principal directions of the material. This reduces to isotropic response when a relationship exists between the normal and shear components; i.e. $\lambda_{44} = \lambda_{11} - \lambda_{12}$.

The analysis for the eigenvalues and eigenvectors is identical to that for isotropic materials. The eigenvalues $\lambda_{\alpha\alpha}^*$, are $\lambda_{11} + 2\lambda_{12}$, $\lambda_{11} - \lambda_{12}$, $\lambda_{11} - \lambda_{12}$, λ_{44} , λ_{44} , λ_{44} for $\alpha = 1$ to 6, respectively.

A.2 Transverse Isotropic Materials

Since a specific application is to metal inelasticity, it is reasonable to impose the condition of incompressibility on the material response. This requires that $\lambda_{iikl} = 0$ in Equation (A.1) for arbitrary values of stress history and current loading. This result was derived by Olzak and Urbanowski [46] and Hill [47] for the general case of plastic flow with an anisotropic yield criterion. Introducing the deviatoric stress components, $s_{ij} = \sigma_{ij} - (1/3)\sigma_{mm}\delta_{ij}$, into Equation (A.1) and imposing the incompressibility and symmetry conditions

$$\lambda_{iikl} = \lambda_{klji} = 0 \quad (\text{A.8})$$

gives

$$\epsilon_{ij} = \lambda_{ijkl}s_{kl} + \lambda_{ijk\rho}(1/3)\sigma_{mm}\delta_{k\rho} = \lambda_{ijkl}s_{kl} \quad (\text{A.9})$$

Thus, for incompressible inelastic material response let ϵ_{α} and s_{α} denote the inelastic strain rate and deviatoric stress vectors respectively, in a six dimensional space. In this space, the restriction of incompressibility can be written as six scalar equations

$$\begin{aligned} \lambda_{11} + \lambda_{21} + \lambda_{31} &= 0 & \lambda_{14} + \lambda_{24} + \lambda_{34} &= 0 \\ \lambda_{12} + \lambda_{22} + \lambda_{32} &= 0 \text{ and } \lambda_{14} + \lambda_{25} + \lambda_{35} &= 0 & (\text{A.10}) \\ \lambda_{13} + \lambda_{23} + \lambda_{33} &= 0 & \lambda_{16} + \lambda_{26} + \lambda_{36} &= 0 \end{aligned}$$

The incompressibility condition specified in Equation (A.10) can be incorporated into the representation for a transverse isotropic materials [48] to yield

$$\begin{Bmatrix} \epsilon_1 \\ \epsilon_2 \\ \epsilon_3 \\ \epsilon_4 \\ \epsilon_5 \\ \epsilon_6 \end{Bmatrix} = \begin{bmatrix} (\lambda_{12} + \lambda_{13}) & -\lambda_{12} & -\lambda_{13} & 0 & 0 & 0 \\ -\lambda_{12} & (\lambda_{12} + \lambda_{13}) & -\lambda_{13} & 0 & 0 & 0 \\ -\lambda_{13} & -\lambda_{13} & 2\lambda_{13} & 0 & 0 & 0 \\ 0 & 0 & 0 & \lambda_{44} & 0 & 0 \\ 0 & 0 & 0 & 0 & \lambda_{44} & 0 \\ 0 & 0 & 0 & 0 & 0 & (2\lambda_{12} + \lambda_{13}) \end{bmatrix} \begin{Bmatrix} s_1 \\ s_2 \\ s_3 \\ s_4 \\ s_5 \\ s_6 \end{Bmatrix} \quad (\text{A.11})$$

Equation (A.11) was written with the coordinate axes in the three-dimensional space oriented parallel to the principal axes of the orthotropy of the body. In this case, coupling does not exist between the shear and normal components of the compliance matrix $\lambda_{\alpha\beta}$. Again applying an elementary analysis gives three unique eigenvalues in the form

$$\begin{Bmatrix} \epsilon_1^* \\ \epsilon_2^* \\ \epsilon_3^* \\ \epsilon_4^* \\ \epsilon_5^* \\ \epsilon_6^* \end{Bmatrix} = \begin{bmatrix} 0 & 0 & 0 & 0 & 0 & 0 \\ 0 & (2\lambda_{12} + \lambda_{13}) & 0 & 0 & 0 & 0 \\ 0 & 0 & 3\lambda_{13} & 0 & 0 & 0 \\ 0 & 0 & 0 & \lambda_{44} & 0 & 0 \\ 0 & 0 & 0 & 0 & \lambda_{44} & 0 \\ 0 & 0 & 0 & 0 & 0 & (2\lambda_{12} - \lambda_{13}) \end{bmatrix} \begin{Bmatrix} s_1^* \\ s_2^* \\ s_3^* \\ s_4^* \\ s_5^* \\ s_6^* \end{Bmatrix} \quad (\text{A.12})$$

The eigenvectors can be arranged to give the transformation specified by Equation (A.6). The eigenvectors for isotropic materials were defined to coincide with the eigenvectors for incompressible transverse isotropic materials.

A.3 Incompressible Orthotropic Materials

The material matrix λ for orthotropic materials with the condition of incompressibility can be written as

$$\begin{Bmatrix} \epsilon_1 \\ \epsilon_2 \\ \epsilon_3 \\ \epsilon_4 \\ \epsilon_5 \\ \epsilon_6 \end{Bmatrix} = \begin{bmatrix} (\lambda_{12} + \lambda_{13}) & -\lambda_{12} & -\lambda_{13} & 0 & 0 & 0 \\ -\lambda_{12} & (\lambda_{12} + \lambda_{23}) & -\lambda_{23} & 0 & 0 & 0 \\ -\lambda_{13} & -\lambda_{23} & (\lambda_{13} + \lambda_{23}) & 0 & 0 & 0 \\ 0 & 0 & 0 & \lambda_{44} & 0 & 0 \\ 0 & 0 & 0 & 0 & \lambda_{55} & 0 \\ 0 & 0 & 0 & 0 & 0 & \lambda_{66} \end{bmatrix} \begin{Bmatrix} s_1 \\ s_2 \\ s_3 \\ s_4 \\ s_5 \\ s_6 \end{Bmatrix} \quad (\text{A.13})$$

where ϵ_α and s_α are again the components of the inelastic strain rate and deviatoric stress vectors.

Solution of Equation (A.13) for the eigenvalues yields six distinct eigenvalues, hence the eigenvectors are all unique. The incompressibility condition requires $\lambda_1^* = 0$ and the first eigenvector $\hat{e}_1 = (1/\sqrt{3}, 1/\sqrt{3}, 1/\sqrt{3}, 0, 0, 0)$ as before. However, the second two eigenvalues cannot be directly calculated; i.e.

$$\lambda_{22}^*, \lambda_{33}^* = (\lambda_{12} + \lambda_{23} + \lambda_{31}) \pm [\lambda_{12}^2 + \lambda_{23}^2 + \lambda_{31}^2 - \lambda_{12}\lambda_{23} - \lambda_{23}\lambda_{31} - \lambda_{31}\lambda_{12}]^{1/2}. \quad (\text{A.14})$$

This further implies that the second and third eigenvectors, \hat{e}_2 and \hat{e}_3 , are functions of the tensor components λ_{12} , λ_{23} and λ_{31} . Since the matrix can be partitioned and analyzed as two independent three space problems, the eigenvectors \hat{e}_1 , \hat{e}_2 , and \hat{e}_3 are all independent and can be arranged as an orthonormal basis. Since \hat{e}_1 is fixed for all incompressible orthotropic materials under any deformation history, the position of the \hat{e}_2 and \hat{e}_3 can be defined by a rotation of \hat{e}_2 and \hat{e}_3 about the \hat{e}_1 vector. Let θ denote the position of \hat{e}_2 and \hat{e}_3 relative to the vectors $(1/\sqrt{2}, -1/\sqrt{2}, 0)$ and $(1/\sqrt{6}, 1/\sqrt{6} - 2/\sqrt{6})$ in the three dimensional subspace, respectively. The first three components of the three eigenvectors can be written as

$$\begin{Bmatrix} \hat{e}_1 \\ \hat{e}_2 \\ \hat{e}_3 \end{Bmatrix} = \begin{Bmatrix} 1 & 0 & 0 & 1/\sqrt{3} & 1/\sqrt{3} & 1/\sqrt{3} \\ 0 & \cos \theta & \sin \theta & 1/\sqrt{2} & -1/\sqrt{2} & 0 \\ 0 & -\sin \theta & \cos \theta & 1/\sqrt{6} & 1/\sqrt{6} & -2/\sqrt{6} \end{Bmatrix} \quad (\text{A.15})$$

The vectors \hat{e}_2 and \hat{e}_3 are still in the deviatoric plane in the subspace.

The angle θ gives the history dependent position of \hat{e}_2 and \hat{e}_3 and the representation reduces to transverse isotropy when $\theta = 0$. The transformation matrix Q , in Equation (A.6), becomes a function of θ for incompressible orthotropic materials.

The angle θ can be evaluated in terms of the components of λ in the initial configuration. Noting that $\underline{\lambda} = Q\lambda Q^T$ and that $\lambda_{11}^* = 0$, the calculation of λ_{11}^* in terms of θ gives

$$\begin{aligned} \tan 2\theta &= \frac{6}{\sqrt{12}} \left\{ \frac{\lambda_{12} - \lambda_{23}}{2\lambda_{12} - \lambda_{13} - \lambda_{23}} \right\} \\ &= \frac{6}{\sqrt{12}} \left\{ \frac{\lambda_{22} - \lambda_{11}}{2\lambda_{33} - \lambda_{11} - \lambda_{22}} \right\} \end{aligned} \tag{A.16}$$

A.4 Conditions Necessary for Stationary Eigenvectors

A.4.1 Transverse Isotropic Materials

The minimum condition for constant eigenvectors can easily be established. If the transformation matrix Q , defined by Equation (A.6), is used to transform the matrix, λ ,

$$\underline{\lambda} = \begin{bmatrix} \lambda_{11} & \lambda_{12} & \lambda_{13} & 0 & 0 & 0 \\ \lambda_{12} & \lambda_{11} & \lambda_{13} & 0 & 0 & 0 \\ \lambda_{13} & \lambda_{13} & \lambda_{33} & 0 & 0 & 0 \\ 0 & 0 & 0 & \lambda_{44} & 0 & 0 \\ 0 & 0 & 0 & 0 & \lambda_{44} & 0 \\ 0 & 0 & 0 & 0 & 0 & (\lambda_{11} - \lambda_{12}) \end{bmatrix} \quad (\text{A.17})$$

for an arbitrary compressible transversely isotropic material, the upper left quadrant of the transformed matrix $[\underline{Q}\lambda\underline{Q}^T]$, becomes

$$\begin{bmatrix} \frac{1}{3} (2\lambda_{11} + 2\lambda_{12} + 4\lambda_{13} + \lambda_{33}) & 0 & \frac{2}{\sqrt{18}} (\lambda_{11} + \lambda_{12} - \lambda_{13} - \lambda_{33}) \\ 0 & \lambda_{11} - \lambda_{12} & 0 \\ \frac{2}{\sqrt{18}} (\lambda_{11} + \lambda_{12} - \lambda_{13} - \lambda_{33}) & 0 & \frac{1}{3} (\lambda_{11} + \lambda_{12} - 4\lambda_{13} + 2\lambda_{33}) \end{bmatrix} \quad (\text{A.18})$$

This implies that the off diagonal term λ_{13}^* , must vanish if Equation (A.18) is in the eigenspace. Thus, the condition

$$\frac{1}{2} \sqrt{18} \lambda_{13}^* = \lambda_{11} + \lambda_{12} - \lambda_{13} - \lambda_{33} = 0 \quad (\text{A.19})$$

is necessary to produce the constant eigenvector result.

A.4.2 Orthotropic Materials

The compliance matrix for compressible orthotropic materials has

nine independent material parameters ($\lambda_{11}, \lambda_{22}, \lambda_{33}, \lambda_{44}, \lambda_{55}, \lambda_{66}, \lambda_{12}, \lambda_{23}, \lambda_{31}$). Using \underline{Q} in Equation (A.6) to transform $\underline{\lambda}$ into the space $\underline{\lambda}^* = \underline{Q}\underline{\lambda}\underline{Q}^T$, also implies that $\lambda_{12}^*, \lambda_{23}^*$ and λ_{31}^* must vanish if $\underline{\lambda}^*$ is in an eigenspace. Thus

$$\sqrt{6} \lambda_{12}^* = (\lambda_{11} - \lambda_{22}) + (\lambda_{13} - \lambda_{23}) = 0$$

$$\sqrt{12} \lambda_{23}^* = (\lambda_{11} - \lambda_{22}) - 2(\lambda_{13} - \lambda_{23}) = 0 \quad (\text{A.20})$$

$$\sqrt{18} \lambda_{31}^* = \lambda_{11} + \lambda_{22} - 2\lambda_{33} + 2\lambda_{12} - \lambda_{23} - \lambda_{13} = 0$$

are the necessary conditions for the eigenvectors to remain stationary. The first two equations of (A.20) can only be satisfied if each of the quantities in brackets are zero. Thus

$$\lambda_{11} = \lambda_{22} \quad , \quad (\text{A.21})$$

$$\lambda_{13} = \lambda_{23} \quad ,$$

and the third equation becomes

$$\lambda_{11} - \lambda_{33} + \lambda_{12} - \lambda_{13} = 0 \quad . \quad (\text{A.22})$$

These conditions are the same as that for transverse isotropy as expressed in Equations (A.17) and (A.19). Hence, materials with symmetry properties defined as orthotropic can never satisfy the stationary eigenvector condition.

The consequences of this result can be further explained by considering an example calculation with the restriction that the

eigenvectors are fixed (this is the case presented in Reference [38]). Let us examine the inelastic response of a strain hardening transverse isotropic metal. Suppose the hardening is calculated by modifying the eigenvalues in Equation (A.12), and let $\underline{\epsilon}$ designate the inelastic strain rates, $\dot{\underline{\epsilon}}^I$. Let λ_{22}^* and λ_{33}^* be the eigenvalues after an arbitrary deformation and transform the eigenspace into the physical space according to Equation (A.6).

The resulting flow equation for the normal strain rates is given by

$$\begin{Bmatrix} \dot{\epsilon}_1^I \\ \dot{\epsilon}_2^I \\ \dot{\epsilon}_3^I \end{Bmatrix} = \begin{bmatrix} (\frac{1}{2} \lambda_{22}^* + \frac{1}{6} \lambda_{33}^*) & (-\frac{1}{2} \lambda_{33}^* + \frac{1}{6} \lambda_{33}^*) & -\frac{1}{3} \lambda_{33}^* \\ (-\frac{1}{2} \lambda_{22}^* + \frac{1}{6} \lambda_{33}^*) & (\frac{1}{2} \lambda_{22}^* + \frac{1}{6} \lambda_{33}^*) & -\frac{1}{3} \lambda_{33}^* \\ -\frac{1}{3} \lambda_{33}^* & -\frac{1}{3} \lambda_{33}^* & \frac{2}{3} \lambda_{33}^* \end{bmatrix} \begin{Bmatrix} s_1 \\ s_2 \\ s_3 \end{Bmatrix} \quad (\text{A.23})$$

Thus, the transverse isotropy assumption is maintained for any choice of λ_{22}^* and λ_{33}^* provided the transformation $\underline{\theta}$ remains constant. As a consequence, the material hardening computed in the eigenspace will also retain the transverse isotropy assumption. This result is unacceptable for general load histories

The eigenvalues and eigenvectors must be functions of the material hardening for general load histories. Relating these functions to actual material response becomes a difficult, if not impossible task. In fact, the mathematical structure bears little relationship to the

physical metallurgy of the problem and merely confuses the situation rather than leading to any significant simplification.

APPENDIX B

DEVELOPMENT OF THE KINEMATIC EQUATIONS

This Appendix contains explicit representations for the local and global stress and inelastic strain rate components. The sign convention for positive slip directions on the (111) octahedral planes are shown in Figure B1. The positive unit normals to the four octahedral planes are given by

$$\begin{aligned}
 \bar{n}^1 &= 1/\sqrt{3} (\bar{i} + \bar{j} + \bar{k}) \quad , \\
 \bar{n}^2 &= 1/\sqrt{3} (-\bar{i} + \bar{j} - \bar{k}) \quad , \\
 \bar{n}^3 &= 1/\sqrt{3} (\bar{i} - \bar{j} - \bar{k}) \quad , \quad \text{and} \\
 \bar{n}^4 &= 1/\sqrt{3} (-\bar{i} - \bar{j} + \bar{k}) \quad , \quad \quad \quad (B.1)
 \end{aligned}$$

where \bar{i} , \bar{j} , and \bar{k} are the unit vectors in the principal material directions. The positive sign convention for the $[1\ 0\ \bar{1}]$ directions on the octahedral planes are:

$$\begin{aligned}
 \bar{e}^{11} &= 1/\sqrt{2} (\bar{i} - \bar{k}) \quad , \\
 \bar{e}^{12} &= 1/\sqrt{2} (-\bar{j} + \bar{k}) \quad , \\
 \bar{e}^{13} &= 1/\sqrt{2} (\bar{i} - \bar{j}) \quad , \\
 \bar{e}^{21} &= 1/\sqrt{2} (\bar{i} - \bar{k}) \quad , \\
 \bar{e}^{22} &= 1/\sqrt{2} (\bar{i} + \bar{j}) \quad , \\
 \bar{e}^{23} &= 1/\sqrt{2} (\bar{j} + \bar{k}) \quad ,
 \end{aligned}$$

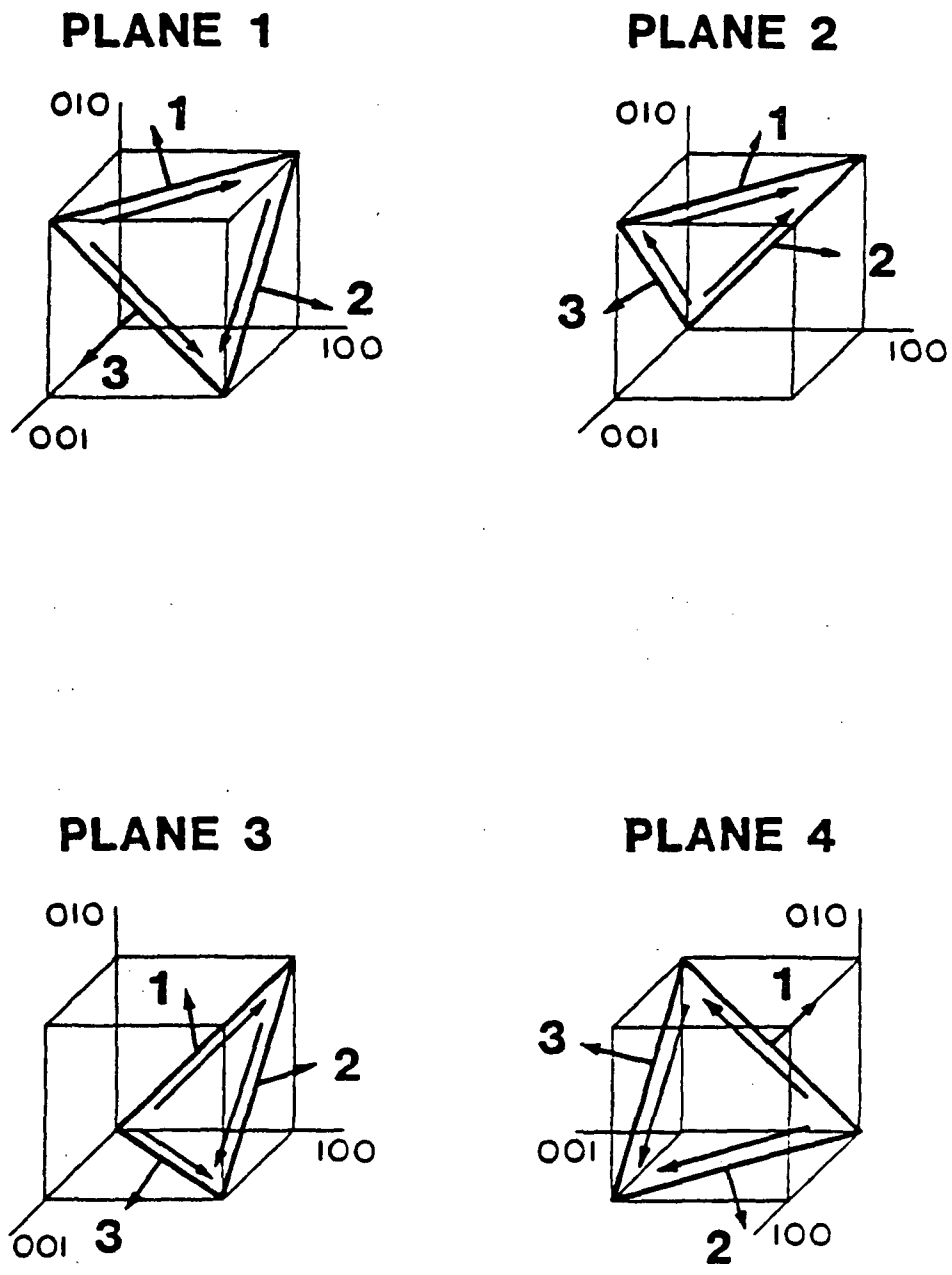


FIGURE B1. OCTAHEDRAL PLANES AND SLIP DIRECTIONS

$$\bar{l}^{31} = 1/\sqrt{2} (\bar{i} + \bar{j}) \quad ,$$

$$\bar{l}^{32} = 1/\sqrt{2} (-\bar{j} + \bar{k}) \quad ,$$

$$\bar{l}^{33} = 1/\sqrt{2} (\bar{i} + \bar{k}) \quad ,$$

$$\bar{l}^{41} = 1/\sqrt{2} (\bar{j} + \bar{k}) \quad ,$$

$$\bar{l}^{42} = 1/\sqrt{2} (\bar{i} + \bar{k}) \quad , \quad \text{and}$$

$$\bar{l}^{43} = 1/\sqrt{2} (\bar{i} - \bar{j}) \quad . \quad (B.2)$$

Substituting Equations (B.1) and (B.2) into (2.6) gives the inelastic strain rate tensor due to shearing in the $[1\ 0\ \bar{1}]$ directions on the octahedral planes as:

$$\begin{bmatrix} \dot{\epsilon}_{11}^I & \dot{\epsilon}_{12}^I & \dot{\epsilon}_{13}^I \\ \dot{\epsilon}_{21}^I & \dot{\epsilon}_{22}^I & \dot{\epsilon}_{23}^I \\ \dot{\epsilon}_{31}^I & \dot{\epsilon}_{32}^I & \dot{\epsilon}_{33}^I \end{bmatrix} = \sqrt{6}/12 \left\{ \dot{\gamma}_{OCT}^{11} \begin{bmatrix} 2 & 1 & 0 \\ 1 & 0 & -1 \\ 0 & -1 & -2 \end{bmatrix} + \dot{\gamma}_{OCT}^{12} \begin{bmatrix} 0 & -1 & 1 \\ -1 & -2 & 0 \\ 1 & 0 & 2 \end{bmatrix} + \dot{\gamma}_{OCT}^{13} \begin{bmatrix} 2 & 0 & 1 \\ 0 & -2 & 1 \\ 1 & -1 & 0 \end{bmatrix} \right.$$

$${}_{\text{OCT}}^{21} \begin{bmatrix} -2 & 1 & 0 \\ 1 & 0 & -1 \\ 0 & -1 & 2 \end{bmatrix} + {}_{\text{OCT}}^{22} \begin{bmatrix} -2 & 0 & -1 \\ 0 & 2 & -1 \\ -1 & -1 & 0 \end{bmatrix} +$$

$${}_{\text{OCT}}^{23} \begin{bmatrix} 0 & -1 & -1 \\ -1 & 2 & 0 \\ -1 & 0 & -2 \end{bmatrix} + {}_{\text{OCT}}^{31} \begin{bmatrix} 2 & 0 & -1 \\ 0 & -2 & -1 \\ -1 & -1 & 0 \end{bmatrix} +$$

$${}_{\text{OCT}}^{32} \begin{bmatrix} 0 & -1 & 1 \\ -1 & 2 & 0 \\ 1 & 0 & -2 \end{bmatrix} + {}_{\text{OCT}}^{33} \begin{bmatrix} 2 & -1 & 0 \\ -1 & 0 & -1 \\ 0 & -1 & -2 \end{bmatrix} +$$

$${}_{\text{OCT}}^{41} \begin{bmatrix} 0 & -1 & -1 \\ -1 & -2 & 0 \\ -1 & 0 & 2 \end{bmatrix} + {}_{\text{OCT}}^{42} \begin{bmatrix} -2 & -1 & 0 \\ -1 & 0 & -1 \\ 0 & -1 & 2 \end{bmatrix} +$$

$${}_{\text{OCT}}^{43} \left. \begin{bmatrix} -2 & 0 & 1 \\ 0 & 2 & -1 \\ 1 & -1 & 0 \end{bmatrix} \right\}$$

(B.3)

The inelastic strain rate vector is relative to the principal material axes. Substituting Equations (B.1) and (B.2) into (2.9) gives the shear stress in each of the $[1\ 0\ \bar{1}]$ directions on the octahedral planes as:

$$\left. \begin{array}{c} \tau^{11} \\ \tau^{12} \\ \tau^{13} \\ \tau^{23} \\ \tau^{22} \\ \tau^{23} \\ \tau^{31} \\ \tau^{32} \\ \tau^{33} \\ \tau^{41} \\ \tau^{42} \\ \tau^{43} \end{array} \right\} = \frac{1}{\sqrt{6}} \begin{bmatrix} 1 & 0 & -1 & 1 & 0 & -1 \\ 0 & -1 & 1 & -1 & 1 & 0 \\ 1 & -1 & 0 & 0 & 1 & -1 \\ -1 & 0 & 1 & 1 & 0 & -1 \\ -1 & 1 & 0 & 0 & -1 & -1 \\ 0 & 1 & -1 & -1 & -1 & 0 \\ 1 & -1 & 0 & 0 & -1 & -1 \\ 0 & 1 & -1 & -1 & 1 & 0 \\ 1 & 0 & -1 & -1 & 0 & -1 \\ 0 & -1 & 1 & -1 & -1 & 0 \\ -1 & 0 & 1 & -1 & 0 & -1 \\ -1 & 1 & 0 & 0 & 1 & -1 \end{bmatrix} \left. \begin{array}{c} \sigma_{11} \\ \sigma_{22} \\ \sigma_{33} \\ \sigma_{12} \\ \sigma_{13} \\ \sigma_{23} \end{array} \right\} \quad (B.4)$$

The stresses σ_{ij} are relative to the material axes.

The positive sign convention for the $[\bar{1} \ 2 \ \bar{1}]$ directions on the octahedral planes are:

$$\bar{l}^{11} = 1/\sqrt{6} (-\bar{i} + 2\bar{j} - \bar{k}) \quad ,$$

$$\bar{l}^{12} = 1/\sqrt{6} (2\bar{i} - \bar{j} - \bar{k}) \quad ,$$

$$\bar{l}^{13} = 1/\sqrt{6} (-\bar{i} - \bar{j} + 2\bar{k}) \quad ,$$

$$\bar{l}^{21} = 1/\sqrt{6} (\bar{i} + 2\bar{j} + \bar{k}) \quad ,$$

$$\bar{l}^{22} = 1/\sqrt{6} (\bar{i} - \bar{j} - 2\bar{k}) \quad ,$$

$$\bar{l}^{23} = 1/\sqrt{6} (-2\bar{i} - \bar{j} + \bar{k}) \quad ,$$

$$\bar{l}^{31} = 1/\sqrt{6} (-\bar{i} + \bar{j} - 2\bar{k}) \quad ,$$

$$\bar{l}^{32} = 1/\sqrt{6} (2\bar{i} + \bar{j} + \bar{k}) \quad ,$$

$$\bar{l}^{33} = 1/\sqrt{6} (-\bar{i} - 2\bar{j} + \bar{k}) \quad ,$$

$$\bar{l}^{41} = 1/\sqrt{6} (-2\bar{i} + \bar{j} - \bar{k}) \quad ,$$

$$\bar{l}^{42} = 1/\sqrt{6} (\bar{i} - 2\bar{j} - \bar{k}) \quad , \text{ and}$$

$$\bar{l}^{43} = 1/\sqrt{6} (\bar{i} + \bar{j} + 2\bar{k}) \quad . \quad (B.5)$$

Substituting Equations (B.1) and (B.5) into (2.9) gives the shear stress

in each of the $[\bar{1} \ 2 \ \bar{1}]$ directions on the octahedral planes as:

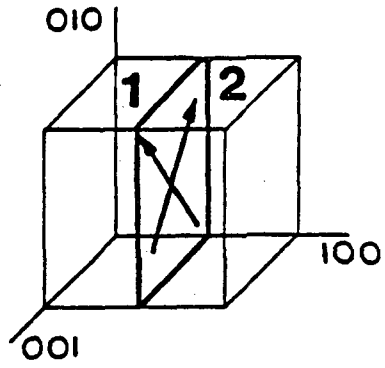
$$\begin{Bmatrix} \tau^{11} \\ \tau^{12} \\ \tau^{13} \\ \tau^{21} \\ \tau^{22} \\ \tau^{23} \\ \tau^{31} \\ \tau^{32} \\ \tau^{33} \\ \tau^{41} \\ \tau^{42} \\ \tau^{43} \end{Bmatrix} = \begin{bmatrix} -1 & 2 & -1 & 1 & -2 & 1 \\ 2 & -1 & -1 & 1 & 1 & -2 \\ -1 & -1 & 2 & -2 & 1 & 1 \\ -1 & 2 & -1 & -1 & -2 & -1 \\ -1 & -1 & 2 & 2 & 1 & -1 \\ 2 & -1 & -1 & -1 & 1 & 2 \\ -1 & -1 & 2 & 2 & -1 & 1 \\ 2 & -1 & -1 & -1 & -1 & -2 \\ -1 & 2 & -1 & -1 & 2 & 1 \\ 2 & -1 & -1 & 1 & -1 & 2 \\ -1 & 2 & -1 & 1 & 2 & -1 \\ -1 & -1 & 2 & -2 & -1 & -1 \end{bmatrix} \begin{Bmatrix} \sigma_{11} \\ \sigma_{22} \\ \sigma_{33} \\ \sigma_{12} \\ \sigma_{13} \\ \sigma_{23} \end{Bmatrix} \quad (B.6)$$

These components influence the orientation dependent yield and tension/compression asymmetry for octahedral slip through the core width effect.

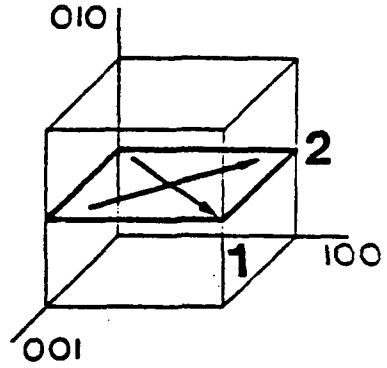
The sign convention for positive slip directions on the (0 0 1) cube planes are shown in Figure B2. The positive unit normals are given by:

$$\begin{aligned}
 \bar{n}^1 &= \bar{i} \quad , \\
 \bar{n}^2 &= \bar{j} \quad , \quad \text{and}
 \end{aligned}$$

PLANE 1



PLANE 2



PLANE 3

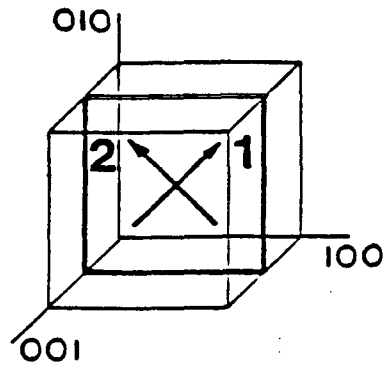


FIGURE B2. CUBE PLANES AND SLIP DIRECTIONS

$$\bar{n}^3 = \bar{k} \quad . \quad (B.7)$$

The sign convention for positive slip directions on the cube planes are:

$$\bar{l}^{11} = 1/\sqrt{2} (\bar{j} + \bar{k}) \quad ,$$

$$\bar{l}^{12} = 1/\sqrt{2} (\bar{j} - \bar{k}) \quad ,$$

$$\bar{l}^{21} = 1/\sqrt{2} (\bar{i} + \bar{k}) \quad ,$$

$$\bar{l}^{22} = 1/\sqrt{2} (\bar{i} - \bar{k}) \quad .$$

$$\bar{l}^{31} = 1/\sqrt{2} (\bar{i} + \bar{j}) \quad , \quad \text{and}$$

$$\bar{l}^{32} = 1/\sqrt{2} (-\bar{i} + \bar{j}) \quad . \quad (B.8)$$

Substituting Equations (B.7) and (B.8) into (2.1) gives the inelastic strain rate tensor due to shearing on the cube planes as:

$$\begin{bmatrix} \dot{\epsilon}_{11}^I & \dot{\epsilon}_{12}^I & \dot{\epsilon}_{13}^I \\ \dot{\epsilon}_{21}^I & \dot{\epsilon}_{22}^I & \dot{\epsilon}_{23}^I \\ \dot{\epsilon}_{31}^I & \dot{\epsilon}_{32}^I & \dot{\epsilon}_{33}^I \end{bmatrix} = \sqrt{2}/4 \left\{ \begin{matrix} \dot{\gamma}_{\text{CUBE}}^{11} \\ \dot{\gamma}_{\text{CUBE}}^{21} \\ \dot{\gamma}_{\text{CUBE}}^{31} \end{matrix} \begin{bmatrix} 0 & 1 & 1 \\ 1 & 0 & 0 \\ 1 & 0 & 0 \end{bmatrix} + \dots \right.$$

$$\begin{aligned}
& \dot{\gamma}_{\text{CUBE}}^{12} \begin{bmatrix} 0 & 1 & -1 \\ 1 & 0 & 0 \\ -1 & 0 & 0 \end{bmatrix} + \dot{\gamma}_{\text{CUBE}}^{21} \begin{bmatrix} 0 & 1 & 0 \\ 1 & 0 & 1 \\ 0 & 1 & 0 \end{bmatrix} + \\
& \dot{\gamma}_{\text{CUBE}}^{22} \begin{bmatrix} 0 & 1 & 0 \\ 1 & 0 & -1 \\ 0 & -1 & 0 \end{bmatrix} + \dot{\gamma}_{\text{CUBE}}^{31} \begin{bmatrix} 0 & 0 & 1 \\ 0 & 0 & 1 \\ 1 & 1 & 0 \end{bmatrix} + \\
& \left. \dot{\gamma}_{\text{CUBE}}^{32} \begin{bmatrix} 0 & 0 & -1 \\ 0 & 0 & 1 \\ -1 & 1 & 0 \end{bmatrix} \right\} \cdot \quad (B.9)
\end{aligned}$$

Substituting Equations (B.7) and (B.8) into (2.9) gives the shear stress in each of the directions on the cube planes as:

$$\begin{Bmatrix} \tau^{11} \\ \tau^{12} \\ \tau^{21} \\ \tau^{22} \\ \tau^{31} \\ \tau^{32} \end{Bmatrix} = 1/\sqrt{2} \begin{bmatrix} 0 & 0 & 0 & 1 & 1 & 0 \\ 0 & 0 & 0 & 1 & -1 & 0 \\ 0 & 0 & 0 & 1 & 0 & 1 \\ 0 & 0 & 0 & 1 & 0 & -1 \\ 0 & 0 & 0 & 0 & 1 & 1 \\ 0 & 0 & 0 & 0 & -1 & 1 \end{bmatrix} \begin{Bmatrix} \sigma_{11} \\ \sigma_{22} \\ \sigma_{33} \\ \sigma_{12} \\ \sigma_{13} \\ \sigma_{23} \end{Bmatrix} \quad (B.10)$$

The total inelastic strain rate tensor is the sum of the contribution from each of the active slip systems as computed in Equations (B.3), (B.6), and (B.9).

REFERENCES

1. Kear, B., and Pearcey, B., "Tensile and Creep Properties of Single Crystals of the Nickel-Base Superalloy Mar-M200", Trans. AIME, Vol. 239, p. 1209, August 1967.
2. Pearcey, B., and Ver Snyder, F., "Single Crystal Alloy Extends Turbine Blade Service Life Four Times", SAE Journal, Vol. 74, p. 36, 1966.
3. Wells, C., "The Elastic Constants of a Directionally Solidified Nickel-Base Superalloy, Mar-M200", Trans. ASM, Vol. 60, p. 270, 1967.
4. Leverant, G., and Gell, M., "The Elevated Temperature Fatigue of a Nickel-Base Superalloy, Mar-M200, in Conventionally Cast and Directionally Solidified Forms", Trans. AIME, Vol. 245, p. 1167, 1969.
5. Gell, M., and Leverant, G., "The Fatigue of a Nickel-Base Superalloy, Mar-M200, In Single-Crystal and Columnar-Grained Forms at Room Temperature", Trans AIME, Vol. 242, p. 1869, 1968.
6. Miner, R., Voigt, R., Gayda, J., and Gabb, T., "Orientation and Temperature Dependence of Some Mechanical Properties of the Single-Crystal Nickel-Base Superalloy Rene N4: Part I. Tensile Behavior", to appear Metallurgical Transaction.
7. Pope, D., and Ezz, S., "Mechanical Properties of Ni_3Al and Nickel-Base Alloys with High Volume Fraction of γ' ", International Metals Reviews, Vol. 29, No. 3, p. 136, 1984.
8. Shah, D., "Orientation Dependence of Creep Behavior of Single Crystal γ' (Ni_3Al)", Scripta Metallurgica, Vol. 17, p. 997, 1983.
9. Umakoshi, Y., Pope, D., and Vitek, V., "The Asymmetry of The Flow Stress In $Ni_3(Al,Ta)$ Single Crystals", Acta Metallurgica, Vol. 32, No. 3, p. 449, 1984.
10. Takeuchi, S., and Kuramoto, E., "Temperature and Orientation Dependence of the Yield Stress in Ni_3Ga Single Crystals", Acta Metallurgica, Vol. 21, p. 415, 1973.
11. Lall, C., Chin, S., and Pope, D., "The Orientation and Temperature Dependence of the Yield Stress of $Ni_3(Al, Nb)$ Single Crystals", Metallurgical Transactions A, Vol. 10A, p. 1323, Sept. 1979.

12. Ezz, S., Pope, D., and Paidar, V., "The Tension/Compression Flow Stress Asymmetry in Ni₃ (Al,Nb) Single Crystals", Acta Metallurgica, Vol. 30, p. 921, 1982.
13. Schulson, E., "Flow and Fracture of Zr₃Al", International Metals Reviews, Vol. 29, No. 3, p. 195, 1984.
14. Wee, D., Pope, D., and Vitek, V., "Plastic Flow of Pt₃Al Single Crystals", Acta Metallurgica, Vol. 32, No. 6, p. 829, 1984.
15. Shah, D., and Duhl, D., "The Effect of Orientation, Temperature and Gamma Prime Size on the Yield Strength of a Single Crystal Nickel Base Superalloy", Proceedings of the Fifth International Symposium on Superalloys, ASM, Metals Park, Ohio, 1984.
16. Pope, D., and Heredia, F., "The Tension/Compression Asymmetry in High γ' Volume Fraction Nickel Base Alloy Single Crystals", Fifth International Symposium on Superalloys, ASM, Metals Park, Ohio 1984.
17. Swanson, G., Life Prediction and Constitutive Models for Engine Hot Section Anisotropic Materials Program, Contract NAS3-23939, Monthly Report PWA-5968-9, August 1984.
18. Swanson, G., Life Prediction and Constitutive Models for Engine Hot Section Anisotropic Materials Program, Contract NAS3-23939, Monthly Report PWA-5968-10, September 1984.
19. Lobotnov, Y., Creep Problems In Structural Members, North Holland Publishing Company, Amsterdam, 1969.
20. Hill, R., Mathematical Theory of Plasticity, Oxford University Press, London, 1950.
21. Basani, J., "Yield Characterization of Metals with Transversely Isotropic Properties", International Journal of Mechanical Engineering Science, Vol. 12, p. 341, 1977.
22. Baladi, G., "Numerical Implementation of a Transverse-Isotropic Inelastic, Work-Hardening Constitutive Model", Transactions of the 4th International Conference on Structural Mechanics in Reactor Technology, San Francisco, August 15-19, 1977.
23. Lee, D., and Zaverl, F., "A Description of History Dependent Plastic Flow Behavior of Anisotropic Metals", Journal of Engineering Materials and Technology, ASME, Vol. 101, p. 59, January 1979.

24. Shih, C., and Lee, D., "Further Developments in Anisotropic Plasticity", *Journal of Engineering Materials and Technology*, ASME, Vol. 100, p. 294, July 1978.
25. Shahabi, S., and Shelton, A., "The Anisotropic, Yield, Flow and Creep Behavior of Pre-Strained EN-24 Steel", *Journal of Mechanical Engineering Science*, Vol. 17, No. 2, p. 93, 1975.
26. Lee, D., and Zaverl, F., "A Generalized Strain Rate Dependent Constitutive Equation for Anisotropic Metals", *Acta Metallurgica*, Vol. 26, p. 1771, 1978.
27. Eisenberg, M., and Yen, C., "A Theory of Multiaxial Anisotropic Viscoplasticity", *Journal of Applied Mechanics*, ASME, Vol. 48, p. 276, 1981.
28. Hill, R., "A Theory of the Yielding and Plastic Flow of Anisotropic Metals", *Proceedings of the Royal Society (London)*, Series A, Vol. 193, p. 281, 1948.
29. Edelman, F., and Drucker, D., "Some Extensions of Elementary Plasticity Theory", *J. Franklin Instr.*, Vol. 251, p. 581, 1951.
30. Lee, D., "A Continuum Description of Anomalous Yielding in Anisotropic Metals", *Metallurgical Transaction A*, Vol. 9A, p. 1495, 1978.
31. Taylor, G., "Plastic Strains in Metals", *J. Inst. Metals*, Vol. 62, p. 307, 1938.
32. Bishop, J., and Hill, R., "A Theory of the Plastic Distortion of a Polycrystalline Aggregate Under Combined Stresses", *Phil. Mag.*, p. 414, 1951.
33. Bishop, J., and Hill, R., "A Theoretical Derivation of the Plastic Properties of a Polycrystalline Face-Centered Metal", *Phil. Mag.*, Vol. 42, p. 1298, 1951.
34. Bishop, J., "A. Theoretical Examination of the Plastic Deformation of Crystals by Glide", *Phil. Mag.*, p. 51, 1952.
35. Paslay, P., Wells, C., and Leverant, G., "An Analysis of Primary Creep of Nickel-Base Superalloy Single Crystals", *Journal of Applied Mechanics*, ASME, p. 759, 1970.
36. Paslay, P., Wells, C., Leverant, G., and Burck, L., "Creep of Single Crystal Nickel-Base Superalloy Tubes Under Biaxial Tension", *Journal of Applied Mechanics*, ASME, Vol. 38, p. 623, 1971.

37. Gabb, T., Gayda, J., and Miner, R., "Orientation and Temperature Dependence of Some Mechanical Properties of the Single-Crystal Nickel-Base Superalloy RENE N4: Part II. Low Cycle Fatigue", to appear Metallurgical Transactions.
38. Stouffer, D., and Bodner, S., "A Constitutive Model for the Deformation Induced Anisotropic Plastic Flow of Metals", International Journal of Engineering Science, Vol. 17, p. 737, 1979.
39. Bodner, S., and Partom, Y., "Constitutive Equations for Elastic-Viscoplastic Strain-Hardening Materials", ASME, Journal of Applied Mechanics, Vol. 42, p. 385, 1975.
40. Bodner, S., Partom, I., and Partom, Y., "Uniaxial Cyclic Loading of Elastic-Viscoplastic Materials", ASME, Journal of Applied Mechanics, Vol. 46, p. 805, 1979.
41. Rice, J., "On the Structure of Stress-Strain Relations for Time-Dependent Plastic Deformation In Metals", ASME, Journal of Applied Mechanics, Vol. 37, p. 728, 1970.
42. Ponter, A., and Leckie, F., "Constitutive Relations for the Time Dependent Deformation of Metals", ASME, Journal of Engineering Materials and Technology, Vol. 98, p. 47, 1976.
43. Ponter, A., "Convexity and Associated Continuum Properties of a Class of Constitutive Relationship", Journal De Mecanique, 5.4, p. 527, 1976.
44. Abuefoutouh, N., "A Thermodynamically Consistent Constitutive Model for Inelastic Flow of Metals", Ph.D. Dissertation, Department of Aerospace Engineering, University of Cincinnati, 1983.
45. Budiansky, B., and O'Connell, R., "Bulk Dissipation in Heterogeneous Media", Solid Earth Geophysics and Geotechnology, ASME-AMD, Vol. 42, 1980.
46. Olszak, W., and Urbanowsky, W., "The Plastic Potential and the Generalized Distortion Energy in the Theory of Non Homogeneous Anisotropic Elastic-Plastic Bodies", Arch. Mech. Stos., Vol. 8, p. 671, 1956.
47. Hill, R., "Theoretical Plasticity of Textured Aggregates", Math Proc. Camb. Phil. Soc., Vol. 85, p. 179, 1979.
48. Jones, R., Mechanics of Composite Materials, McGraw Hill, New York, 1975.

49. Sutcu, M., and Krempl, E., "A Transversely Isotropic Formulation of the Viscoplasticity Theory Based on Overstress", Report MML 84-5, Rensselaer Polytechnic Institute, 1984.
50. Bodner, S., and Stouffer, D., "Comments on Anisotropic Plastic Flow and Incompressibility", International Journal of Engineering Science, Vol. 21, No. 3, p. 211, 1983.
51. Stouffer, D., and Bodner, S., "A Relationship Between Theory and Experiment for a State Variable Mechanical Testing for Deformation Model Development", ASTM STP 765, American Society for Testing and Materials, p. 239, 1982.
52. Stouffer, D., "A Constitutive Representation for IN100", Air Force Materials Laboratory, AFML-TR-81-4039, January 1981.
53. Merzer, A., and Bodner, S., "Analytical Formulation of a Rate and Temperature Dependent Stress-Strain Relation", ASME, Journal of Engineering Materials and Technology, Vol. 101, p. 254, 1979.
54. Bodner, S., "Representation of Time Dependent Mechanical Behavior of Rene 95 by Constitutive Equations", Air Force Materials Laboratory, AFML-TR-79-4116, August 1979.
55. Bodner, S., and Lindholm, U., "An Incremental Criterion for Time-Dependent Failure of Materials", ASME, Journal of Engineering Materials and Technology, April 1976.
56. Rosen, A., and Bodner, S., "The Influence of Strain Rate and Strain Ageing on the Flow Stress of Commercially-Pure Aluminum", Journal of Mechanics and Physics of Solids, Vol. 15, p. 47, 1967.
57. Anand, L., "Constitutive Equations for the Rate-Dependent Deformation of Metals at Elevated Temperatures", ASME, Journal of Engineering Materials and Technology, Vol. 104, p. 12, 1982.
58. Merzer, A., "Steady and Transient Creep Behavior Based on Unified Constitutive Equations", ASME, Journal of Engineering Materials and Technology, Vol. 104, p. 18, 1982.
59. Bodner, S., and Merzer, A., "Viscoplastic Constitutive Equations for Copper with Strain Rate History and Temperature Effects", ASME, Journal of Engineering Materials and Technology, Vol. 100, p. 388, 1978.
60. Dame, L., Stouffer, D., and Abuelfoutouh, N., "Finite Element Analysis of Notch Behavior Using a State Variable Constitutive Equation", Proceedings of 2nd Symposium on Nonlinear Constitutive Relations for High Temperature Applications, NASA Lewis, June 13-15, 1984.

61. Gilman, J., Micromechanics of Flow, McGraw-Hill, New York, 1969.
62. Gilman, J., "Dislocation Mobility in Crystals", J. Appl. Phys., Vol. 36, p. 3195, 1965.
63. Giamei, A., "Deformation and Fracture of Advanced Anisotropic Superalloys", Final Technical Report, Contract No. F44620-76-C-0028, Air Force Office of Scientific Research, 1979.
64. Asaro, R., "Crystal Plasticity", Journal of Applied Mechanics, ASME, Vol. 50, p. 921, 1983.
65. Havner, K., and Shalaby, A., "A Simple Mathematical Theory of Finite Distortional Latent Hardening in Single Crystals", Proc. R. Soc. Lond. A 358, p. 47, 1977.
66. Havner, K., and Salpekar, S., "Theoretical Latent Hardening of Crystals in Double-Slip-II. F.C.C. Crystals Slipping on Distinct Planes", J. Mech. Phys. Solids, Vol. 31, No. 3, p. 231, 1983.
67. Weng, G., "Kinematic Hardening Rule In Single Crystals", Int. J. Solids Structures, Vol. 15, p. 861, 1979.
68. Wukusick, C., "Directional Solidification Alloy Development", NADC-78136-60, Naval Air Systems Command, 1980.
69. Davies, R., and Johnston, T.: in "Ordered Alloys", (ed. B. Kear et. al.), p. 447, 1970, Baton Rouge, Louisiana, Claiborne's Publishing Division.
70. Tien, J., Kear, B., and Leverant, G., "On the High Activation Energy for Steady State Creep of Particle Strengthened Systems", Scripta Metallurgica, Vol. 6, p. 135, 1972.
71. Witmer, E., and Kotanchik, J., "Progress Report on Discrete-Element Elastic and Elastic-Plastic Analyses of Shells of Revolution Subjected to Axisymmetric and Asymmetric Loading", Proceedings of the Second Conference on Matrix Methods in Structural Analysis, Wright-Patterson Air Force Base, Dayton, Ohio, pp. 1341-1453, October 1968.
72. Salmon, M., Berke, L., and Sandhu, R., "An Application of the Finite Element Method to Elastic-Plastic Problems of Plane Stress", Air Force Flight Dynamic Laboratory, Tech. Report AFFDL-TR-68-39, May 1978.
73. Hildebrand, F., Introduction to Numerical Analysis, New York, McGraw-Hill, 1974.
74. Carnahan, B., Luther, H., and Wilkes, J., Applied Numerical Methods, New York, Wiley, 1969.

75. Bonneville, J., and Escaig, B., "Cross-Slipping Process and the Stress-Orientation Dependence in Pure Copper", *Acta Metallurgica*, Vol. 27, p. 1477, 1979.
76. Orowan, E., "The Creep of Metals", *Trans. West of Scotland Iron and Steel Inst.*, Vol. 54, p. 45, 1947.
77. Peirce, D., Asaro, R., and Needleman, A., "An Analysis of Nonuniform and Localized Deformation in Ductile Single Crystals", *Acta Metallurgica*, Vol. 30, p. 1087, 1982.
78. Yang, S., "Elastic Constants of a Monocrystalline Nickel-Base Superalloy", *Metallurgical Transactions A.*, Vol. 16A-No. 4, p. 661, 1984.

1. Report No. NASA CR-175015		2. Government Accession No.		3. Recipient's Catalog No.	
4. Title and Subtitle Anisotropic Constitutive Model for Nickel Base Single Crystal Alloys: Development and Finite Element Implementation				5. Report Date March 1986	
				6. Performing Organization Code	
7. Author(s) L.T. Dame and D.C. Stouffer				8. Performing Organization Report No. None	
				10. Work Unit No.	
9. Performing Organization Name and Address University of Cincinnati Dept. of Aerospace Engineering and Engineering Mechanics Cincinnati, Ohio 45221-0070				11. Contract or Grant No. NAG 3-511	
				13. Type of Report and Period Covered Contractor Report	
12. Sponsoring Agency Name and Address National Aeronautics and Space Administration Washington, D.C. 20546				14. Sponsoring Agency Code 533-04-11	
15. Supplementary Notes Final report. Project Manager, Robert L. Thompson, Structures Division, NASA Lewis Research Center, Cleveland, Ohio. This research was funded by the NASA Lewis HOST Project and Wright-Patterson Air Force Base, Dayton, Ohio (Theodore Nicholas).					
16. Abstract <p>The purpose of this research is to develop a tool for the mechanical analysis of nickel base single crystal superalloys, specifically René N4, used in gas turbine engine components. This objective is achieved by developing a rate dependent anisotropic constitutive model and implementing it in a nonlinear three dimensional finite element code. The constitutive model is developed from metallurgical concepts utilizing a crystallographic approach. A non Schmid's law formulation is used to model the tension/compression asymmetry and orientation dependence in octahedral slip. Schmid's law is a good approximation to the inelastic response of the material in cube slip. The constitutive equations model the tensile behavior, creep response and strain rate sensitivity of these alloys. Methods for deriving the material constants from standard tests are presented. The finite element implementation utilizes an initial strain method and twenty noded isoparametric solid elements. The ability to model piecewise linear load histories is included in the finite element code. The constitutive equations are accurately and economically integrated using a second order Adams-Moulton predictor-corrector method with a dynamic time incrementing procedure. Computed results from the finite element code are compared with experimental data for tensile, creep and cyclic tests at 760°C. The strain rate sensitivity and stress relaxation capabilities of the model are evaluated. Limitations and future development needs are discussed.</p>					
17. Key Words (Suggested by Author(s)) René N4; Fatigue; Single Crystal; Creep; Constitutive equation; Tensile; Mechanical properties			18. Distribution Statement Unclassified - unlimited STAR Category 39		
19. Security Classif. (of this report) Unclassified		20. Security Classif. (of this page) Unclassified		21. No. of pages 129	22. Price* A07

National Aeronautics and
Space Administration

Lewis Research Center
Cleveland, Ohio 44135

Official Business
Penalty for Private Use \$300

SECOND CLASS MAIL

ADDRESS CORRECTION REQUESTED



Postage and Fees Paid
National Aeronautics and
Space Administration
NASA-451

NASA
